**Centro de Investigación y de Estudios Avanzados del Instituto Politécnico Nacional
Unidad Saltillo**

"EVALUATION OF ORDERED MESOPOROUS CARBON AND A BIOCARBON AS CATALYSTS OF BIOANODES CONTAINING *Bacillus subtilis* FOR ENERGY GENERATION IN MFC."

THESIS

for the degree of:

Doctor en Ciencias

En:

Sustentabilidad de los Recursos Naturales y Energía

By:

Selvia García Mayagoitia

Thesis advisors:

Dr. Francisco Javier Rodríguez Varela
Dr. Fabián Fernández Luqueño

Ramos Arizpe, Coahuila   August 2023

Centro de Investigación y de Estudios Avanzados del Instituto Politécnico Nacional Unidad Saltillo

"EVALUACIÓN DE CARBÓN MESOPOROSO ORDENADO Y UN BIOCARBÓN COMO CATALIZADORES DE BIOÁNODOS CONTENIENDO *Bacillus subtilis* PARA GENERACIÓN DE ENERGÍA EN CCM."

Tesis que presenta:

Selvia García Mayagoitia

Para obtener el Grado de

Doctora en Ciencias

En

Sustentabilidad de los Recursos Naturales y Energía

Directores de Tesis:

Dr. Francisco Javier Rodríguez Varela
Dr. Fabián Fernández Luqueño

Ramos Arizpe, Coahuila.   Agosto de 2023

This project was dedicated to my family,

My kids Andrea, Abigail and Adrian who are my motor in life.

To my mother Selvia who was always supporting

Thanks for believing in this dream.

Acknowledgements

Table of contents

List of figures

List of tables

Glossary of Abbreviations and Acronyms

B. subtilis   *Bacillus subtilis*

BC   Biocarbon

BC015   Biocarbon functionalized with 0.15 M methanol

BC05   Biocarbon functionalized with 0.5 M methanol

BC1   Biocarbon functionalized with 1 M methanol

CE   Coulombic Efficiency

CHNS   Determination of Carbon, Hydrogen, Nitrogen, and Sulfur

CV   Cyclic Voltammograms

EET   Extracellular Electron Transfer

FESEM   Field Emission Scanning Electron Microscopy

MFC   Microbial Fuel Cells

COD   Chemical Oxygen Demand

OMC   Ordered Mesoporous Carbon

OMC015   Ordered Mesoporous Carbon functionalized with 0.15 M methanol

OMC05   Ordered Mesoporous Carbon functionalized with 0.5 M methanol

OMC1   Ordered Mesoporous Carbon functionalized with 1 M methanol

ORR   Oxygen Reduction Reaction

PD   Power Density

PWW   Pharmaceutical Wastewater

RHE   Reversible Hydrogen Electrode

SEM   Scanning Electron Microscopy

TEM   Transmission Electron Microscopy

Abstract

In this study, Ordered Mesoporous Carbon (OMC) and biocarbon (BC) from sewage sludge were evaluated as catalysts in bioanodes containing a biofilm of *Bacillus subtilis* (*B. subtilis*) as electrochemically active microorganism (EAM) to generate energy from pharmaceutical wastewater (PWW) in a dual-chamber Microbial Fuel Cell (MFC).

OMC and BC were functionalized with methanol as chemical agent at different concentrations (0.15, 0.5 y 1 M), with the intermittent microwave heating (IMH) method, resulting in a project with eight catalysts: OMC, OMC015, OMC05, and OMC1; as well as BC, BC015, BC05, and BC1.

In the first stage, cyclic voltammograms (CVs) in PWW obtained in half cell probe, showed an enhanced bioelectrochemical behavior of the OMC + *B. subtilis* and OMC015 + *B. subtilis* bioanodes compared to OMC05 + *B. subtilis* and OMC1 + *B. subtilis*. Therefore, the two former bioanodes were evaluated in the MFC containing PWW as substrate.

The results showed differences in the behavior of the bioanodes in long-term tests (7 days) in the MFC. OMC + *B. subtilis* showed a decrease in Open Circuit Voltage (OCV) and current density (*j*) values from Day 0 to Day 3, followed by a significant increase in *j* and a slightly higher OCV at day 7 (compared to Day 3). Meanwhile, OMC015 + *B. subtilis* showed a more stable bioelectrochemical behavior, with slight variations in OCV and *j* at Days 0, 3 and 7. The highest power density (P_{cell}) of the MFC was 12.32 mW m^{-2} with OMC015 + *B. subtilis* at Day 3 of operation.

In the second stage, CVs in PWW showed that BC + *B. subtilis* and BC015 + *B. subtilis* are more active than BC05 + *B. subtilis* and BC1 + *B. subtilis* to oxidize the organic matter contained in PWW. During the 7 days test in the MFC, BC + *B. subtilis* suffered a drastic decrease in OCV from Day 0 to Days 3 and 7, nevertheless with an increase in *j*, particularly at Day 3. Meanwhile, BC015 + *B. subtilis* decreased in OCV from Day 0 to Day 3, followed by an increase at Day 7, which included the generation of the highest *j* value. BC015 + *B. subtilis* generated the highest P_{cell} (11.66 mW m^{-2}) at Day 7.

The results showed the biocompatibility between the OMC015 and BC015 catalysts and *B. subtilis* as EAM, and their catalytic activity as bioanodes to oxidize organic matter contained in PWW, generating bioenergy from the MFC.

Resumen

En esta investigación, Carbón Mesoporoso Ordenado (OMC), y biocarbón (BC) proveniente de lodos residuales, fueron evaluados como bioánodos conteniendo una biopelícula de *Bacillus subtilis* (*B.subtilis*), como microorganismo electroquímicamente activo (EAM) para generar energía de agua residual farmacéutica (PWW) en una celda de combustible microbiana (MFC) de doble cámara.

OMC y BC fueron funcionalizados con metanol como agente químico a diferentes concentraciones (0.15, 0.5 y 1M), con el método de calentamiento intermitente de microondas (IMH) resultando en un proyecto con 8 catalizadores: OMC, OMC015, OMC05, y OMC1, así como BC, BC015, BC05, Y BC1.

En la primera etapa, los voltamperogramas cíclicos (CVs) obtenidos de los bioánodos de OMC + *B.subtilis* y OMC015 + *B.subtilis* mostraron un mejor comportamiento bioelectroquímico comparado con OMC05 + *B.subtilis* y OMC1 + *B.subtilis*, utilizando PWW como sustrato en las pruebas de media celda. Por lo tanto, los bioánodos formados fueron evaluados en una MFC conteniendo PWW.

Los resultados mostraron diferencias en el comportamiento de los bioánodos en las pruebas de larga duración (7 días) en la MFC. Los valores de Voltaje de Circuito Abierto (OCV) y de densidad de corriente (*j*) de OMC + *B.subtilis* se disminuyeron del Día 0 al Día 3, seguido de un incremento significativo en j y una OCV ligeramente mayor en el día 7 (comparado al Día 3). Mientras tanto, se observó que OMC015 + *B.subtilis* mantiene un comportamiento bioelectroquímico estable, con ligeras variaciones en OCV y j en los días 0, 3, y 7. La mayor densidad de potencia (P_{cell}) de la MFC fue de 12.32 mW m^{-2} utilizando el bioánodo con OMC015 + *B.subtilis* en el Día 3 de la operación.

En la segunda etapa, los CVs obtenidos utilizando PWW, mostraron que BC + *B.subtilis* y BC015 + *B.subtilis* fueron más activos que BC05 + *B.subtilis* y BC1 + *B.subtilis* para oxidar la materia orgánica presente en el sustrato. Durante los 7 días de prueba en la MFC, BC + *B.subtilis* demostró una disminución en OCV del Día 0 al Día 3 y al 7, pero se observó un incremento en j, particularmente en el Día 3. Mientras que la OCV obtenida utilizando BC015 + *B.subtilis* disminuyó del Día 0 al Día 3, posteriormente se observó una mayor generación de *j* (11.66 mW m^{-2}) en el día 7.

Los resultados observados, demostraron la biocompatibilidad entre los catalizadores OMC015 y BC015 con *B.subtilis* como EAM, y su actividad catalítica como bioánodos para oxidar materia orgánica presente en PWW, generando bioenergía a partir de la MFC.

Introduction

Introduction

With the world population rapidly increasing, the energy demand has grown at a high rate, while the reserves of natural resources have decreased, including the everyday scarcer drinking water. Recently, the United Nations Climate Change Conferences (COP 21 and COP 22) set as a priority to limit the effects of anthropogenic activities on climate change and other environmental issues, with the objective of reducing the prominent role of fossil fuels in the world economy by 2050 [1].

Over the last 25 years approximately, several environment-friendly technologies have been developed that might contribute to solving some of the current energy generation problems while also aiding in providing good quality water, have been developed. In this sense, there is an increasing interest in promoting the use of biomass as an energy resource, adding value to residues, and contributing to the so-called bio-economy [1]. Such green technologies are aimed for the treatment of wastewater from the food industry, agriculture, cattle raising, homes, and industrial activities in general [2, 3].

Among those technologies, Microbial Fuel Cells (MFCs) have been studied because of their advantages for sustainable wastewater treatment and energy generation [4, 5]. MFCs make use of bacteria as electrochemically active microorganisms (EAM) at the bioanode to promote the oxidation of organic compounds contained in a substrate (anode chamber) in a bioelectrochemical process that generates electrons which are transferred to a catalyst that also enhances the kinetic reaction. The electrons are transported through an external circuit to the cathode where the Oxygen Reduction Reaction (ORR) occurs (cathode chamber), closing the circuit for electricity generation.

In the last 15 years, research on MFC has focused on enhancing their performance. Some improvements have increased biocompatibility between the catalyst and the EAM. High biocompatibility allows for the homogeneous growth of an extracellular matrix resulting in a biofilm, increasing the electron transfer kinetics from the substrate to the external circuit [6]. Nonetheless, MFCs also have important drawbacks that must be addressed to increase their performance. One of them is to enhance the biocompatibility between EAM and catalyst at the bioanode, since achieving this objective will result in a higher rate of organic compounds oxidation and therefore an increased wastewater treatment. From a

bioelectrochemical point of view, the result will be a higher power density generated by the MFC.

Opposite to other types of fuel cells, carbon-based metal-free porous materials such as Vulcan, Ordered Mesoporous Carbon (OMC), graphite [2], and graphene oxide, among others [3], can be used as high-performance catalysts at the bioanodes of MFCs. OMC is a relatively new member of the carbonaceous family, with a high specific surface area (up to 2000 m^2 g^{-1}), tunable pore size, large pore volume, and high thermomechanical stability [7]. OMCs are attractive for electrochemical applications because of their high electronic conductivity. Moreover, their porous surface increases the catalyst-bacteria contact area. At the interface, the production of flagella by the microorganism is stimulated, anchoring it onto the carbon surface and promoting the charge transfer [4]. With this approach of avoiding the using of noble metals, the cost of MFC is significantly reduced [5].

As an alternative to OMCs, applying biocarbons (BCs) derived from biomass in bioanodes of MFC has gained the attention of research groups worldwide. Several biomass sources have been proposed as carbon sources to produce BCs, which surface properties from micro to mesoporosity enhance the mass transport and speed up the charge flow and the organic oxidation of the substrate [8]. For instance, Tyagi and Lo proposed that sewage sludge from industrial wastewater can be processed to produce biocarbon catalysts, offering economic and environmental advantages for wastewater treatment and energy generation in MFCs [6].

On the other hand, one of the most challenging substrates to be treated leading to the generation of energy in MFCs is pharmaceutical wastewater (PWW), which characterizes by its complex composition, high toxicity, and high chemical oxygen demand (COD), containing a variety of organic and inorganic constituents [9]. Therefore, developing methodologies for treating these wastewaters, which must be affordable, highly biodegradable, and environmentally benign, are necessary [10].

Several electrochemically active microorganisms, capable of oxidizing the organic matter at the substrate to produce electrons by using the cell respiration cycle have been identified [11], such as *Geobacter sp.*, *Klebsiella sp.*, and *Pseudomonas aeruginosa.*

Nonetheless, these bacteria have some disadvantages for MFCs applications. For example, *Geobacter sp.* are strictly anaerobic microorganisms, while *Pseudomonas aeruginosa* are opportunistic pathogens [12].

Meanwhile, *Bacillus subtilis* (*B. subtilis*), a gram-positive aerobic bacterium, is not a pathogenic microorganisms found naturally in soils, and its culture does not necessarily require specific nutritive media. These characteristics make it an excellent candidate for MFC applications, since it has been shown that these bacteria can promote the oxidation of organic matter and, therefore the production of electrons from different substrates mainly due to the mediators' redox compounds [13].

In this thesis, the behavior of non-functionalized OMC and BC from sewage sludge and functionalized with methanol at different concentrations (0.15, 0.5 and 1 M, labeled as OMC015, OMC05, and OMC1; as well as BC015, BC05, and BC1, respectively), forming bioanodes with *B. subtilis* as the electrochemically active microorganism (EAM), is evaluated in half-cell and in a dual-chamber MFC. The substrate of choice is PWW obtained from a local company. Long-term test of 7 days has been carried out in the MFC, aiming to characterize the bioelectrochemical performance of the bioanodes.

1. Background

1.1 Bioelectrochemical System (BES)

The use of fossil fuels as an energy source has environmental consequences such as climate change, which led to the signing of the Paris Agreement in 2015, in which the objective is to maintain the global surface temperature below 2 °C than the actual [14, 15]. The mitigation of climate change is one of the aims of the scientific society, searching for the development of devices capable of producing alternative energy from waste, such as wastewater, and friendly to the environment.

The device proposed for safely extracting the energy stored in wastewater in the form of electricity or valuable chemicals such as hydrogen with no or low energy, is the BES. This system has minimum or non-environmental impacts compared to the traditional treatments. Many studies that have been carried out and summarized in several works, including: the application of BES for metal removal and recovery, the degradation of volatile organic materials, and the desalination among others [15].

Early studies of BES, such as that of Potter in 1911, described the development of an electric potential difference at a platinum electrode immersed in a glucose solution (cane sugar and ordinary glucose in distilled water) in the presence of microorganisms like *Saccharomyces*, but the power generation obtained was low [16]. Previous studies showed that the particular physiological character of fungi and bacteria required the disintegration of organic compounds as a necessary energy source. Even more, the evolution of caloric energy during fermentation or putrefaction was also acknowledged as a source of electrical energy during these processes [16, 17].

The first breakthrough was in 1931, when Barnet Cohen produced 35 V with various microbial half fuel cells connected in series, with this approach, the attention of researchers was on these devices. In the next fifty years, the scientist looked to understand the basic concepts of MFC and started working on various experiments by currently improving the performance of this alternative energy generator [18].

In 1984, Roller et al. established the importance of promoting the electron transfer in BES by studying the reduction of several redox dye's mediators by bacteria. The authors concluded that the efficiency of the biosystems varies with the amount of oxygen

consumed depending on the microorganism and the type of electron transfer mechanism. In that study, the microorganisms that promoted the higher oxygen consumption rate and reduction of dyes were *Escherichia coli* and *Proteus vulgaris* [19]. Elsewhere, it was found that electron transfer to the electrode, i.e., enhancing the efficiency of the bioelectrochemical system, was achieved by implementing an electron transfer mediator, which in fact increases the substrate consumption rate.

One of the first patents of BES was awarded to Kim et al. Their system was a "Mediator-less biofuel cell", for wastewater treatment, using different substrates and microorganisms. It was claimed that the device could consume the electrons generated from the fermentative metabolism of microorganisms through an electron metabolism without energy conservation [20]. When wastewater was the substrate in the biosystem, a lower amount of sludge was produced and the efficiency of the metabolization of organic materials was increased [20, 21].

Some BES can harvest the energy stored in the organic matter of substrates such as wastewater to generate electricity or valuable chemicals like hydrogen, with relatively low energy consumption in a safe manner. These systems have minimum or non-environmental impacts compared to traditional treatments. The advantageous use of BES for several applications, including metal removal and recovery, degradation of volatile organic materials, and desalination, among others, has been summarized elsewhere [15].

BES can be classified into electron-producing microbial fuel cells (MFCs) and electron-consuming microbial electrolysis cells (MECs). The anodic oxidation reactions are similar, but the reducing reactions at the cathodes are different. In MFCs, the goal is to produce electrical energy, while that in MEC is energy-consuming leading the overall reaction to the production of chemicals of interest such as hydrogen [22]. Another type of BES is the enzymatic fuel cell (EFC), in which isolated enzymes are in direct contact with the substrate during operation, in comparison with MFC, in this last one, the microbial cell wall or cell membrane prevents direct contact of enzymes with the substrate [23]. Meanwhile, the microbial electrosynthesis system (MES), are defined as an electrically driven synthesis of microbial products from sources like CO_2 or wastewater feedstocks, providing a highly attractive and novel route for the generating biochemicals and biofuels [24].

Several possible applications for BES have been identified using different substrates such as acetate, cellulose, and starch, and with interest in domestic, industrial, brewery, and paper-recycling wastewater sectors. BES are systems with the potential to be utilized in several industries and sectors, such as the synthesis of fine and bulk chemicals, energy conversion and storage, and remediation processes. The application of these technologies is related to the oxidation of organic matter and several different sources of oxidizable material at the bioanode. To make the BES suitable, it is important to consider the value of products (energy, fuels, and chemicals) obtained as well as the possibility of producing treated water, which has to be higher than the capital and operational costs, i.e., the novel systems must be, ideally, cost-effective [25].

1.2 Scaling up the BES: The case of MFCs

One of the existing challenges for BES is scaling up the technology to the industrial level [26]. Some of the limitations that must be overcome to achieve it are: i) the fabrication of electrodes with adequate surface-to-volume ratio, ii) the development of biocompatible surfaces, iii) the reduction of costs, and iv) the assuring of long-term stability of the components. Some suggestions to improve the BES are to combine biocatalysts and electrochemical reaction steps to yield a scaled and stable bioelectrochemical process [26].

Nonetheless, devices of a relatively large scale are still uncommon due to the complexity of installation and operating procedures as well as other engineering and environmental factors [27]. Nevertheless, regarding the MFCs, research groups have developed relatively large systems. Table 1.1 shows examples of large-scale MFCs with several configurations, indicating their capacity, microorganism, and power density. As can be seen, MFCs can utilize not only wastewater effluents, but also soil or sediment matrix as the substrate, or as the bacterial source for its implementation in bioremediation [28].

Table 1.1 Examples of scaled Microbial Fuel Cells (MFCs) operating with different substrates.

MFC Configuration	Anode Material	Substrate	MFC Capacity	Microorganism	Power Density	COD	Ref.
5 Baffled MFC (12.7 cm X 4.3 cm X 0.6 cm)	Graphite brush	Acetate	0.0008 L	Bacteria consortia	16 W m^{-3}	-	[29]
6 continuous MFC Units, stacked configuration	Graphite granules	Sodium acetate	0.36 L	Gram-positive bacteria consortia	146 ± 2 2 W m^{-3} after 5 h and remaining for 11 more h	2.17 gL^{-1}	[30]
Serpentine type MFC (40 air-cathode MFC units)	Graphite felt (0.5 cm thick, 15.0 X 9.5 cm)	Brewery wastewater	10 L	Anaerobic bacteria consortia	4.1 W m^{-3}	1.06 gL^{-1}	[31]
Trickling MFC (TMFC)	Carbon cloth	Acetate-containing medium solution, also municipal and brewery waste streams	13.4 L	Consortia containing *Geobacter, Aminiphilus, Sedimentibacter, Acetoanaerobium* and *Spriochaeta*	3.43 W m^{-3} (diluted brewery) 12.7 W m^{-3} (20 mM acetate) <0.05 W m^{-3} (municipal)	4.011 gL^{-1} (Diluted brewery) 2.560 gL^{-1} (20 mM acetate) 0.0156 gL^{-1} (municipal)	[32]
Stack of 64 MFC Units of 16.25 L each (67.0 X 46.4 X14.1 cm).	Reticulated vitreous carbon (RVC) anodes	Household Wastewater	1000 L	*Geobacter*, in consortia with nitrifying and denitrying bacteria as *Candidatus nitroga, Denitratisoma*, and *Thermomonas*.	15 - 60 W m^{-3} in 1 h	224 - 469 gL^{-1}	[33]
Up-flow Anaerobic Sludge Blanket (UASB)-MFC Hybrid reactor	Granular activated carbon bed	Synthetic textile wastewater	~10 L	Microbial consortia	10.67 W m^{-3}	0.416 ± 0.032 gL^{-1}	[34]

16 Bioelectrochemical Wastewater Treatment Units (BE-WWTUs)	Carbon fabric	Raw municipal wastewater	1200 L pilot scale	*Deltaproteobacteria, Geobacter spp. Anaeromyxobacter dehalogenans, Geothrix spp.*	73.3 mA m^{-2}	0.3 gL^{-1}	[35]

When scaling up an MFC, it is important to consider its two main goals: generate power density and wastewater treatment. However, it is also relevant to consider that the MFC must be cost-effective, using low-cost materials for the configuration of the MFC [28]. The most common MFCs arrangement is a dual chamber, where the anode and cathode are separated between an ion exchange membrane, or a salt bridge. Besides the scaling-up, the stacking of MFC consists of arranging numerous MFCs in series or parallel to generate a higher power output [28].

1.3 MFCs: Operation principles and configuration

Over the past 15 years, MFCs have gained the attention of the scientific community, because of their capability of transforming organic waste into electricity through microbial catalytic metabolisms. Figure 1.1 shows the publications related to MFCs, in the 2010-2023 period. It is observed that over time, the research in these devices has increased.

MFCs take advantage of the bioelectrochemical activity of microorganisms at the bioanode to oxidize the organic matter of a substrate (for example, wastewater) with minimum environmental pollution. Due to those reactions, electrons are generated, producing electrical energy [36]. Therefore, some workers consider the substrate as the fuel of the MFC [11]. The MFC technology has faced different challenges that limit its power: the system architecture, the type of materials used for the electrodes, the microbial community, the electrode arrangement, and the protonic exchange membrane [37, 38, 39].
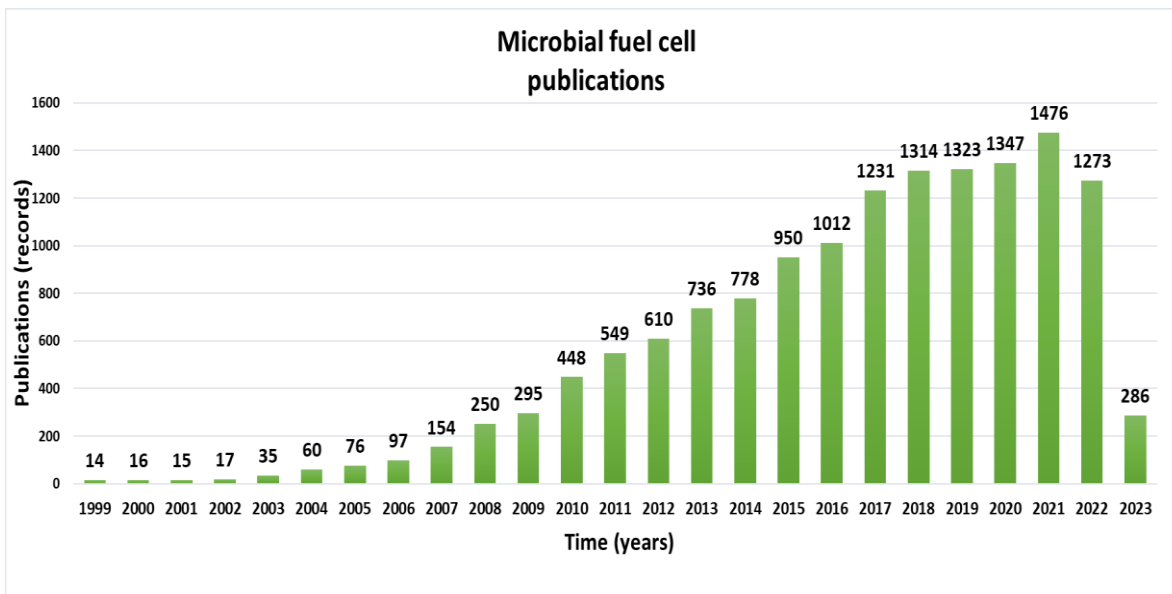
Figure 1.1 Quantitative analysis of the scientific literature on microbial fuel cells (Source: ISI WEB OF SCIENCE, April 2023).

Different configurations of MFCs that have been proposed and developed over the years. MFCs can be divided into single-chamber and dual-chamber cells [40]. A dual-chamber MFC consists of anodic and cathodic compartments in an H-type form, separated by an ion-exchange membrane (Figure 1.2). The membrane acts as an electrolyte, between the anodic and cathodic chambers. The membrane must have a high ionic conductivity, along with excellent mechanical properties.

Proton exchange membranes (PEM) are frequently used in MFCs [40], because of their high proton conductivity and chemical and thermal stability [41, 42, 43]. As an example, Nafion® is a commercially available polymer widely used in MFCs [44]. Notably, MFCs can produce power without a separating material, but the efficiency would be reduced [45].

Some research has focused on the bioanode, where electron transfer is promoted. Despite the progress, there is still plenty of room for improving the overall performance of MFCs through anode manipulation. There are generally two ways to improve the performance of bioanodes: i) selecting suitable bacteria for better bioelectrochemical catalysis, and ii) improving the electron transfer between bacteria and the anode surface [45].
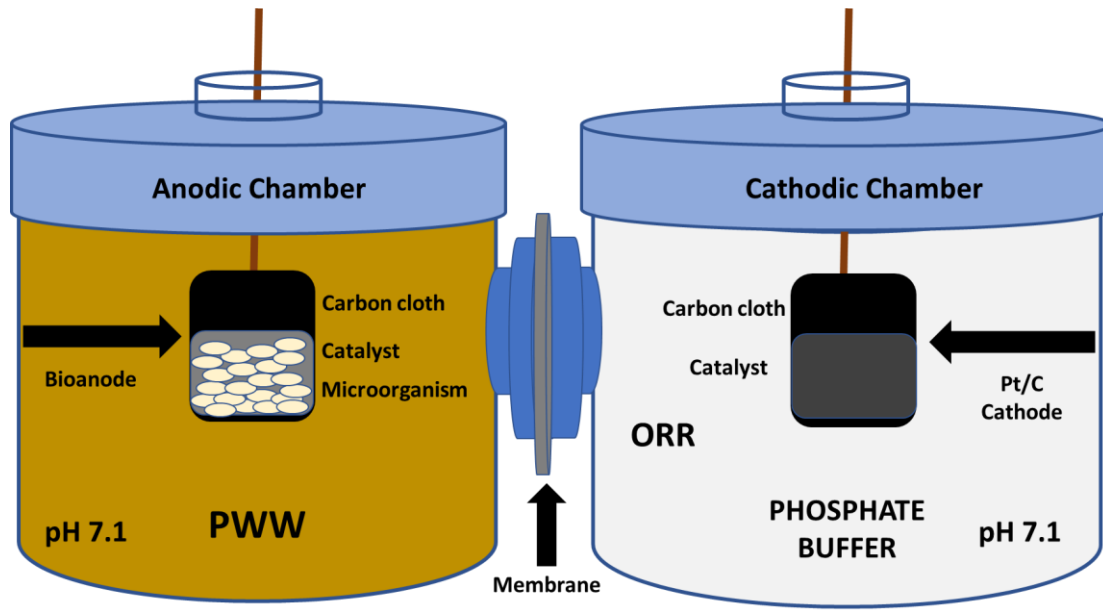
Figure 1.2 Scheme of a dual-chamber MFC.

The potential benefits of the MFC, from a technological point of view are not only related to energy generation but also with wastewater treatment [11]. Moreover, the operational stability of the process offers advantages, along with the continuous reproduction of the microorganisms and its good resistance to environmental stress [11].

The bioelectrochemical reactions in MFCs start when the microorganisms in the bioanode oxidize the organic matter in the substrate to produce electrons and ions. MFCs are attractive since Hendrick et al. have reported that municipal wastewater contains 9.3 times more energy than the energy needed for its treatment [46]. The electrons are transferred to the anode surface and through an external circuit to the cathode at the cathodic chamber (Figure 1.2). Meanwhile, the ions diffuse through the membrane to the cathodic chamber, and react with the electrons, promoting the oxygen reduction reaction (ORR) [45, 47, 48, 49].

Table 1.2 show some oxidation and reduction reactions in MFCs, utilizing different substrates, giving an approach to the reactions catalyzed by the microorganisms, the bioanode and the cathode [50].

Table 1.2. Oxidation and reduction reactions in MFCs.

ANODE OXIDATION REACTIONS (electron donors)

Acetate

$CH_3COO^- + 3H_2O \longrightarrow CO_2 + HCO_3^- + 8H + 8e^-$

Glucose

$C_6H_{12}O_6 + 6H_2O \longrightarrow 6CO_2 + 24H+ + 24e^-$

Glycerol

$C_3H_8O_3 + 6H_2O \longrightarrow 3HCO_3^- + 17H+ + 14e^-$

Domestic wastewater

$C_{10}H_{19}O_3N + 18H_2O \longrightarrow 9CO_2 + NH_4^+ + HCO_3^- + 50H^+ + 50e^-$

CATHODE REDUCTION REACTIONS (electron acceptors)

Oxygen

$O_2 + 4H^+ + 4e^- \longrightarrow 2H_2O$

$O_2 + 2H^+ + 2e^- \longrightarrow H_2O_2$

Nitrate

$NO_3 + 2e^- + 2H^+ \longrightarrow NO_2 + H_2O$

$2NO_3^- + 12H^+ + 10e^- \longrightarrow N_2 + 6H_2O$

Ferric Ion

$Fe^{3+} + e^- + H^+ \longrightarrow Fe^{2+} + 1/2H_2O$

The complete oxidation of organic matter from the wastewater at the bioanode leads to the production of carbon dioxide, protons (in acid media), and electrons [51]. At the cathode, the reactions give water as one of the products. It has been reported that the products of these reactions may have a lower impact on climate change than other secondary byproducts like as methane; thus, pollution risk is decreased by implementing MFCs compared with other wastewater treatment technologies [50].

1.4 Carbon catalysts

The properties of the bioanode play an important role in the effectiveness of oxidation of organic matter and electron transfer. Materials used at the bioanode have been the subject of research, searching for novel catalysts and microorganisms that increase the efficiency of MFCs [49, 52, 53].

Several elements constitute the bioanode of MFCs: i) a support (for example, a gas diffusion carbon cloth), ii) a catalyst layer, and iii) a biofilm of the microorganism. As mentioned, some of the most performing bioanode catalysts are: i) activated carbon, ii) carbon felt, iii) activated carbon fiber felt, iv) graphite, v) graphite felt, and vi) tungsten carbide, among others [54]. Therefore, low-cost carbon-based catalysts that facilitate the microbial attachment and its extracellular matrix growth into a biofilm are preferable over noble metals. This type of configuration at the bioanode promotes the metabolism of organic matter in the substrate, and enhances the extracellular electron transfer EET, improving the performance of MFCs [54].

An appropriate anode catalyst for MFCs must be biocompatible with microorganisms. It needs to have textural properties to promote microbial attachment, allowing the development of an extracellular matrix resulting in a biofilm. Moreover, it must have a high catalytic activity to enhance the oxidation reaction. Additionally, it needs to exhibit high electric conductivity and chemical inertness [37].

Besides the carbons mentioned above, the use of Ordered Mesoporous Carbon (OMC) as catalysts in MFCs has been proposed [2]. Typically, the average pore diameter of OMC falls between 2 and 50 nm. OMC has mesoporous channels arranged in hexagonal, cubic, laminar, or worm-like structures, and a high specific surface area ($416.3 \ m^2 \ g^{-1}$) [38, 39, 55]. These characteristics make OMC appropriate for biofilm growth [56]. When used as bioanode catalyst in an MFCs, OMC has generated a higher current density than a Pt/C catalyst [2].

Even more, biocarbons from biomass have also been proposed as catalysts for bioanodes of MFCs. Typically, these materials possess textural (average pore size reported in the mesoporous range and specific surface area in some cases above $1300 \ m^2 \ g^{-1}$ [57, 58]), structural, and electrical properties which make them interesting for this application [59]. The use of biocarbon in MFCs may be beneficial for the environment because of their properties as adsorbent of contaminants in soil and water [59]. Therefore, biocarbon are a promising alternative to replace catalysts based on more expensive conventional nanostructured carbons such as graphene [60].

Another benefit of using biomass for the environment is producing add-value biocarbon from a cheap earth-abundant resource. For instance, in Mexico sewage sludge production from about 2.029 wastewater treatment plants, is about 640.000 to 10 million of tons per year [61]. Sewage sludge is a waste with high carbon content, and it can be used to obtain biocarbon via pyrolysis for electrode materials in different electrochemical applications, e.g., for supercapacitors, oxygen reduction electrocatalysts, or in lithium-ion batteries application [62].

A recent work shows that a biocarbon from sewage sludge has the following characteristics, the presence of 10 chemical elements as C, O, and heteroatoms as Mg, Ca, Al, Fe, Si, S, and P. After the heat treatment, the Si increased by about 8 % compared to the biosolid. The textural properties in this material, was the presence of mesoporous with a maximum diameter of 4.38 nm and a surface area of 412 m^2 g^{-1}, being 1.6 times larger than commercial Vulcan XC-72 [57].

Besides the advantageous intrinsic properties of carbon-based catalysts for MFCs applications, their surface and structural characteristics may be modified, aiming to enhance their biocompatibility with the EAM and the stability of the bioanode [63]. For instance, the thermal treatment of carbon mesh bioanode catalysts resulted in a 3% increase in the overall power density of an MFC. The treatment promoted a higher surface area of the catalyst, facilitating the adhesion and inoculation of the microorganisms. Carbon fiber brush anodes exhibit an increment in the power density up to 15% after heat treatment, compared to unmodified anodes [63].

Even more, the chemical surface modification with different methods like plasma and functionalization increases the hydrophilicity of the carbon catalysts, promoting the attachment and growth of the biofilm and, therefore, the electron transfer [64]. It has been reported that the surface treatment of carbon nanotubes (CNT) significantly affected the bacteria composition and distribution in the biofilm, increasing the current density generated by a MFC [65].

1.5 Microorganisms

Microorganisms play critical roles in the anode chamber and generate electrons; a good selection of microorganisms may improve the MFC performance [66]. One of the most important limitation in the performance of MFC is the slow electron transfer from the substrate to the external circuit. Such limitation is directly related to the microbial community diversity and abundance at the bioanode (biofilm) and its efficiency for extracellular electron transfer.

The biofilm formation is a continuous and sequential process, which includes the transport, attachment, microcolony formation, and maturation of the biofilm over the electrode surface in the MFC. The efficiency of the electroactive biofilm depends on three parameters as i) system design, ii) operation and iii) biological process made from the microorganism [67].

Bacteria adhesion is influenced mainly by long-range forces (e.g. hydrophilic, electrostatic, and Van Der Waals interactions) and short-range forces such as hydrogen bonding. Hydrophilic surfaces make the surfaces more approachable for the planktonic bacteria because of hydrophilic interaction and can potentially form hydrogen bonds that adhere bacteria to the electrode surface. The surface modification of the carbonaceous anodes can be used to improve MFC performance [65].

Different types of microorganisms (including bacteria, archaea, and fungus) that have proven to be active in MFC. A community of microorganisms in a biofilm is ideally a synergetic community, where each species has a specific role to play in the "ecosystem nutrient cycle". For example, some of them digest nutrients, while others contribute to defending the biofilm against harmful environmental conditions [68].

The electron transfer mechanism has been reported to proceed directly via cytochrome C membrane proteins or nanowires, through active-redox metabolization. Both routes may guide the development and selection of effective microorganisms to improve the power output of an MFC [36].

Some examples of bacteria genera used in the MFC include *Shewanella sp. Pseudomonas sp., Geobacter sp.* and *S. putrefaciens*, the last one is a gram-negative

facultative anaerobic bacterium with the ability to metabolically reduce iron and manganese [69]. *P.aureginosa* is also a gram-negative aerobic bacteria. Rabaey and Verstraete [64] demonstrated that these bacteria produce chemical mediators, such as pyocyanin, that can serve as an electron shuttle for charge transfer into the electrode, producing a high current density in the MFC. *Geobacter sp.*, is an anaerobic bacterium capable of oxidizing organic compounds, metals and petroleum compounds. This last one is the most widely studied for MFC applications [12].

A microorganism that has been less studied, but its characteristics make it interesting for use in MFC, is *Bacillus sp.*, gram-positive aerobic facultative bacterium. *B. subtilis* is one of the most used hosts in fermentation production because it is simple to cultivate, and its products (proteins and metabolites) are often secreted in the growth medium [13].

These bacteria have been applied in some phenolic compound degradation studies [70]. Equally, *B. subtilis* has been used for chlorophenols degradation and electricity generation while degrading organic compounds in the MFC. In the literature, it has been demonstrated that the bacteria biofilm generated long-term power output. The *in situ* voltammogram of the bacterial growth phase showed that the electrochemical activity was mainly due to excreted redox mediators [13].

An important characteristic of *B. subtilis* is the ability to biodegrade cephalexin in treated sewage effluents and it is multi-resistant to antibiotics due to the potential to produce β-lactamase, which is a mechanism used by many bacteria to protect itself from the action of β-lactam antibiotics. When these bacteria are utilized in treated sewage effluents medium, conduce to the biodegradation of β-lactam antibiotics, including amoxicillin and penicillin [71]. The above-mentioned biological properties make it a potential microorganism for MFC on pharmaceutical sewage effluents.

1.6 Electron-transfer mechanisms

The microorganisms that are capable of transferring electrons in the anodic chamber, in the literature, have been called with different names, as examples are included: anodophiles, electricigens, exoelectrogens, electrogenic microorganisms, anode-

respiring bacteria, and as it was mentioned before, electrochemically active bacteria (EAB). These terms describe microorganisms capable to conserve energy to support its growth by completely oxidizing the organic compounds present in the substrate to carbon dioxide with direct electron transfer to the anode [72].

Electricigens microorganisms, such as *G.sulfurreducencs*, are already studied at the gene level, in which the complete genome sequence has been obtained, to understand and describe how the bacteria transfer electrons to the anode. Three mainly mechanisms for electron-transfer are explained in Figure 1.3: i) c-type cytochromes; ii) electrochemical mediators; and iii) conductive pili. These mechanisms are present in many microorganisms as *B. subtilis*, which can occur simultaneously, enhancing the electron transference from the bacteria to the electrode [72].
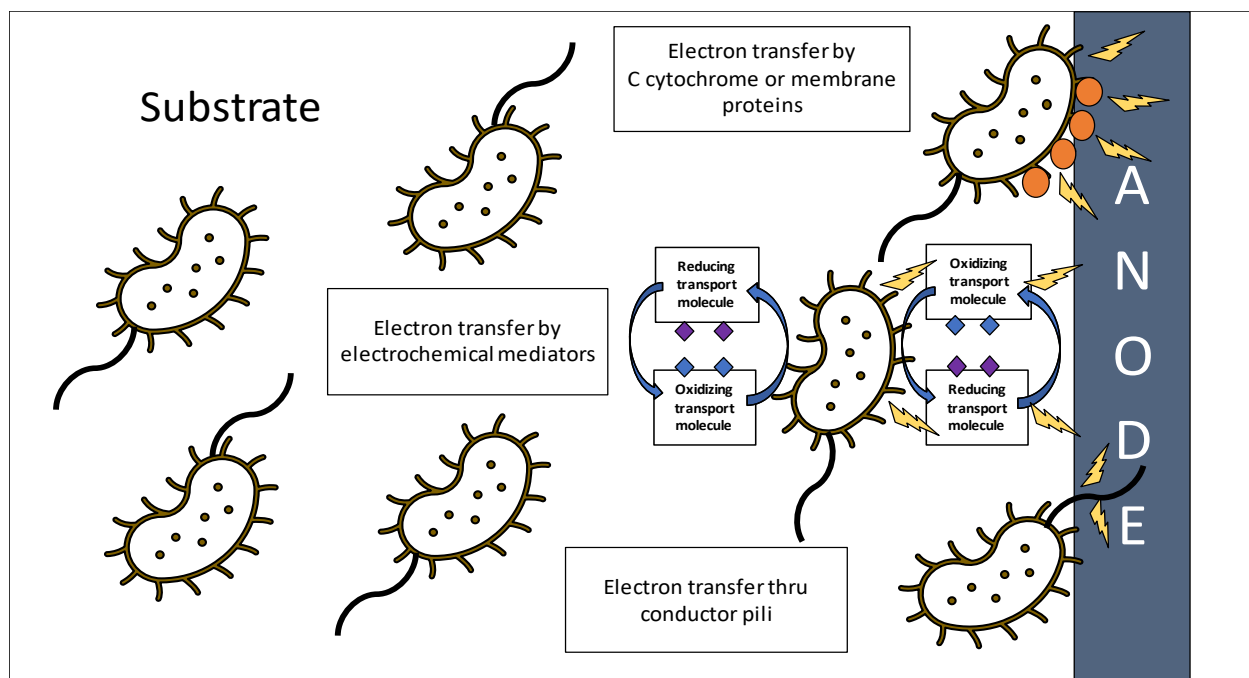
Figure 1.3 Electron-transfer mechanisms

These electron transfer mechanisms can also be classified as direct electron transfer (DET) and mediated electron transfer (MET). The DET occurs via a direct physical contact between the microbial cell wall and the anode surface or via pili that links the two. Gene

expression studies and electrochemical analysis demonstrated that there are active sites for cytochrome proteins on the outer cell surface. When the bacteria contact the anode surface, the cytochromes can transfer electrons from inside of the microbial cell wall to the outer well wall and then to the anode surface. One disadvantage is that only a monolayer of sessile cells in a biofilm participates in the transfer. This may explain why the power and current densities of MFCs are low sometimes since the MET can utilize more than one monolayer [73].

Lately, some researchers have observed that some microorganisms as *S. oneidensis* and *G. sulfurreducens*, can produce conductive pili, forming physical conductive connections between the cell wall at a short distance from the anode. An extensive pilus network allows several layers of sessile cells to donate electrons to the anode, thus multiplying the MFC power output. It has been recently discovered that filamentous bacteria in marine sediments, are capable of transferring electrons over centimeter-long distances via conductive filaments which are 200 nm or more in diameter, indicating that the DET could occur in contact with the electrode and via a pili or conductive filament linkage [73, 74].

In an MFC, the EET has been primarily studied in microorganisms that transfer electrons to insoluble Fe (III) or Mn (IV) oxides or to humic substances too large to enter through cells. The bacterial yield depends on the potential difference between the electron donor and acceptor, translating into the energy available for the bacteria. The potential difference between donor and acceptor is calculated with the Nernst equation and is directly proportional to the amount of oxidized and reduced compounds [64, 75].

In the chambers of an MFC, the potential of the electron donor and acceptor are defined by the anode and cathode potentials, respectively. Nonetheless, the microorganism did not always take advantage of the actual potential of the electron donor at MFC bioanodes, because of the losses occurring between bacteria and electrodes. These losses are identified as activation and ohmic polarizations [75].

The electrochemical reactions at the electrode surface must surmount activation energy for the electron transfer either from the electron donor at the anode or from the electron acceptor at the cathode. Energy losses result from the formation of the anode-biofilm, due to the unique environment created by the microorganisms. These losses can be explained

in the first place, by the microbial metabolism, in which bacteria must capture energy from the potential difference between their electron donor and the terminal electron carrier to support their growth and maintenance. In the second place, the biofilm formed consumes energy [76].

1.7 Bioelectrochemical Phenomena at the Anodic Chamber

As it was mentioned, oxidation reactions occur in the anodic chamber of an MFC, where microorganisms act analogous to a catalyst, interacting with the anode electrode through direct and indirect processes producing output current. However, some energy from the process must be self-used by the microorganism for survival and growth, being considered a loss [72].

MFCs are complex systems in which bioelectrochemical reactions and mass transfer occur in the anodic chamber. To comprehend the interactions between the anode electrode and the biofilm by the bacteria, research groups have focused on understanding the biochemical and bioelectrochemical phenomena in the cells. Studies using synthetic substrates or modeling the microbial consortia, are being used for this objective. Reaching a deeper understanding of such phenomena will help to improve the performance of MFCs and the possibility of scaling them up [77].

Electrochemistry refers to the use of electricity to drive a chemical reaction or produce electricity from chemical reactions. Redox reactions are involved in electron transfer from one species to another. When species are oxidized, it means there is a loss of electrons, while when reduced, there is a gain of electrons. If one species takes electrons from another and becomes reduced, is called the oxidizing agent or oxidant. Opposite, when it transfers electrons to another species becoming oxidized, it is called the reducing agent or reductant [78].

Utilizing these concepts may help in understanding the relevance of MFCs components. For instance, the organic compounds contained in the substrate are oxidized by the oxidizing agent (i.e., the EAM) through the different metabolism chains inside its cell, transferring electrons to the bioanode.

Rabaey, K., *et al* (2007), suggest the importance to widespread the information about the interactions between bacteria and anodes and how the electron transfer mechanisms occur. In Figure 1.4, the metabolic diversity of microorganisms is shown, indicating how bacteria transform the organic compounds contained in a substrate in different metabolic pathways. Among them, some microorganisms partially oxidize the substrates using fermentation pathways. At the same time, those exoelectrogenic take advantage of side products from the first group of fermentative bacteria over the anode, resulting in a total oxidation of the complex organic compounds, while electrons are transferred [75].
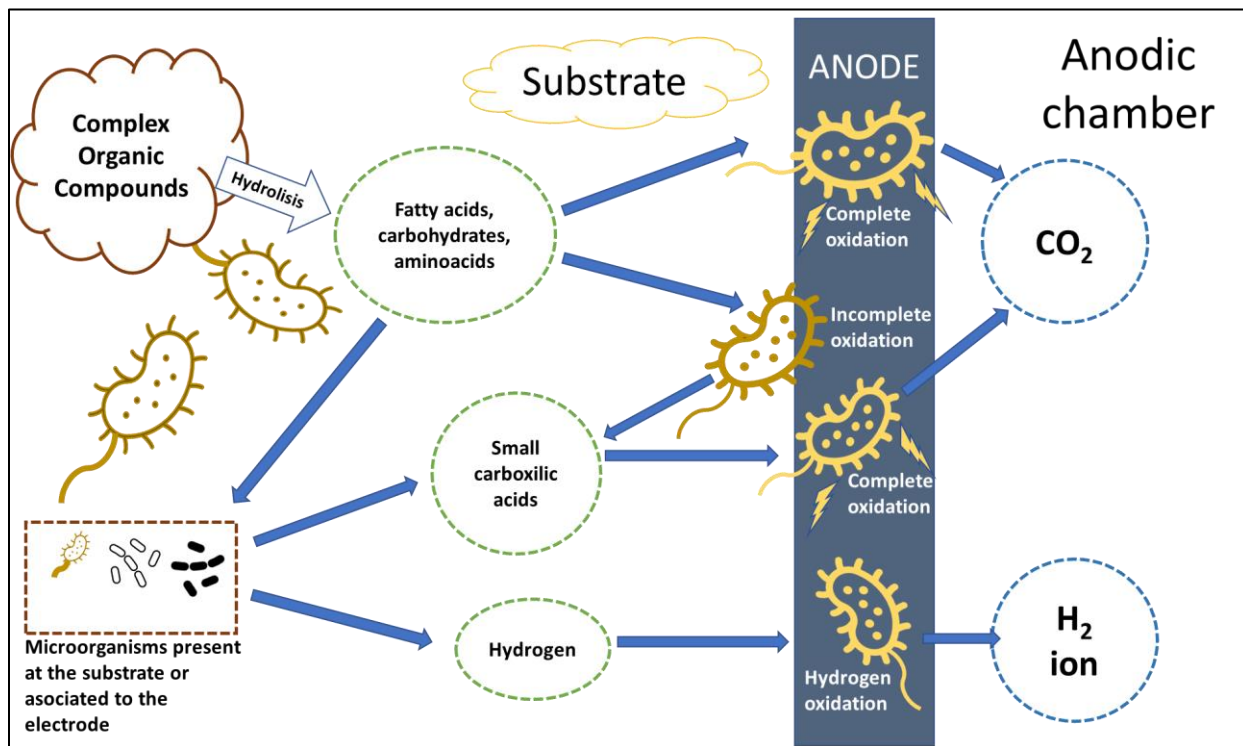
Figure 1.4 Metabolic substrate transformation of substrate by different microorganisms

A manner to explain the bioelectrochemical reactions occurring in the MFC involves the cell metabolism, in which the aerobic heterotrophic bacteria harvest energy by transferring electrons generated from their respiration to terminal oxygen electron acceptors. The nicotinamide adenine dinucleotide (NAD^+) is involved in the redox reactions

(NAD+/NADH), delivering electrons from to another reaction. An important issue is that NAD+ is an oxidizing agent (accepting electrons) and becomes reduced, forming NADH. In anaerobic conditions (no terminal oxygen electron acceptors), the re-oxidation of NADH to NAD+ can occur when alternative electron acceptors are present (solid electrodes in MFC) [79].

Without the terminal electron acceptors, bacteria promote fermentation under anaerobic conditions to drive the re-oxidation of NADH, but the energy output is substantially lower than respiration. In the anaerobic conditions of anolytes in MFC, the solid anode acts as a terminal electron acceptor allowing respiration and re-oxidation of NADH to NAD+. Nonetheless, the degradation of organic matter in wastewater can be achieved in anaerobic conditions [79].

1.8 Substrates and Wastewater

A substrate can act as carbon and energy source, being important for most biological processes. In the case of MFCs, the efficiency and economic viability of converting organic wastes into bioenergy depend on the physicochemical characteristics and the nature of the compounds at the substrate. The chemical composition and the concentration can be converted into products or fuels, and the last ones have a major interest because of their potential in bioelectrochemical systems (BES) [80].

Pant *et al.* [80], mentioned that the substrate influences not only the composition of the bacterial community at the anode biofilm, but it also influences the performance of an MFC in terms of power density and Coulombic efficiency. Many substrates can be used in MFC for electricity production ranging from pure compounds to complex mixtures of organic matter in wastewater. Acetate and glucose are the substrates more utilized in MFC, because their simple chemical composition is extensively used as carbon sources [80].

The wastewater employed as substrate in MFCs can be of different sources and compositions. For instance, wastewater from brewery has a high quantity of organic matter and low concentration of inhibitory substances. Wastewater from the starch process shows a high content of carbohydrates, sugars, and proteins. Synthetic dyes from

the textile manufacturing industry are also used as substrates in MFCs, since the microorganisms can generate energy by oxidizing the dyes contained in the effluent [80].

Meanwhile, domestic wastewater contains organic matter like feces, fat, food scraps, detergents, and pharmaceuticals. This type of wastewater, in chemical terms, contains 300-600 g of carbon rich organic matter (also known as carbonaceous chemical oxygen demand or COD) in one cubic meter, 40-60 g of nitrogen (e.g., ammonium and organic compounds), 5-10 g of phosphorus (e.g., phosphates and organic compounds), 10-20 g of sulfur (e.g., sulfate), and traces of heavy metal ions [81].

Wastewater treatment aims to produce relatively clean effluents that can be discharged for example into a surrounding river, preventing pollution. Conventional wastewater treatment plants are designed to remove dissolved organic matter, particles, and suspended colloids through multiple process units. Different effluent treatment processes are available, including biological, physical, and chemical processes, to remove organic and inorganic pollutants [82]. As a wastewater treatment example, there exist sewage treatment plants, which generally involve pretreatment, primary, secondary, and tertiary processes. The biological degradation of organic matter in wastewater consumes a large quantity of electricity continuously, because of the aerobic digestion of organic wastes [83, 79].

It should be mentioned that industrial effluents are among the most challenging substrates for MFCs, in particular pharmaceutical wastewater (PWW). PWW is typically composed of non-biodegradable organic matter such as animal and plant steroids, anti-inflammatory drugs, antibiotics, other prescription and non-prescription drugs, reproductive hormones, beta-lactamides, analgesic, lipid regulators, flame retardants, antidepressants, cytostatic agents, detergents metabolites, personal care products, and other extensively used chemicals and spent solvents [84].It also contains contaminants with low biodegradability and inhibitory compounds from conventional biological treatments [9]. This type of wastewater is characterized by its toxicity and high chemical oxygen demand (COD).

Hypothesis

The use of ordered mesoporous carbon (OMC) and biocarbon (BC) as catalysts of bioanodes will enhance the performance of B. subtilis for oxidize organic compounds contained in pharmaceutical wastewater (PWW), improving the kinetics of the bioelectrochemical reactions for energy production in an MFC.

Objectives

General

To study the behavior of bioanodes containing OMC and BC catalysts with a biofilm of *B. subtilis* by evaluating their electrochemical performance for the oxidation of organic matter present in PWW, for their possible use in MFCs.

Particular

- To demonstrate the feasibility of obtaining a BC from sewage sludge with suitable properties for MFCs applications.
- To evaluate the electrochemical behavior of OMC and BC in PWW forming bioanodes with B. subtilis as EAM in half-cell and MFCs set-ups.
- To evaluate the effect of functionalizing OMC and BC with methanol on their electrochemical behavior.
- To study the biocompatibility between the OMC and BC catalysts with *B. subtilis* in electrochemical testing with PWW as substrate.
- To characterize a MFC equipped with OMC + *B.subtilis* and BC + *B. subtilis* bioanodes operating with PWW at the anodic chamber.

2. Scientific Methodology

2.1 Development of catalysts for anodes and bioanodes

2.1.1 Synthesis of Ordered Mesoporous Carbon (OMC)

OMC was synthesized by a organic-organic self-assembly process. A mixture of resorcinol (8.8 g), formaldehyde (24 mL), and sodium carbonate (0.04 g, alkaline catalyzer) was stirred in a magnetic agitator for 1 h. Afterwards, a mixture containing Pluronic F127 triblock copolymer (6.2 g), water (16 mL), and ethanol (25 mL) was added maintaining stirring for 1 h. Pluronic F127 was used as the template to promote the formation of a hexagonal mesostructure. In the condensation stage, 8 mL of 2 M HCl were adjusted to the solution, which was submitted to vigorous agitation for 1 h.

The obtained resin was dried at 80°C for 24 h (Figure 2.1), then pyrolyzed at 900°C in N2 atmosphere in a tubular furnace (Thermo Scientific®, Thermolyne model) for 3 h at a heat rate of 1°C min^{-1}. The resulting solid was pulverized in a Fritsh® Pulverisette planetary mill for 10 min and sieved in a 100 mesh (Figure 2.2).
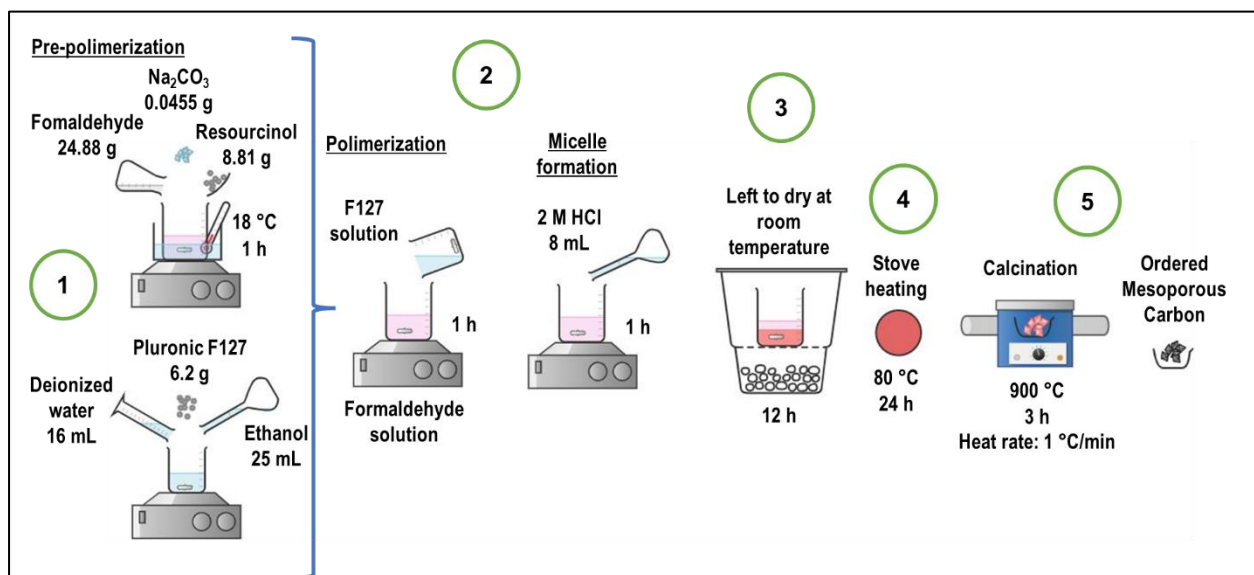
Figure 2.1 Diagram of the synthesis of OMC
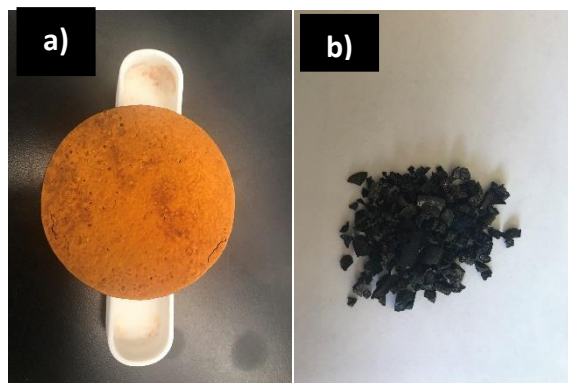
Figure 2.2 Images of a) pre-pyrolyzed powder and b) OMC after pyrolisis

2.1.2 Synthesis of biocarbon (BC) from sewage sludge

The biosludge (BS) utilized here was collected at Reciclagua (Sistema Ecológico de Regeneración de Aguas Residuales Industriales, S.A. de C.V.), in Lerma, State of México. This biosludge is originated by different sources, of which ca. 90% is produced mainly from the textile industry and the rest from households [85].

To obtain the BC, 120 g of BS were dried at 100°C for 72 h in a Thermo Scientific® Heratherm oven, pulverized in a mortar and pyrolyzed at 700°C in N_2 atmosphere for 90 min in the same tubular furnace indicated above. The obtained powder was mixed with KOH in a 1:2 weight ratio in a 20 mL water solution for its chemical activation. The mixture was left in the oven for 24 h, then pyrolyzed at 750°C in N_2 atmosphere for 90 min in a heating ramp of 8°C min^{-1}.

Afterwards, the material was washed with 1 M HCl and 100 mL of deionized water, dried at 100°C for 12 h, pulverized in the same planetary mill for 10 min, and sieved in a 250 mesh. The diagram of the synthesis of the BC is shown at Figure 2.3.
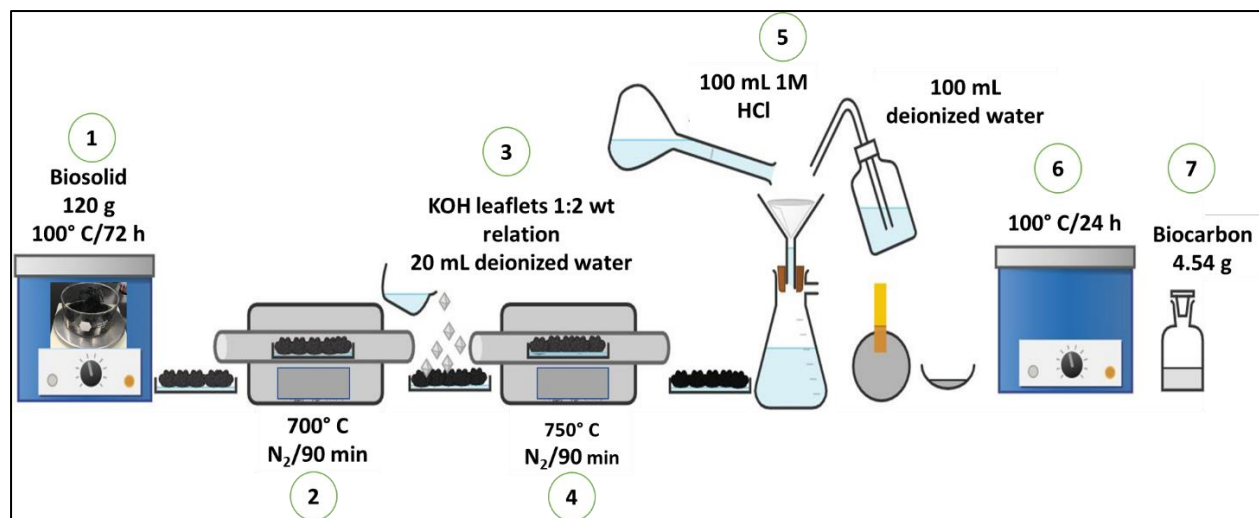
Figure 2.3 Diagram of the synthesis of BC.

2.1.3 Functionalization of the carbon catalysts

OMC and BC powders were functionalized by the intermittent microwave heating process. For this, 2 g of carbon samples were separately sonicated in 0.15, 0.5 and 1 mol L^{-1} methanol solutions graded to 200 mL with deionized water for 30 min, followed by stirring for 1 h. The mixtures were thermally treated in a microwave oven for 8 min applying 25 s on/15 s off pulses under agitation and refluxing conditions. The powders were filtered, washed, left to dried for 24 h and then calcined at 200ºC for 30 min in a Thermo Scientific® Thermolyne muffle. The functionalized OMC (or BC) catalysts were labeled as OMC015 (BC015), OMC05 (BC05) and OMC1 (BC1) after functionalization with 0.15, 0.5 and 1 M methanol, respectively. The diagram of the functionalization procedure is shown in figure 2.4.
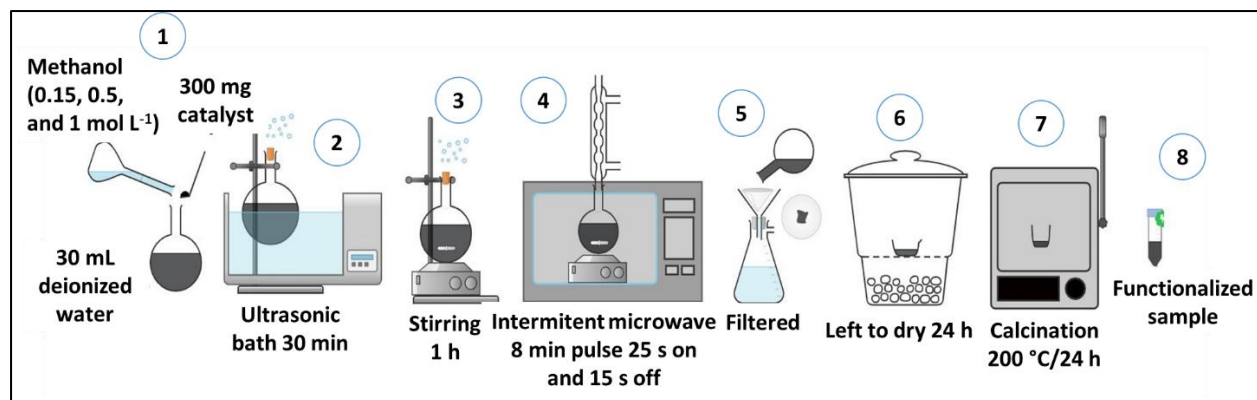
Figure 2.4 Diagram of the functionalization of the carbon catalysts with methanol at different concentrations.

2.2 Physicochemical characterization of the carbon materials

Chemical composition and morphology were determined utilizing an EDAX® Genesis Phillips Scanning Electron Microscope (SEM), equipped with an Energy Dispersive Spectroscopy (EDS) detector, under an accelerating voltage of 20 kV. Chemical mapping was performed in a 7800 F Jeol Field Emission Scanning Electron Microscope (FESEM) equipped with a Quantax EDS detector.

CHNS characterization was carried out in a Flash 2000 Thermo Scientific elemental analyzer, reporting here the average wt. % of carbon, hydrogen, nitrogen, and sulfur from 3 measurements. High Resolution Transmission Electron Microscopy (HRTEM) analysis was implemented to analyze the morphology of the samples using a Talos 200 FEI® apparatus. The textural properties were characterized by N_2 adsorption/desorption analysis in a Autosorb1 Quantachrome Automated Gas Sorption System apparatus, Version 1.16 for OMC and Version 11.03 for BC. The surface area of the carbon samples was obtained using the Brunauer–Emmett–Teller (BET) methodology.

 X-Ray Diffraction (XRD) patterns were obtained in an Empyrean PANalytical equipment in a of 7-100 (2 theta) sweep, with 0.026 space and 30 s permanence. Fourier Transform Infrared Spectroscopy (FT-IR) spectra were acquired using a Tensor II Bruker spectrometer in the 4000-500 cm^{-1} interval using the ATR technique. The experimental spectra were evaluated using de MATCH software.

Raman spectra were acquired in a DXR2 Thermo Scientific spectrometer at a wavelength of 633 nm, in the 100 to 3500 cm^{-1} range. The surface chemical composition was determined by X-Ray Photoelectron Spectrometry (XPS) with a K-Alpha Thermo Scientific Spectrometer using an Al Kα monochromatic X-ray source (1486.68 eV). The analysis conditions for the high-resolution regions were energy pass of 50 eV, dwell time of 50 mS, 90° of "take-off angle" with 0.1 eV pass.

2.3 Sampling and conservation of pharmaceutical wastewater (PWW).

PWW was collected following the sampling design as by composite sample technique, in which: each 30 min, 1 L plastic bottles were filled out at the factory effluent, reaching a total volume of 14 L that was homogeneously mixed, stored, and transported in a cooler to avoid chemical or physical changes that could alter its composition. The PWW was characterized taking 7 aleatory samples by triplicate to determine its temperature, pH, specific conductance, turbidity, oxidation and reduction potential, using an Orion Star A211 Thermo Scientific potentiometer and an Orion Star A222 Thermo Scientific conductometer. It was stored at -20 ºC to avoid microbial growth and to keep the water sample in adequate state until its use [86].

2.4 Inoculum

The microbial strain B. subtilis (CDBB 1349), provided by the Colección Nacional de Cepas Microbianas y Cultivos Celulares of the Centro de Investigación y de Estudios Avanzados del Instituto Politécnico Nacional, was the microorganism studied in this work.

Petri dishes containing approximately 15 mL of LB agar (SigmaAldrich®) were sterilized in an All-American® sterilizer. *B.subtilis* was inoculated by placing the Petri dishes in an INO VICHI incubator for 72 h at a controlled temperature of 28 °C. Afterwards, culture media with grown bacteria was separated in test tubes with 10 mL of LB agar and cooled at -4 °C for its later use.

2.5 Fabrication of anodes and bioanodes

The anodes were composed of a gas diffusion electrode and a catalyst layer of the OMC and BC series of catalysts. Their fabrication was as follows: carbon cloths (ELAT LT-1200W, BASF) were cut into pieces, to which back face a copper wire was fixed to assure electrical contact. A 1 cm^2 geometric area was exposed, while the rest of the electrode surface was covered by epoxy. Catalytic inks were prepared by ultrasonically mixing for 30 min powders of the different catalysts with Nafion® solution (5 wt. %, Sigma-Aldrich) and 2-propanol (J.T. Baker) in a 3.5:1:1 ratio (wt. %). Then, 5 mg cm^{-2} of the carbonaceous catalyst were deposited on the exposed area of the electrode using a 20 µL micropipette (Socorex, Acura 825), forming the catalyst layer.

The bioanodes were composed of anodes containing a biofilm of *B. subtilis*. For their fabrication, anodes were placed in flasks containing 100 mL of sterile nutritive broth, inoculated with 2 mL of bacteria inoculum. The flasks were left in the orbital incubator for six days at 28 °C, allowing the biofilm to grow over the electrode surface, forming the bioanode. All the processes were performed in clean and sterilized atmosphere.

2.6 Bioanodes characterization by SEM

The morphology of the bioanodes was characterized in an XL30 Philips SEM apparatus at 10 kV acceleration voltage. The biological material was fixed in samples of bioanodes cut into small pieces using Tromps solution (4 mL of 25% grade I glutaraldehyde, 10 mL of 37% formaldehyde, 1 g of anhydrous monobasic sodium phosphate, 0.27 g of sodium hydroxide) in 1 mL Eppendorf tubes, then refrigerated for 24 h. The samples were dehydrated by passing them subsequently in 40%, 50%, 60%, 70%, 80%, 90%, and twice in 100% (v/v) ethanol solutions, for 30 min each (Figure 2.5), then left to dry in a desiccator for 24 h.

Figure 2.5 Photograph showing samples of bioanodes submitted to dehydration in ethanol solutions.

2.7 Electrochemical characterization of anodes and bioanodes in half cell

The catalytic activity of the OMC and BC series of catalysts was characterized in an electrochemical half-cell using a VSP-300 BioLogic SAS bipotentiostat. The cell consisted of a three-electrode arrangement: an Ag/AgCl reference electrode (in saturated NaCl 3M, standard potential: 0.209 V), a Pt wire counter electrode, and the working electrode. i.e, anodes and bioanodes described in the previous section.

Cyclic voltammograms (CVs) were acquired in the 50 - 1200 mV potential interval in the Reversible Hydrogen Electrode (RHE) scale. Conversion from the Ag/AgCl to the RHE scale was made with the Nernst equation:

$$E_{RHE} = E^0 + 0.059\,(pH) + E_{Ag/AgCl} \tag{1}$$

where:

E_{RHE}= Potential in the Reversible Hydrogen Electrode scale

E^o= Standard potential of the Ag/AgCl electrode

$E_{Ag/AgCl}$= Potential measured with the Ag/AgCl electrode (0.209 V)

pH= pH of the electrolyte

0.059= constant obtained from $\frac{RT}{nF}$ in which R is the constant of gases (8.31 J mol^{-1}), T is the Absolut temperature in °K (298 °K), n is the transferred electrons (1) and F is the Faraday constant (96,406 J V^{-1})

First, the anodes and bioanodes were activated by obtaining 40 CVs at 50 mV s^{-1}, resulting in reproducible voltammograms. Then, 3 CVs were acquired at 20 mV s^{-1} of which the third one was reported in this work.

2.8 Characterization in Microbial Fuel Cell (MFC)

The bioanodes showing enhanced electrochemical behavior in half cell were evaluated in the MFC. Thus, OMC + *B. subtilis*, OMC015 + *B. subtilis*, BC + *B. subtilis*, and BC015 + *B. subtilis* were evaluated in the dual-chamber MFC connected to the already mentioned bipotentiostat. The cathode was an electrode containing the commercial Pt/C nanocatalyst (where C= Vulcan XC-72), with a 20:80 Pt:C wt. ratio. The bioanodes were placed in the anodic chamber, at which 200 mL of PWW where adjusted. Meanwhile, the cathode chamber contained 200 mL of phosphate buffer (8.06 g NaCl, 0.22 g KCl, 1.15 g Na$_2$HPO$_4$, 0.20 g KH$_2$PO$_4$, gauge to 1000 mL with distilled water), with pH= 7.1, saturated with O$_2$ (Figure 2.6).
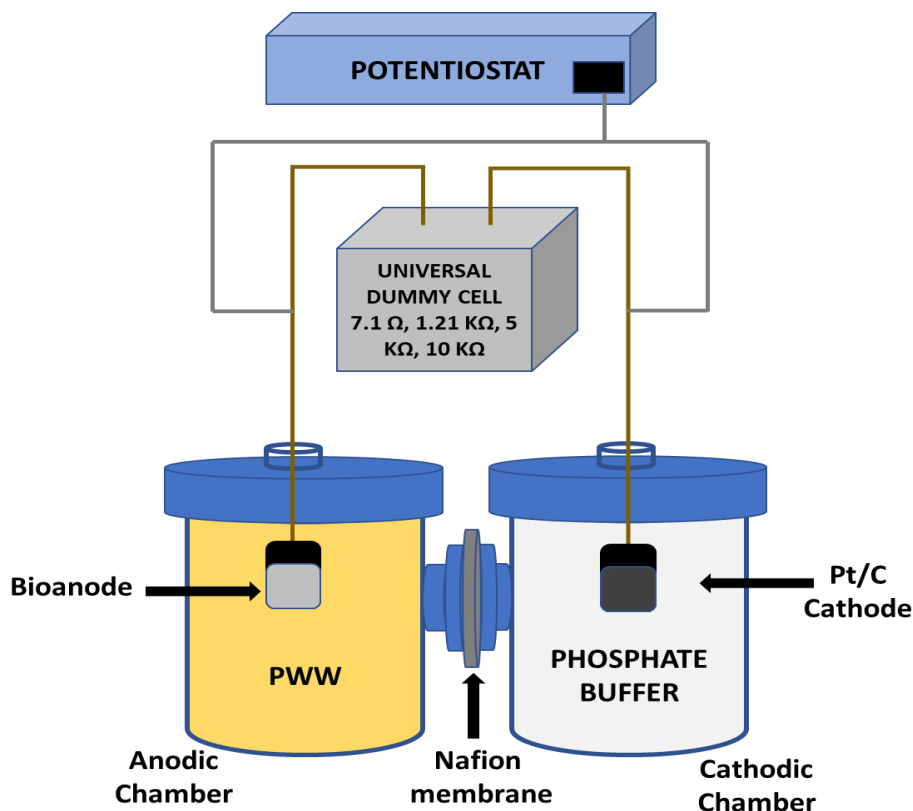
Figure 2.6 Scheme of the dual-chamber MFC.

2.8.1 Nafion membrane activation

Nafion samples having 25 cm^2 geometrical area were activated prior to their test in the MFC. Samples of the polymer were immersed in 10% v/v H_2O_2 for 1 h at 60 °C, washed with boiling deionized water for 30 s, placed in 0.5 M H_2SO_4 at 85 °C for 1 h, and washed with boiling deionized water for 5 min. The activated membranes already were stored in deionized water for their later use.

2.8.2 Electrochemical impedance spectroscopy (EIS) of the bioanodes

EIS is a sensitive, non-destructive, and powerful technique, that can provide information that helps understanding interface phenomena, such as charge transfer resistance, solution resistance, capacitance, and inductance [87]. EIS spectra of some bioanodes were obtained by implementing a three-electrode arrangement in the MFC in a frequency range between 10 kHz and 1 mHz, in a bipotentiostat BioLogic SAS, VSP-300, with an amplitude of 10 mV at Day 0, before obtaining the polarization curves described in the following section. For this purpose, the working electrode was the corresponding bioanode, the Ag/AgCl reference electrode was placed in the anodic chamber, while the cathode acted as counter electrode. The Nyquist plots obtained were fitted with the EC lab software by implementing an equivalent circuit (see Chapter 3).

2.8.3 Polarization and power density curves of the MFC

The cell voltage (E_{cell}) vs current density (j) polarization curves were obtained using the bipotentiostat and a set of external resistances (Figure 2.7 a). First, the open circuit voltage (OCV) of the cell was measured. Then, external resistances (R_{ext}) of 0.0071, 1.21, 5, and 10 kΩ were applied to measure E_{cell} and from such values, the cell current (I_{cell}) from Ohm's law (eq 2) was determined. The j values were obtained by normalizing I_{cell} by the geometric area of the electrodes (A_{geo}), as shown in eq 3. Meanwhile, the cell power density (P_{cell}) was obtained with eq. 4 and used to plot P_{cell} vs j curves:

$$I_{cell} = {E_{cell}}/{R_{ext}} \qquad (2)$$

$$j = {I_{cell}}/{A_{geo}} \qquad (3)$$

$$P_{cell} = E_{cell} * j \qquad (4)$$
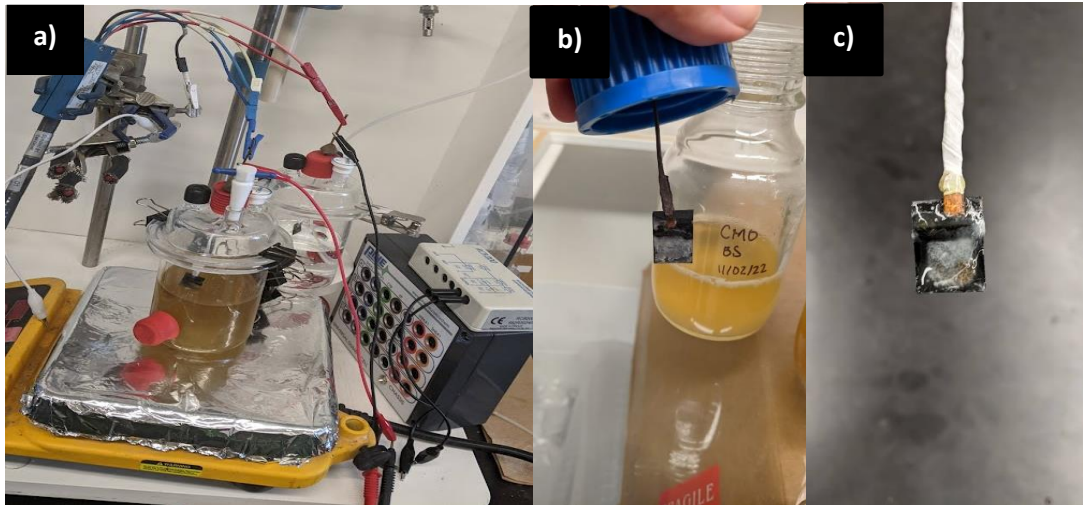
Figure 2.7 Photographs of a) the dual-chamber MFC set-up and b-c) details of bioanodes showing the whitish *B. subtilis* biofilm.

E_{cell} vs j and P_{cell} vs j curves were acquired at Days O, 3, and 7 of operation of the MFC.

2.9 PWW characterization

2.9.1 Determination of settleable solids in PWW

For the determination of settleable solids in PWW, three aleatory samples of 1 L were adjusted into Imhoff cones. After 10 min, the sediments were measured with the scale. Subsequently, the solids attached to the walls of the cone after 45 min, were detached from the vessel wall using a glass rod, allowing for sedimentation for 15 min. The sediments were measured using the scale after 60 min of initiated the determination (Figure 2.8).

The results were expressed in mL of settleable solids/L of the samples at 10 and 60 min. The lower measurable limit of this methodology has been reported in the range of 0.1 to 1 mL/L [88].

Figure 2.8 Imhoff cones with PWW for the measurement of settleable solids.

2.9.2 Chemical Oxygen Demand (COD) measurements

The values of COD were obtained using the spectrophotometric method, reported in the Standard Methods for the Examination of Water and Wastewater [89]. The standard establishes that the COD is the measured oxygen equivalent to the organic matter which is susceptible to be oxidized by a strong chemical oxidant, in specific conditions of temperature and time. In this method, a sample is oxidized by a known quantity of potassium dichromate ($K_2Cr_2O_7$) in excess and is expressed as equivalent of oxygen as: eq.m. of $Cr_2O_7^{-2}$ = 8 mg of O_2. The residual potassium dichromate is determined using a spectrophotometer at 600 nm.

The preparation of the solutions used were as follows [88]:

Digestion solution: A mixture of 500 mL of distilled water and 10.216 g of $K_2Cr_2O_7$ previously dried at 103 °C for 2 h was adjusted to a volumetric flask, followed by the addition of 167 mL of concentrated H_2SO_4 and 33.3 g of mercuric sulfate ($HgSO_4$). The mixture was dispersed with continuous agitation and left to cool down to room temperature. Finally, it was gauged to 1000 mL of distilled water.

Sulfuric acid solution: Argentum sulfate (Ag_2SO_4) was added to a solution of concentrated H_2SO_4 in a 5.5 g / 1 kg of H_2SO_4 ratio. The dissolved mixture was left to cool dawn to room temperature previous for its use.

Potassium hydrogen phthalate (KHP) solution. Calibration curve for 2000 mg O_2/L: The KHP reagent was dried at 120°C for 1 h. Then, 1.7 g of dried KHP was diluted in 1000 mL of distilled water and kept in refrigeration at 4 °C in a volumetric flask until its use.

Calibration curve

3   Six 15 mL test tubes were used to obtain the calibration curve, which was used to evaluate the digestion of 1, 2, 3, 4, 5, and 10 mL of KHP solution gauged to 10 mL with distilled water. These concentrations correspond to 200, 400, 600, 800, 1000, and 2000 mg O_2/L.

4   The reagent blank was prepared with 2 mL of distilled water in a test tube.

5   1.3 mL of digestion solution and 2.6 mL of H_2SO_4 solution were added to each test tube having 2 mL of KHP dissolution.

6   The test tubes were capped, vigorously agitated, and placed in a metallic rack that was introduced in a Heratherm ThermoScientific oven to be treated at 150°C for 2 h. The tubes were left to cool down to room temperature and the digestions were transferred to the cells of a Jenway 7305 Spectrophotometer (Figure 2.9)

7   The dissolutions were allowed for the solids to sediment before taking the data of absorbance at 600 nm.

8   The data of absorbance was plotted versus mg O_2/L, and the best curve was traced using lineal regression in Excel.
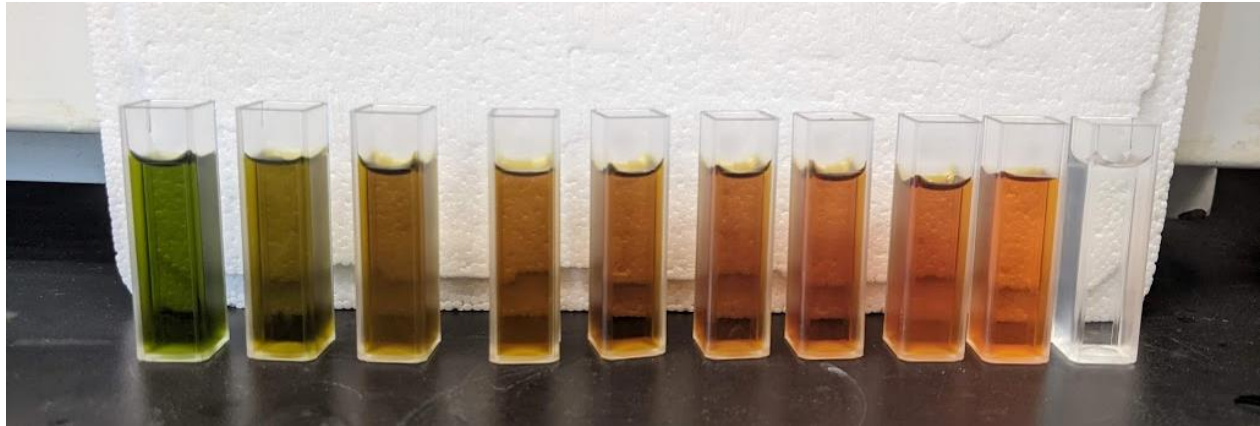
Figure 2.9 Photograph of cells for the determination of calibration curve of COD measurements

Determination of COD of PWW samples.

The determination was done, sampling 2 mL of PWW at Day 0, Day 3, and Day 7, during the MFC experiment. The samples due its nature were diluted 1:10 with distilled water, 2 mL of each dissolution were processed following the steps from numerals 2.9.2.1 a) to e). The measurements were done by triplicate as it can be observed in Figure 2.10.
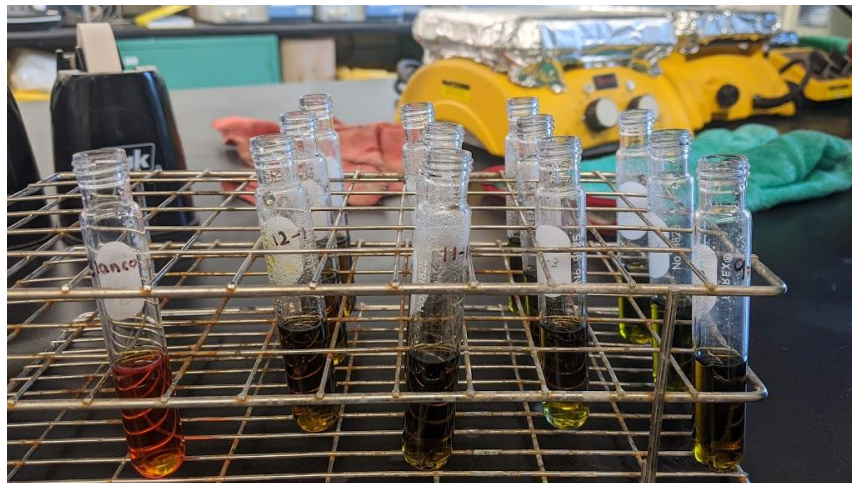
Figure 2.10 Image of digestions of PWW samples

Calculations for results of COD

For the COD calculation, the least squares method was applied to the calibration curves of samples of PWW used in the MFC, as proposed in the Mexican NMX-AA-030-SCFI-2001 norm [90], The calibration curves were adjusted to the best straight. A model was obtained to correlate the adjustment with the COD concentration after digestion. The equations utilized to calibrate the curves were [90]:

$$y = mx + b \qquad\qquad (5)$$

$$A = mc + b \qquad\qquad (6)$$

where:

y= variable dependent on the equation

x= variable dependent on the equation

A= Absorbance

m= slope of the curve

c= concentration

b= origin at the ordinate

The results were expressed in mg O_2/L.

3. Results and Discussion of OMC

3.1 Physicochemical characterization of OMC

3.1.1 XRD patterns of the OMC

In Figure 3.1 depicts the XRD patterns of OMC, OMC015, OMC05, and OMC1. The catalysts show reflections at 22.5 and 43.6° (2θ), attributed to the (002) and (100) carbon planes (JCPDS 41-1487), characteristic of graphitic structures. The broad feature of the peaks indicates the amorphous nature of the OMC catalysts [91]. No significant differences can be observed between non-functionalized and functionalized OMC.
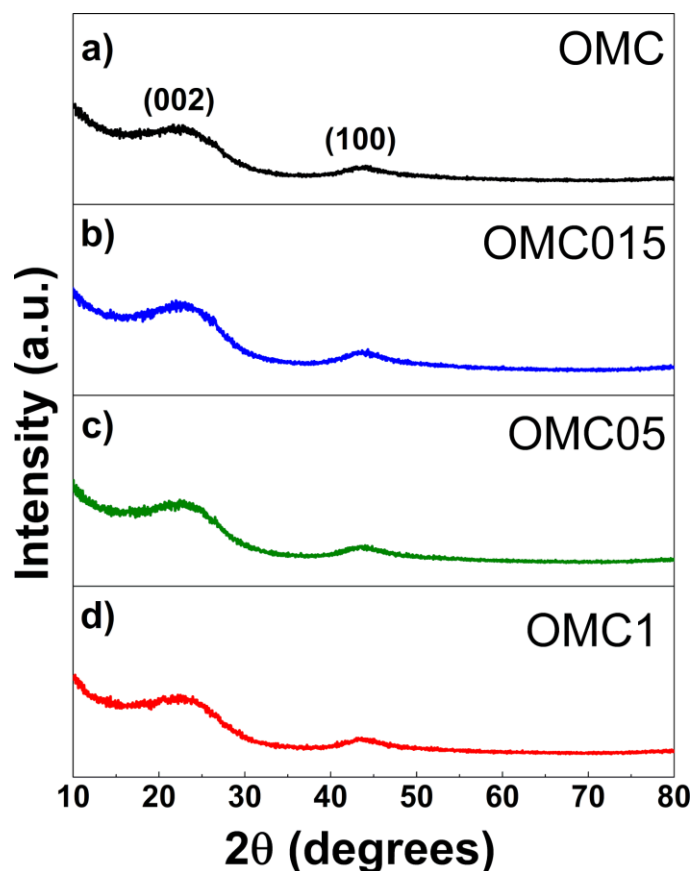
Figure 3.1 XRD patterns of a) OMC); b) OMC015; c) OMC05; d) OMC1.

3.1.1 Chemical composition by EDS.

The chemical composition and standard deviation of non-functionalized and functionalized OMC is shown in Table 3.1. The concentration of C and O at OMC is ca. 98.78 and 1.22 (wt. %), respectively. The IMH affects the chemical composition of the catalysts, because of the presence of MeOH during treatment and due to the fact that carbon materials are sensitive to microwave radiation [92]. With 0.15 M MeOH, the main influence is on the O content at the OMC015 catalyst since its concentration decreases. It is likely that the microwave heat treatment in the relatively low MeOH concentration causes removal of residual oxygen-containing species. At higher MeOH concentrations, the C content decreases at OMC05 and OMC1, reaching a minimum at the former. Conversely, the O content increases to 7.03 (wt. %) at OMC05 with a slight decrease at OMC1, apparently because of a surface saturation with oxygen-like species at higher MeOH concentrations.

Table 3.1 Chemical composition of the OMC catalysts by EDS.

Catalyst	Chemical Composition (wt. %)					
	C			O		
OMC	98.78	±	0.36¥	1.22	±	0.36
OMC015	99.89	±	0.24	0.11	±	0.24
OMC05	92.97	±	0.15	7.03	±	0.15
OMC1	93.67	±	0.12	6.33	±	0.12

¥ Standard deviation

3.1.2 Raman Spectroscopy of OMC materials

In figure 3.2, shows the Raman spectra of non-functionalized and functionalized OMC. The D (associated with structural disorder or defects, at ca. 1320 cm^{-1}) and G (attributed to structural order or sp^2 carbon hybridization, at ~1580 cm^{-1}) bands, typical of carbon-based materials, are observed [93]. The ratio of the intensities between the D and G bands (I_D/I_G) of OMC is 1.08, decreasing to 1.03 after functionalization with 0.15 M MeOH. The results indicate that microwave heating with a low MeOH concentration slightly increases the graphitic structural order i.e., a more intense G band of OMC015 than non-

functionalized OMC. Meanwhile, the opposite occurs at OMC05 and OMC1, at which a higher MeOH concentration during IMH provokes an increase in their I_D/I_G ratio (1.16 and 1.46, respectively), compared to OMC and OMC015.
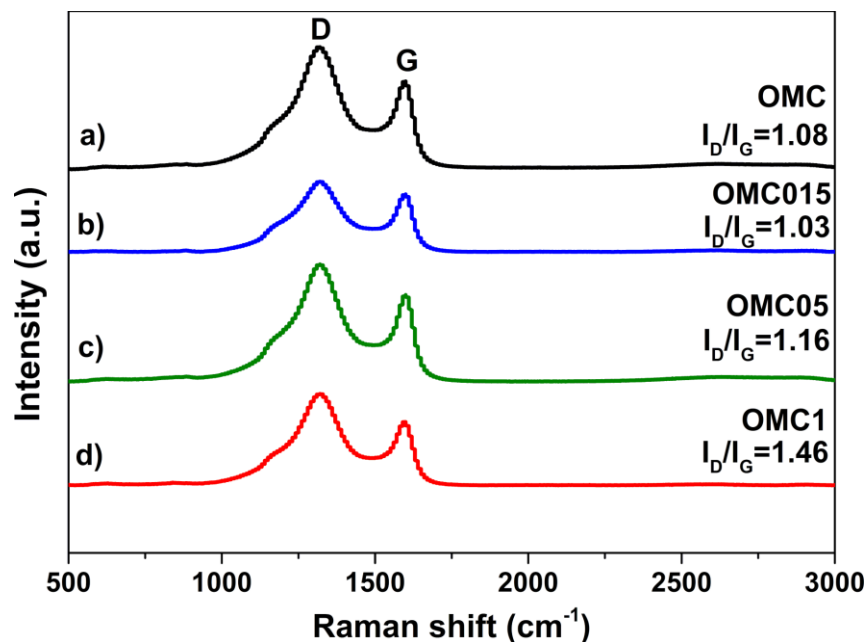
Figure 3.2 Raman spectra of a) OMC); b) OMC015; c) OMC05; d) OMC1.

3.1.3 Identification of functional groups utilizing Fourier Transform Infrared (FT-IR) Spectroscopy

The FTIR spectra of OMC, OMC015, OMC05, and OMC1 are shown in Figure 3.3. The non-functionalized catalyst shows low intensity bands at 3773 and 3718 cm^{-1} ascribed to v(O-H) stretching vibrations, and relatively more intense signals at 1629 cm^{-1} due to C=C vibrations of carbonyl groups [94]. While OMC015 shows the same bands, it calls the attention that the relative intensity of the v(O-H) and C=C bonds increases compared to OMC. Meanwhile, the relative intensity of the v(O-H) vibrations at OMC05 and OMC1 is higher than that of OMC015. Such feature is ascribed to the IMH functionalization with higher MeOH concentrations, promoting the formation of O-H functional groups. On the other hand, it should be mentioned that the relative intensity of the C=C signal is lower at OMC05 and not detected at OMC1, compared to OMC015.
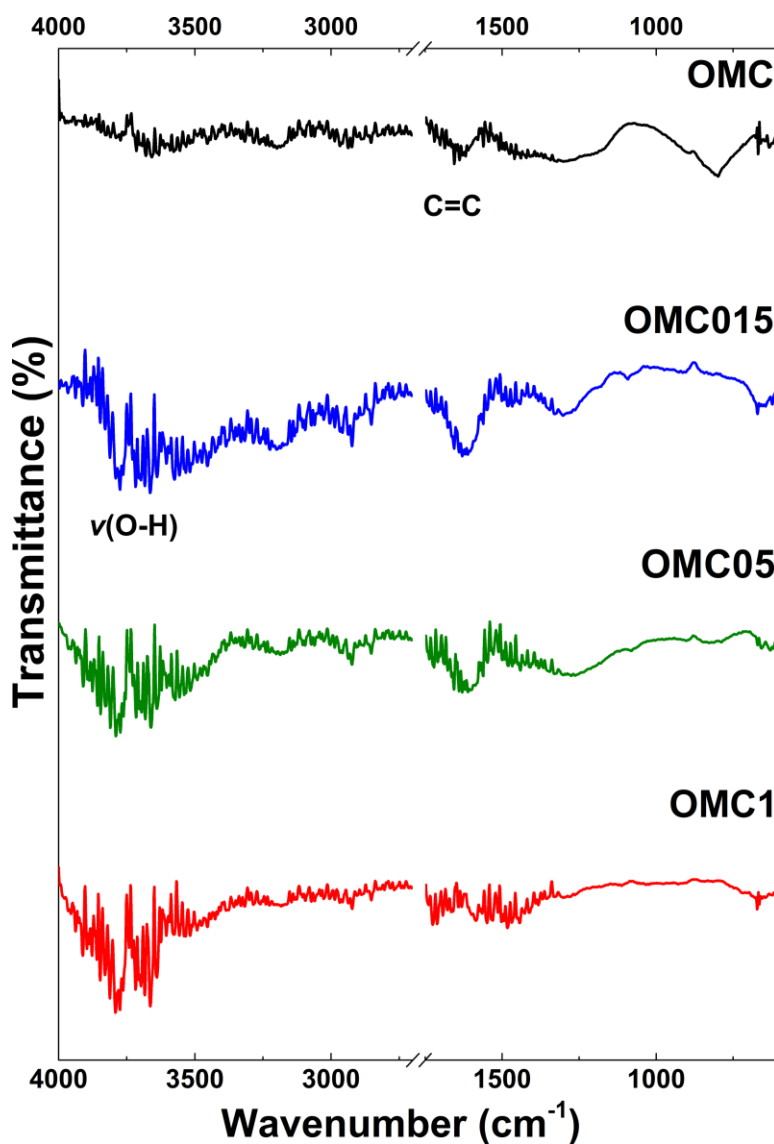
Figure 3.3 FTIR spectra of a) OMC, b) OMC015, c) OMC05, and d) OMC1.

3.1.4 FESEM Analysis

The morphology and chemical mapping of the OMC catalysts are shown in Figure 3.4. The micrographs show a rather similar morphology, with large particles of irregular shape. As already mentioned in the SEM-EDS analysis, the most abundant elements at the catalysts are C and O, although with the FESEM technique traces of K and Ca have been detected. This morphology is expected based on previous studies on similar OMC materials [95].
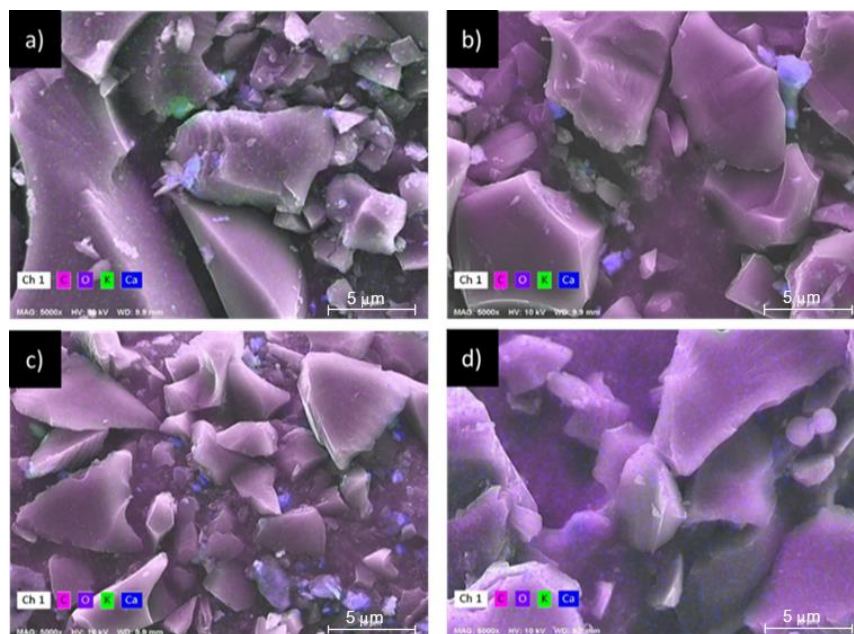
Figure 3.4 FESEM micrographs and chemical mapping of a) OMC, b) OMC015, c) OMC05, and d) OMC1.

3.1.5 HRTEM Analysis

The functionalization with MeOH, a soft chemical agent, has no effect on the morphology of the carbon-based catalysts. Figure 3.5 shows a HRTEM micrograph of OMC, at which the ordered arrangement of lattice fringes corresponding to its graphitized structure (e.g., the area highlighted by a red square) can be distinguished. This feature has been ascribed to the partial crystallinity of OMC [96].
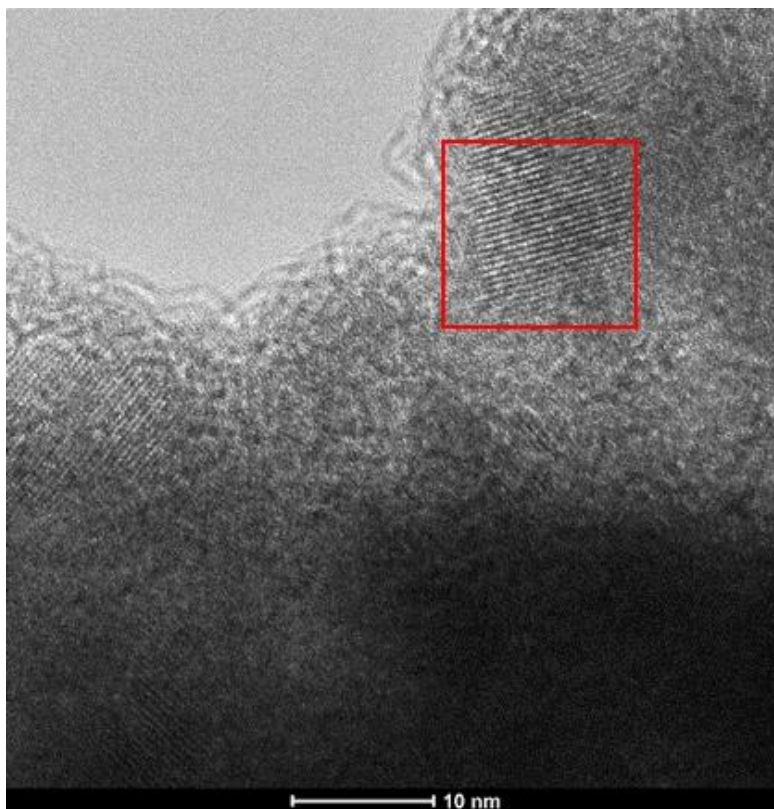
Figure 3.5 HRTEM micrograph of OMC.

3.1.6 Desorption of N_2- BET Analysis

The N_2 adsorption-desorption isotherms of the OMC catalysts are shown in Figure 3.6. All isotherms have open hysteresis at low P/P0. The open characteristic is typical of slit or bottle-shaped pores, at which the adsorbate penetration is kinetically slow due the narrowness of the intrachannels of the carbon materials [93, 97]. The isotherms fall in the type IVa classification [98, 99]. Moreover, the materials show a steep increase in adsorption at high P/P0 while a hysteresis loop appears as a typical feature of micro-mesoporous structures [93].
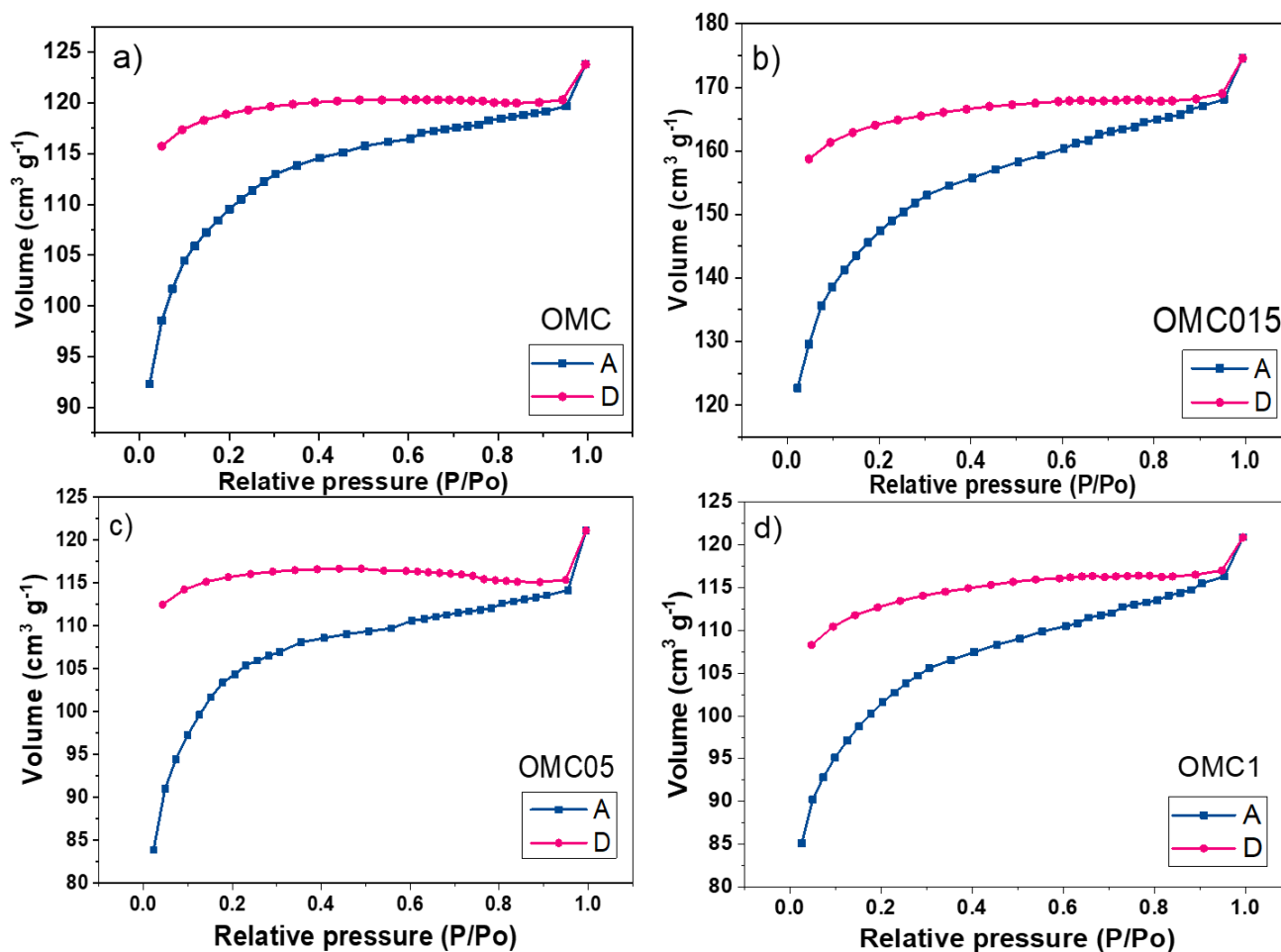
Figure 3.6 N$_2$ adsorption (A)-desorption (D) isotherms of a) OMC, b) OMC015, c) OMC05, and d) OMC1.

It can be seen in Table 3.2 that the surface area increases from 410.6 at OMC to 550 m^2 g^{-1} at OMC015 after functionalization with 0.15 M MeOH. The average pore size (reaching ca. 2 nm) and the total pore volume also become higher at the latter (0.270 vs. 0.191 cm^3 g^{-1}, respectively). The microwave radiation falls between the infrared and the radio waves (ca. 10-3 to 1 m, [100]). It has been reported that carbon materials are active to microwave radiation [92]. It is hypothesized that exposure of OMC to microwave radiation in 0.15 M MeOH removes some impurities, which can be correlated with the chemical composition in Table 3.3 [92]. The results show that OMC and OMC015 have a C content of ca. 98.78 and 99.89 wt. %, respectively, with less O at the latter. A slightly similar tendency can be seen in Table 3.4. Simultaneously, the relatively diluted MeOH solution can impregnate

available pores, increasing their volume under intermittent heating, therefore producing a higher surface area at OMC015.

At OMC05 and OMC1, a contrary effect is observed compared to OMC015, i.e., their content of C and O decreases and increases, respectively, compared to OMC. Apparently, the relatively higher MeOH concentration inhibits the removal of impurities, avoids the activation of pores, or even provokes a collapse of a number of them under radiation, thus limiting the surface area. Even though more studies, out of the scope of this work, may be needed to determine an optimal MeOH concentration to generate a higher surface area, it seems that lower concentrations promote enhanced textural properties of OMC. Overall, the average pore size of the OMC catalysts falls within the micro-mesoporosity limit.

Table 3.2 Textural properties of OMC, OMC015, OMC05 and OMC1

Sample	Surface Area (m^2g^{-1})	Average pore size (nm)	Total pore volume (cm^3g^{-1})
OMC	410.6	1.865	0.1915
OMC015	550.0	1.964	0.2700
OMC05	380.1	1.971	0.1873
OMC1	382.0	1.958	0.1870

3.1.7 Analysis of the carbon catalysts by X-Ray Photoelectron Spectrometry

Table 3.3 depicts the surface chemical composition from the XPS survey of the OMC catalysts, composed mainly of C and O, with traces of Na at the non-functionalized catalyst because of the precursor used in the synthesis process, which was not detected after functionalization. There was an increase in the relative concentration of surface C after functionalization, with a slight decrease in that of O.

Table 3.3 XPS survey parameters of OMC, OMC015, OMC05, and OMC1

Catalyst	(at. %)					
	C 1s	O 1s	F 1s	Si 2p	K 2s	Na 1s
OMC	88.75	8.54	ND	ND	2.24	0.48
OMC015	91.44	7.75	0.81	ND	ND	ND
OMC05	91.23	7.64	0.78	0.36	ND	ND
OMC1	90.58	8.38	1.04	ND	ND	ND

In Figure 3.7, the high-resolution XPS spectra of the OMC catalysts in the C 1s region can be observed. It depicts characteristic peaks ascribed to C=C sp^2, C-C sp^3, C-OH, C=O, and O-C=O species [101, 102, 103, 104]. The relative atomic concentration and the binding energy (BE) of the species are shown in Table 3.4. As can be observed, the highest concentration (roughly 80 at. %) is that of the sp^2 nanodomains (at ca. 284 eV) in the four OMC catalysts.
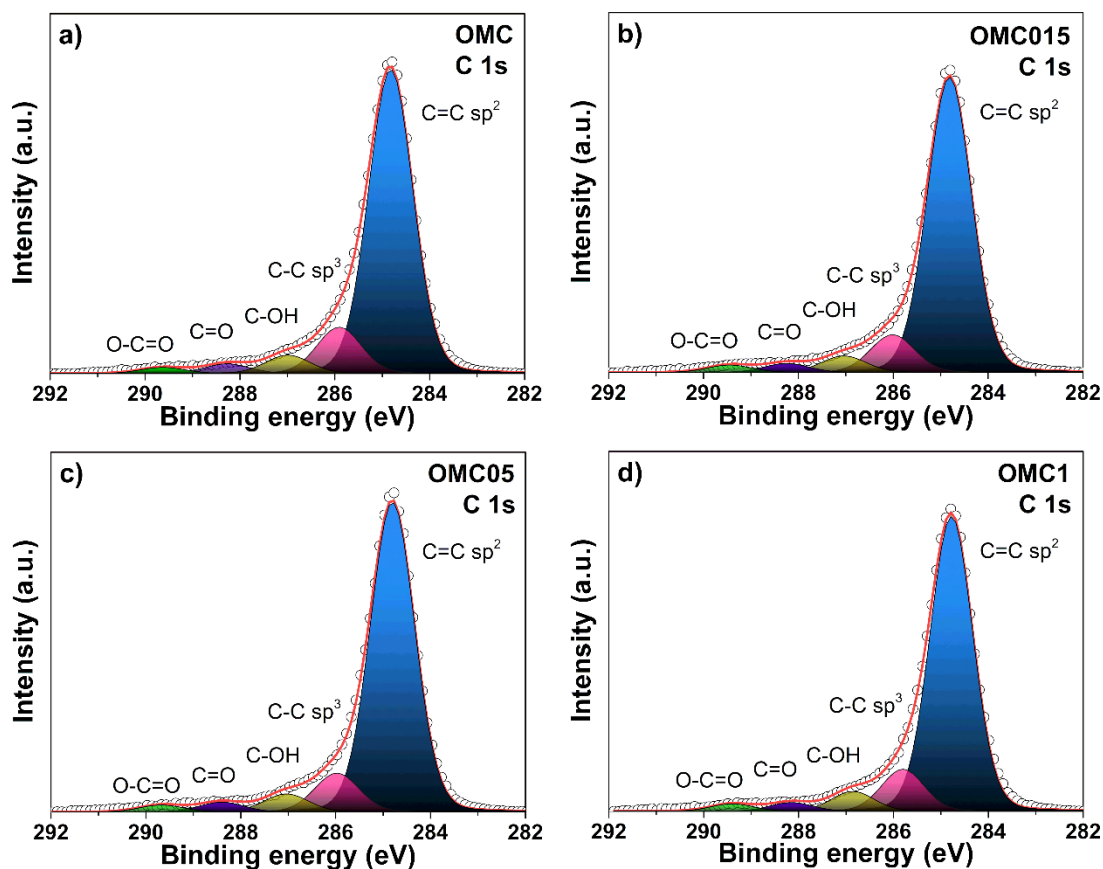
Figure 3.7 High resolution spectra in the C 1s region of OMC, OMC015, OMC05, and OMC1.

Meanwhile, the high-resolution spectra in the O 1s region (Figure 3.8) shows the presence of the C=O, C-O, and O-C=O species [105]. Table 3.4 shows the relative atomic concentration of the species, the higher corresponding to the C-O species (BE about 532 eV). Overall, the C and O bonds in Figures 3.7 and 3.8 correspond to those normally observed elsewhere for carbon-based catalysts.
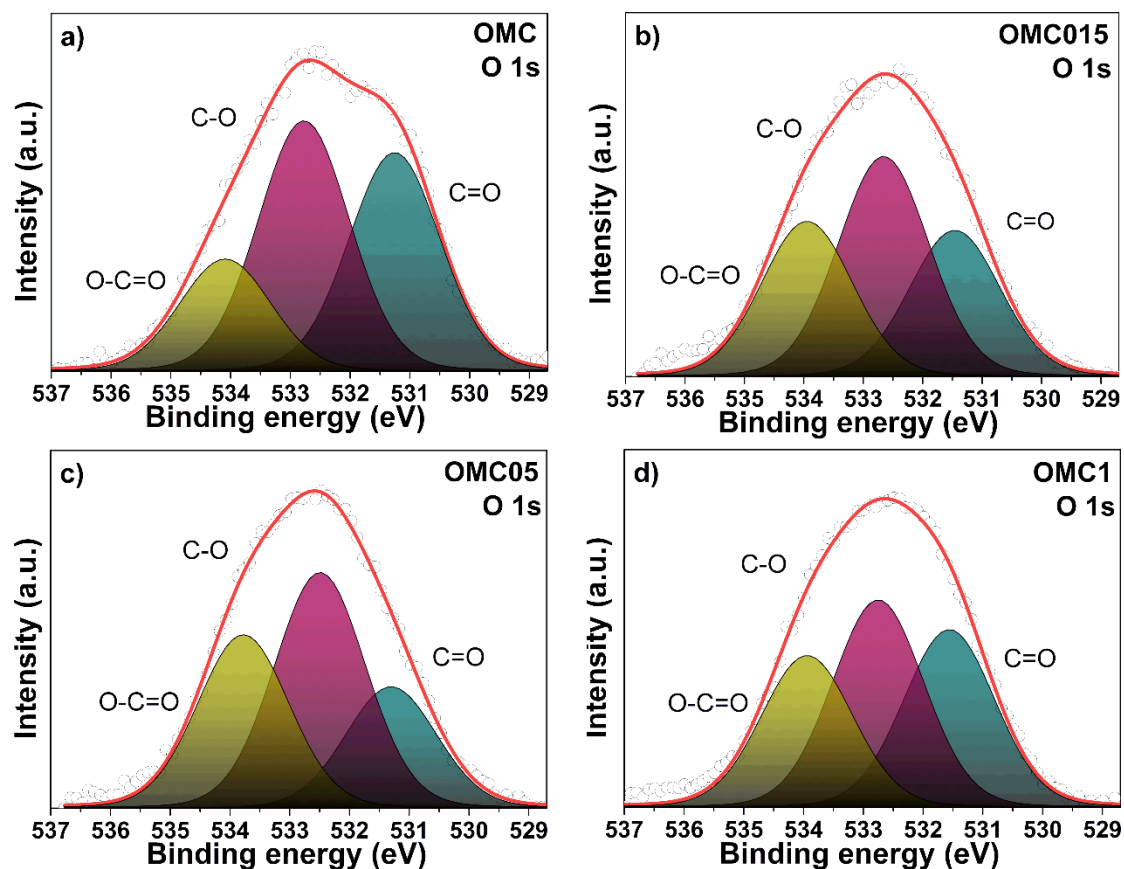
Figure 3.8 High resolution spectra in the O 1s region of a) OMC b) OMC015 c) OMC05 and d) OMC1.

Table 3.4 High resolution XPS data of OMC catalysts.

Catalyst	Species	State	BE (eV)	Composition (at. %)
OMC	C=C sp^2	C 1s	284.82	79.1
	C-C sp^3	C 1s	285.91	12.0
	C-OH	C 1s	286.99	4.8
	C=O	C 1s	288.27	2.5
	O-C=O	C 1s	289.62	1.6
	C=O	O 1s	531.26	37.6
	C-O	O 1s	532.77	43.1
	O-C=O	O 1s	534.09	19.3

OMC015	C=C sp^2	C 1s	284.82	80.7
	C-C sp^3	C 1s	286.01	10.3
	C-OH	C 1s	287.04	4.5
	C=O	C 1s	288.25	2.5
	O-C=O	C 1s	289.45	2.0
	C=O	O 1s	531.46	28.1
	C-O	O 1s	532.66	42.1
	O-C=O	O 1s	533.95	29.8
OMC05	C=C sp^2	C 1s	284.80	80.7
	C-C sp^3	C 1s	285.98	10.2
	C-OH	C 1s	287.04	4.7
	C=O	C 1s	288.40	2.6
	O-C=O	C 1s	289.67	1.8
	C=O	O 1s	531.30	22.9
	C-O	O 1s	532.49	44.4
	O-C=O	O 1s	533.78	32.7
OMC1	C=C sp^2	C 1s	284.78	79.1
	C-C sp^3	C 1s	285.80	11.3
	C-OH	C 1s	286.86	5.3
	C=O	C 1s	288.15	2.3
	O-C=O	C 1s	289.40	2.0
	C=O	O 1s	531.56	33.1
	C-O	O 1s	532.75	38.6
	O-C=O	O 1s	533.94	28.3

3.1.8 Morphology of the bioanodes

Figure 3.9 shows SEM micrographs of the bioanodes formed by the OMC catalysts and a biofilm by *B. subtilis* at two magnifications. The non-functionalized (Figure 3.9 a-b) and functionalized (Figures 3.9 c-h) bioanodes show a high degree of coverage by the biofilm over the carbonaceous catalysts, as confirmed by the well-developed extracellular matrix

with rod-like shape bacteria. The formation of the biofilm can be attributed in part to the highly hydrophilic nature of the carbon surface, resulting in a carbon/EAM interface that suggests biocompatibility between the OMC catalysts and *B. subtilis*, [65] a fundamental feature to promote the electron transfer at the bioanodes [106].
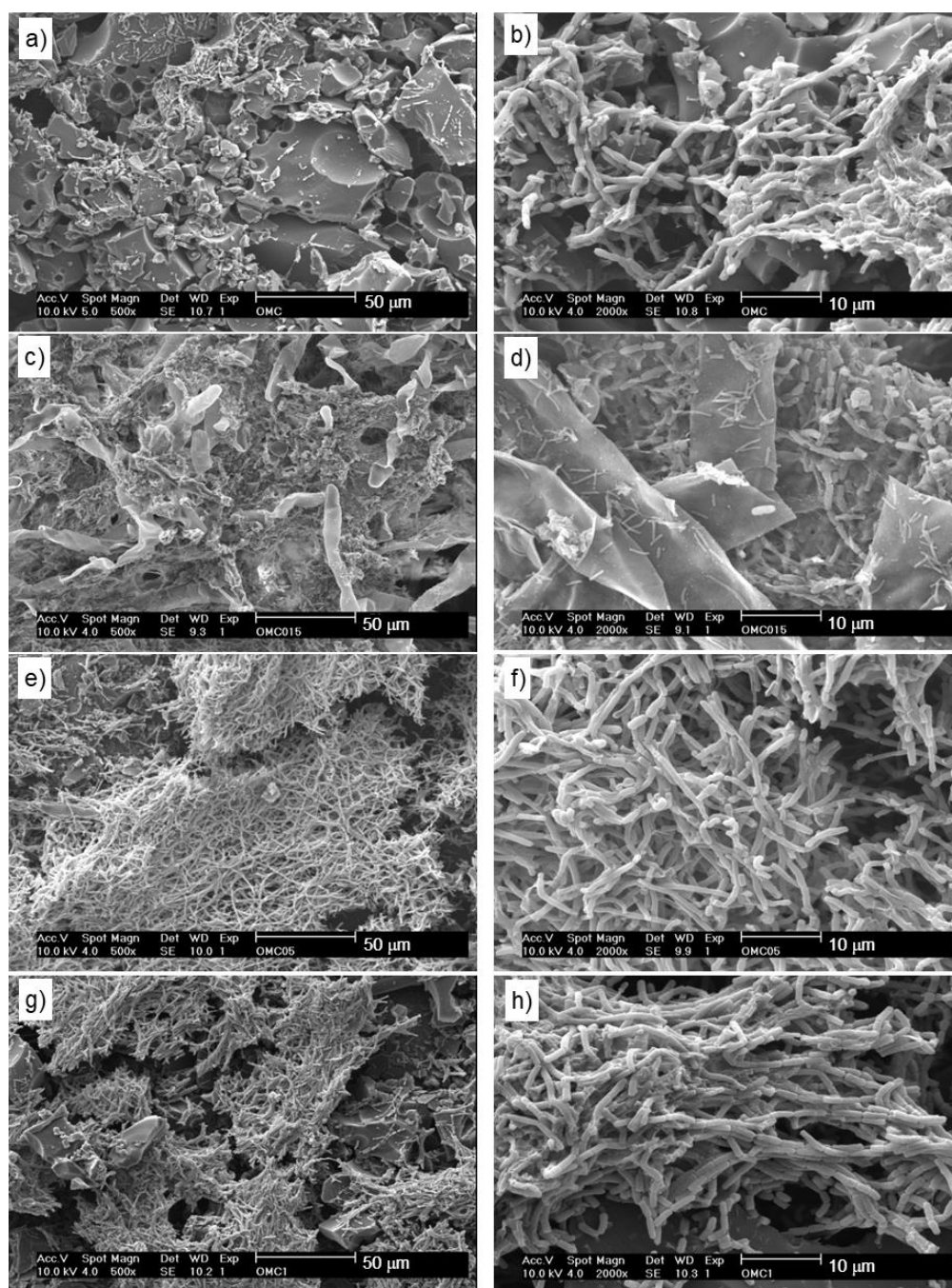
Figure 3.9 SEM micrographs of the bioanodes: a-b) OMC + *B. subtilis*, c-d) OMC015 + *B. subtilis*, e-f) OMC05 + *B. subtilis*, and g-h) OMC1 + *B. subtilis*.

3.2 Evaluation of electrochemical behavior of OMC in half cell

3.2.1 Electrochemical behavior of OMC in half cell

In the Figure 3.10 displays the CVs of the non-functionalized and functionalized OMC anodes (i.e., without biofilm) in N_2-saturated PWW. OMC015, OMC05, and OMC1 generate higher j values at the most negative and positive potentials than OMC. Among the functionalized catalysts, OMC015 shows a slightly enhanced performance compared to OMC05 in terms of higher j, followed by OMC1. Thus, initially the functionalization with a relatively low concentration of MeOH has a positive effect on the electrochemical behavior of OMC, but a gradual increase in alcohol content during IMH hinders the generation of j. This behavior may be related to the development of OH^- functional groups at the active surface of the functionalized OMC catalysts, as shown in Figure 3.3.
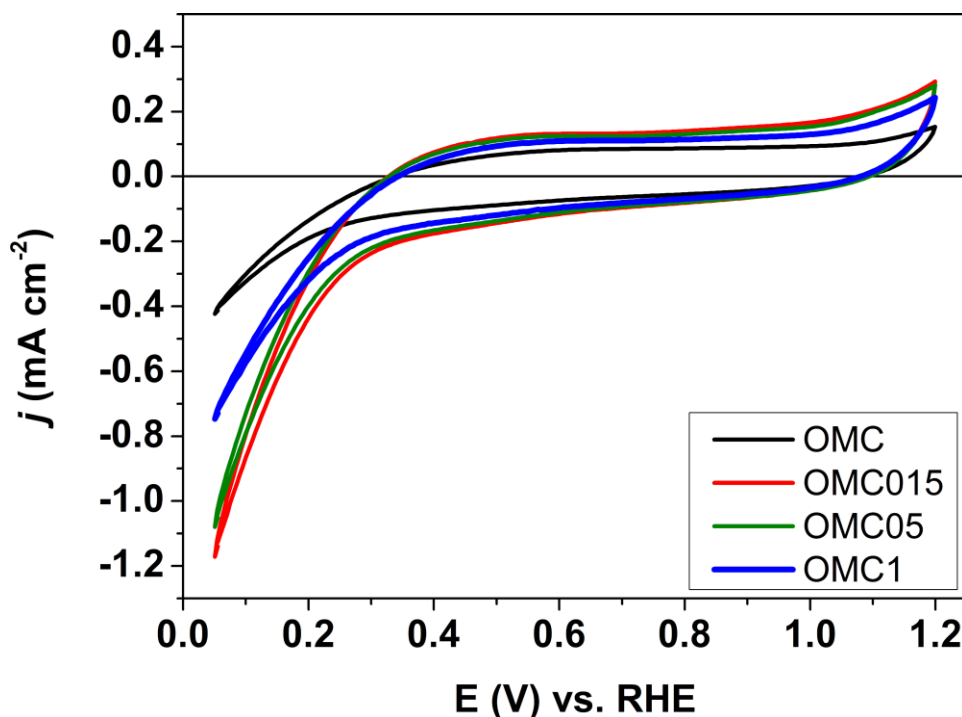
Figure 3.10 CVs of the non-functionalized and functionalized OMC catalysts in N_2-saturated PWW. Scan rate: 20 mV s^{-1}.

3.2.2 Electrochemical behavior of the OMC + *B.subtilis* bioanodes

Figure 8 shows a comparison of the bioelectrochemical behavior of the anodes depicted in Figure 3.11 and the corresponding bioanodes: a) OMC + *B. subtilis*, b) OMC015 + *B. subtilis*, c) OMC05 + *B. subtilis*, and d) OMC1 + *B. subtilis*. It is seen that the presence of the EAM at the OMC + *B. subtilis* bioanode increases the *j* values at the more positive and negative potentials. Consequently, the slope of its CV changes compared to the OMC anode, indicating an enhancement in biocatalytic activity at the carbon/EAM interface, thus improving the oxidation of organic matter from PWW and the EET at the bioanode [107, 108]. Such behavior can be correlated to the coverage of the catalyst layer by the biofilm, as seen in Figures 3.9 a-b.
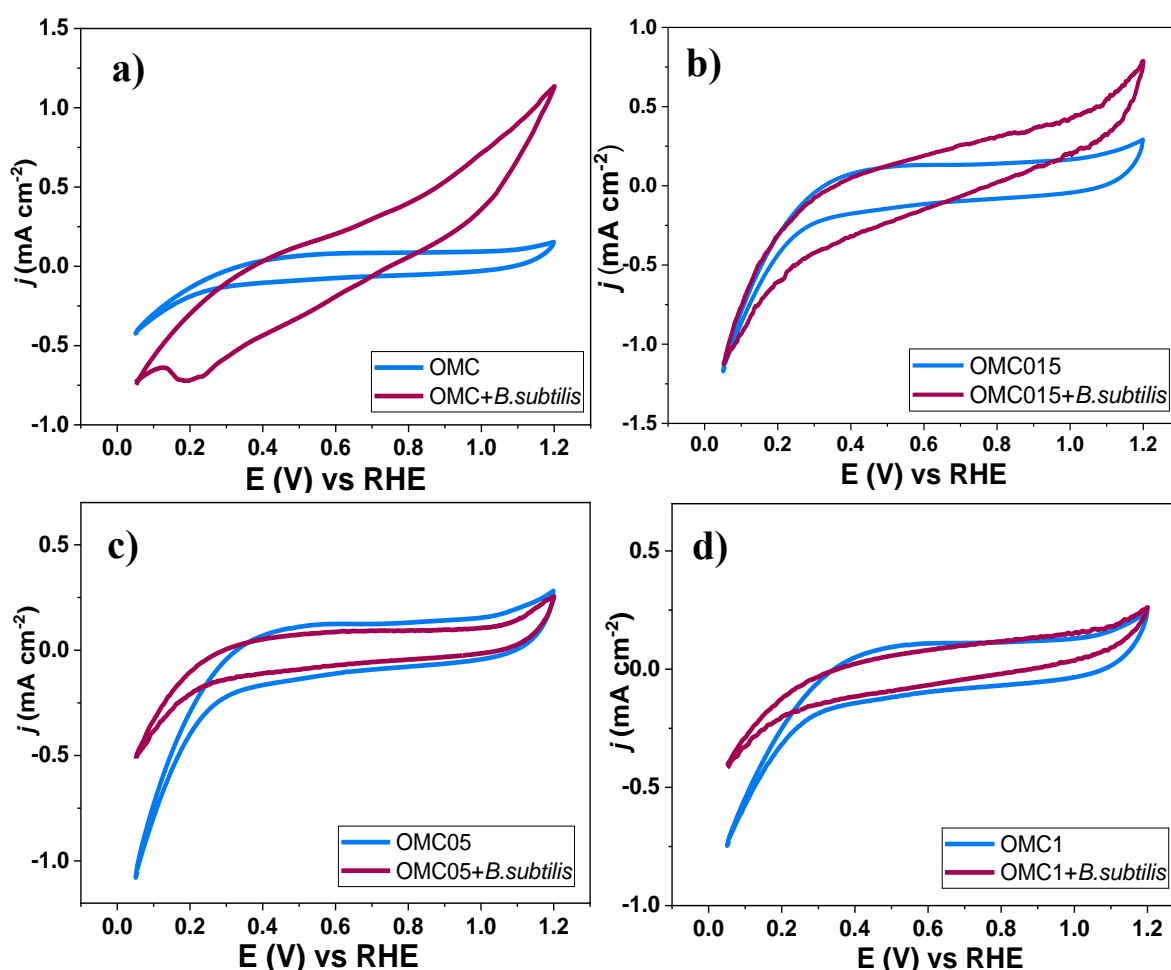
Figure 3.11 CVs of the bioanodes of OMC/*B. subtilis* and the anodes formed only by the carbon catalysts in N_2-saturated PWW. Scan rate: 20 mV s^{-1}.

Similarly, the CV of OMC015 + *B. subtilis* shows a change in slope due to the generation of higher *j* values at the most positive potential, compared to OMC015 without EAM. Nevertheless, *j* at the more negative potentials is about the same at both bioanode and anode. As reported elsewhere, a change in slope as those shown by OMC + *B. subtilis* and OMC015 + *B. subtilis* compared to OMC and OMC015, respectively, may be ascribed to c-type cytochromes promoting the bioelectrochemical reaction by enhancing the EET via a direct mechanism [109]. Moreover, as indicated previously, higher *j* values in the anodic and cathodic scans can be ascribed to improved oxidation reactions and/or faster electron transfer, and to the reduction of accumulated metabolic intermediates, respectively [107].

In the case of the OMC05 + *B. subtilis* and OMC1 + *B. subtilis* bioanodes, their *j* values become smaller than their anode counterparts (i.e., OMC05 and OMC1, respectively), thus showing a lower bioelectrochemical performance with the microorganisms. Such results demonstrate that, despite the biofilm growth (see Figures 3.9 e-h), the EET between the catalyst layer and biofilm is rather poor at these bioanodes, limiting the oxidation of organic matter from PWW. It is hypothesized that the thickness of the biofilm at these bioanodes is higher than an optimal value expected for a fast EET, becoming rather resistive and resulting in low *j* values generated with the EAM. Moreover, one factor that may have affected the performance of OMC05 and OMC1 is their lower surface area, compared to OMC and OMC015 (Table 3.2). Considering this behavior, only the OMC + *B. subtilis* and OMC015 + *B. subtilis* bioanodes have been further evaluated in the full MFC.

3.2.3 Polarization and Power density curves

Figures 3.12 a-b) show the polarization and power density curves of the MFC equipped with the OMC + *B. subtilis* bioanode, with PWW as the substrate, at Days 0, 3 and 7 of testing. At Day 0, the OCV is 0.20 V, delivering a maximum j of 115.7 mA m^{-2}, with P_{cell}= 6.56 mW m^{-2} (Table 3.6). After 3 days of operation, the overall performance decays drastically in terms of OCV and *j*, delivering P_{cell}= 1.22 mW m^{-2}. Such decrease in bioelectrochemical activity can be attributed partially to the so-called microbial log phase,

at which during a given time lapse the microorganisms utilize the metabolic energy for their extracellular development [110, 111], thus there is a clear decrease in P_{cell}.

Table 3.5. Parameters of the MFC operating with the OMC + *B. subtilis* and OMC015 + *B. subtilis* bioanodes, with PWW as the substrate.

Bioanode	V_{cell} (V)			j (mA m^{-2})			P_{cell} (mW m^{-2})		
	Day 0	Day 3	Day 7	Day 0	Day 3	Day 7	Day 0	Day 3	Day 7
OMC + *B. subtilis*	0.20	0.06	0.15	115.7	44.6	49.5	6.56	1.22	2.02
OMC015 + *B. subtilis*	0.35	0.33	0.30	132.2	148.8	140.4	11.2	12.3	10.6

At Day 7, the OCV increases compared to Day 3, but remains lower than Day 0 (i.e., 0.15 V). The j generated by the MFC at Day 7 is also lower than Day 0, with P_{cell}= 2.02 mW m^{-2} (Table 3.5), suggesting an adaptation of the microorganism, reaching a growth stationary phase, enhancing the electron transfer from the PWW related to Day 3, but not reaching the initial performance of Day 0. The oscillating behavior of the MFC can also be a result of the dynamic features of the OMC + *B. subtilis* bioanode, where the biofilm can be evolving during the operation, probably forming/eliminating other bacteria [110, 111].
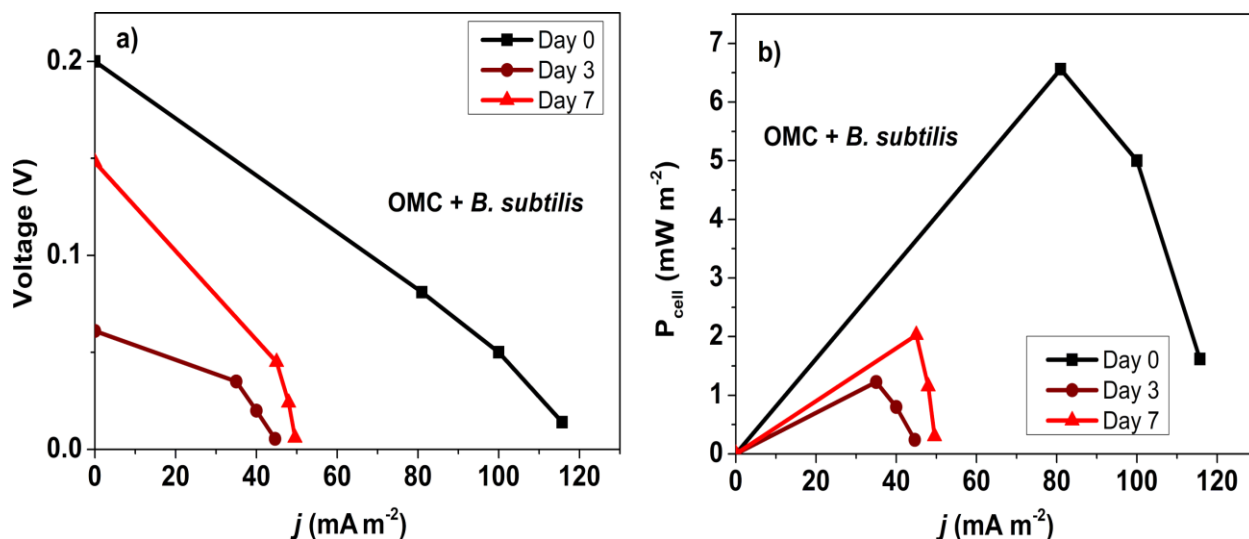
Figure 3.12 a) V-*j* and b) P_cell-*j* curves of the MFC equipped with the OMC + *B. subtilis* bioanode at Days 0, 3 and 7. Membrane: Nafion 117. Cathode: Pt/C. Anode substrate: PWW. Cathode electrolyte: O_2-saturated phosphate buffer solution. T_cell: ambient.

Figures 3.13 a-b) show the polarization and power density curves of the MFC equipped with the OMC015 + *B. subtilis* bioanode. In this case, the behavior is less oscillating, resulting in a more stable operation of the MFC. For instance, the OCV is 0.35, 0.33, and 0.30 V at Days 0, 3, and 7, respectively. The highest *j* is 148.8 mA m^{-2} at Day 3, which is relatively similar to the Day 7 (Table 3.6). The maximum P_cell is 12.3 mW m^{-2} at Day 3, which is higher than the maximum in Figure 3.12 b). Opposite to the behavior observed in Figure 3.13, where the performance of the MFC with the OMC015 + *B. subtilis* bioanode in the 7-days test indicates a fast extracellular development in the biofilm formed by the EAM, along with a high biocompatibility between OMC015 and the bacteria, resulting in relatively equal EET from the PWW during the long-term test [112].
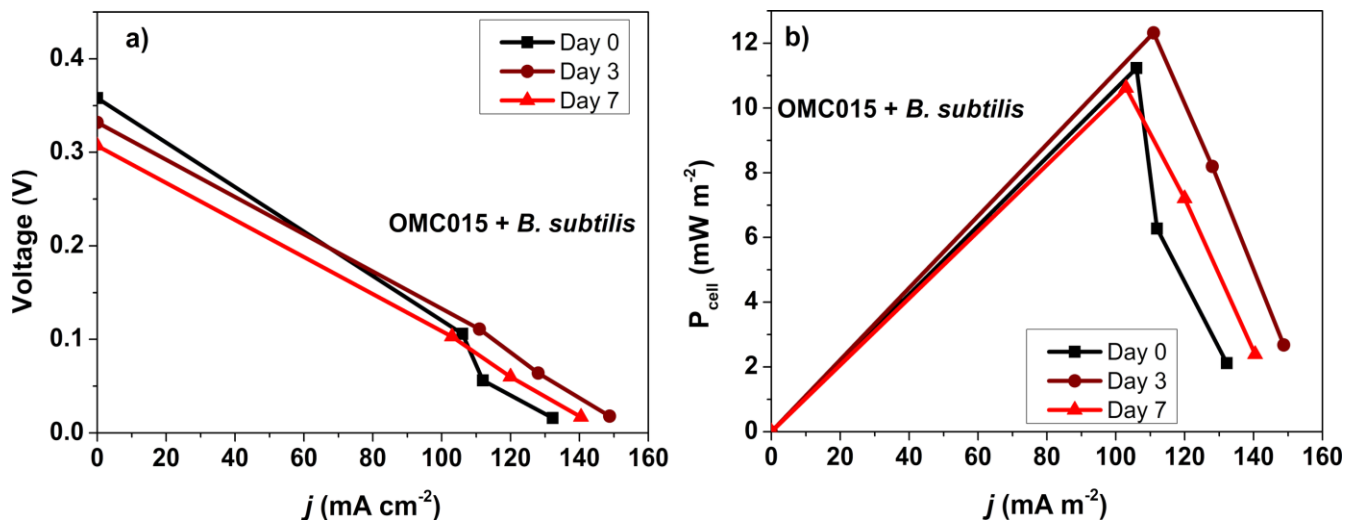
Figure 3.13 a) V-j and b) P$_{cell}$-j curves of the MFC equipped with the OMC015 + *B. subtilis* bioanode at Days 0, 3 and 7. Membrane: Nafion 117. Cathode: Pt/C. Substrate: PWW. Cathode electrolyte: O2-saturated phosphate buffer solution. T$_{cell}$: ambient.

3.2.4 Electrochemical Impedance

Figure 3.14 shows the Nyquist plots of the OMC + *B. subtilis* and OMC015 + *B. subtilis* bioanodes. The fit was performed using a Randles equivalent circuit (inset) to determine the ohmic (R1) and charge transfer resistance of the bioanodes (Rct, identified as R2), the non-ideal capacitive behavior (constant phase element, Q), and the limitations due to diffusion of species (Warburg element, W) [113]. The R2 values of OMC + *B. subtilis* and OMC015 + *B. subtilis* have been determined as 6730 and 3638 Ω, respectively. Moreover, with the OMC015 + *B. subtilis* bioanode, the linear behavior due to diffusion limitations at low frequencies is more important than that of OMC + *B. subtilis*.

Nevertheless, the results indicate that the Rct decreases when the OMC is functionalized with methanol (OMC015 catalyst), which agrees with the previous reports by our research group [108]. This lower Rct correlates well with the higher performance of the MFC equipped with the OMC015 + *B. subtilis* bioanode at Day 0 (Figure 3.14) compared to that with OMC + *B. subtilis* at the same Day (Figure 3.13) in terms of j and P$_{cell}$.

A comparison with previous reports shows that bioanodes with modified carbon cloth (CC) using a microalgae-derived nitrogen-rich biocarbon (CCP-CC) have Rct values of 264.7 and 59.3 Ω, respectively [114]. Elsewhere, the polarization resistance of carbon felt + *S. oneidensis* and carbon felt only electrodes has been reported as 10.2 and 7790 kΩ, respectively [115]. The authors report that the Rct is the major contribution to the total internal resistance of the MFC, which is lower for MFC that contained the microbial biofilm. Other studies agree that the Rct values decrease due to the biofilm presence [116]. In such report, a carbon paper has been implemented as anode material, with an initial Rct of 9 kΩ, which decreases to 2.5 kΩ after two weeks of operation because of the biofilm growth on the anode surface.

Although it is a hard task to compare different MFC bioanode systems, the previous reports indicate that the Rct values calculated for the OMC + *B. subtilis* and OMC15 + *B. subtilis* bioanodes are within the range expected for this type of bioelectrochemical devices. Here, it is shown that the functionalization treatment with methanol modifies the structural properties and increases the presence of O-H bonds, which in addition to promoting the biocompatibility between the catalyst and the EAM, has a positive effect reducing the charge transfer resistance. The lower R2 value, along with the fact that OMC015 has the highest specific surface area, can explain why the OMC015 + *B. subtilis* bioanode generates the highest *j* values in the polarization curves with a more stable behavior.
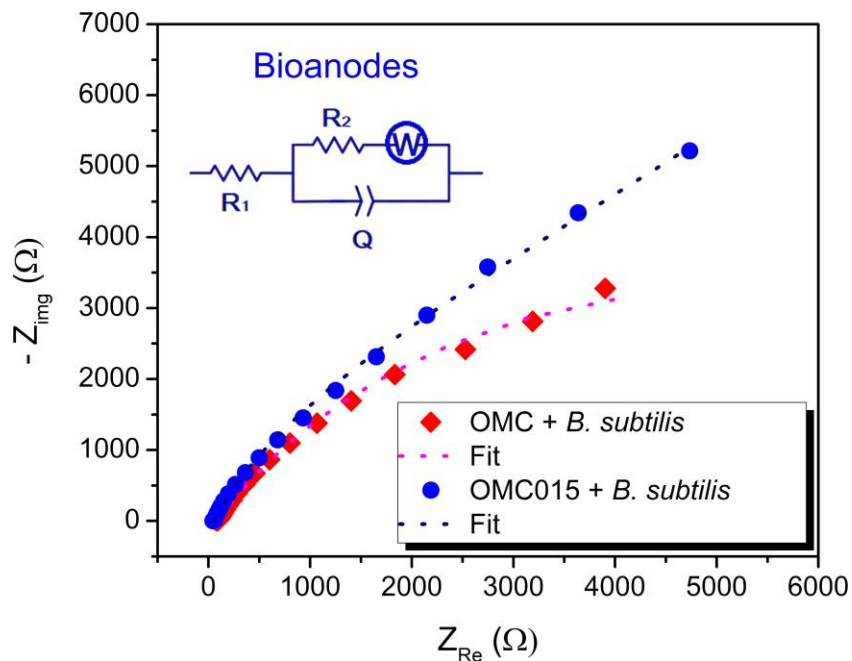
Figure 3.14 Nyquist plots and Randles equivalent circuit (inset) of the OMC + *B. subtilis* and OMC015 + *B. subtilis* bioanodes evaluated at Day 0 of the MFC testing. Anode substrate: PWW; cathode electrolyte: O_2-saturated phosphate buffer solution.

4. Results and discussions of BC

4.1 Physicochemical chemical characterization of BC

4.1.1 XRD patterns of biocarbon and functionalized biocarbon

In Figure 4.1 the XRD patterns of BS, BC, BC015, BC05, and BC10. In the case of BS, the (100) and (110) reflections attributed to quartz (SiO_2) at 21.81° and 35.96° (2θ) respectively, are observed [117, 118, 119]. The pattern also shows a peak at 29.42°(2θ), attributed to the (104) plane of calcite ($CaCO_3$) (JCPDS 47-1743). SiO_2 and $CaCO_3$ are two of the most commonly found crystalline salts in carbonized biomass [120]

In the pattern of BC, i.e., after BS has been pyrolyzed and activated with KOH, which is an effective reagent for removing impurities and generating biocarbons with relatively high carbon content [120], there is a shift in the peaks towards higher 2θ angles. Moreover, some new reflections emerge, such as those at 28.40° and 37.06° corresponding to the (111) and (102) planes of SiO_2 [121], as well as three peaks at 29.50°, 31.02° and 34.11°(2θ), attributed to the (104), (006), and (110) planes of $CaCO_3$ (JCPDS 47-1743) [122, 123, 124, 125].

Meanwhile, BC015 shows a low intensity $CaCO_3$ (006) plane, with the emerging of the (110) and (113) reflections of SiO_2 and $CaCO_3$ at 36.09° and 39.41° (2θ), respectively. BC05 and BC1 show similar characteristics than BC015, without the $CaCO_3$ (006) reflection. These features indicate that the functionalization with methanol slightly modifies the structure of the amorphous materials. Moreover, due to the high intensity of the peaks associated to these crystalline phases, the characteristic (002) plane of C is not observed at the BC series of catalysts [126].
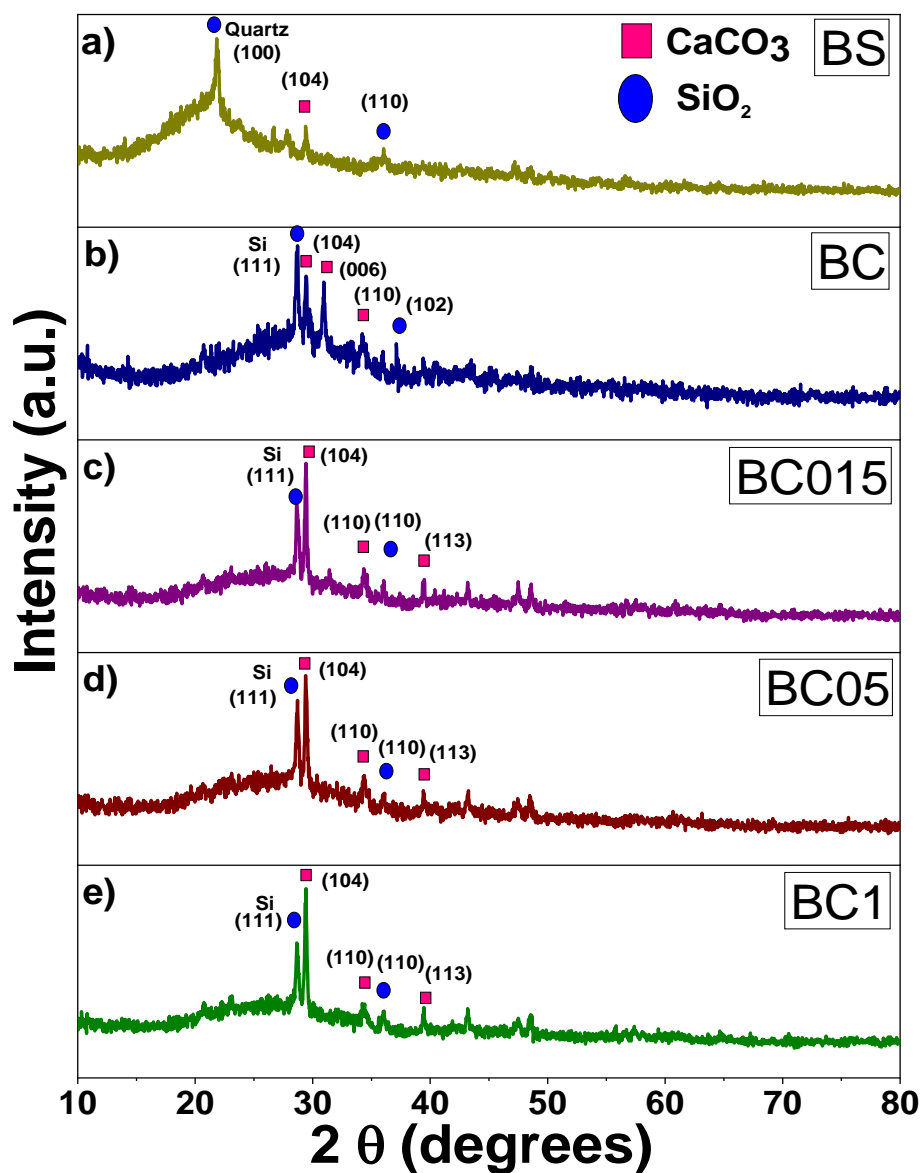
Figure 4.1 XRD patterns of a) BS; b) BC; c) BC015; d) BC05; and e) BC1.

4.1.2 Raman Spectroscopy of BC materials

The Raman spectra of non-functionalized and functionalized BC in Figure 4.2 shows two typical peaks of carbon materials, i.e., the D and G bands (at ca. 1333 and 1591 cm^{-1}, respectively) [120] . The I_D/I_G ratio increases as the concentration of MeOH during functionalization is higher, indicating that the IMH with the alcohol increases the graphitic order of the BC catalysts. Except for the functionalization with 0.15 M MeOH, the structural

behavior of the BC catalysts is similar to that of the OMC materials in the previous Chapter, demonstrating the activity of these carbon-based materials to microwave radiation [92].
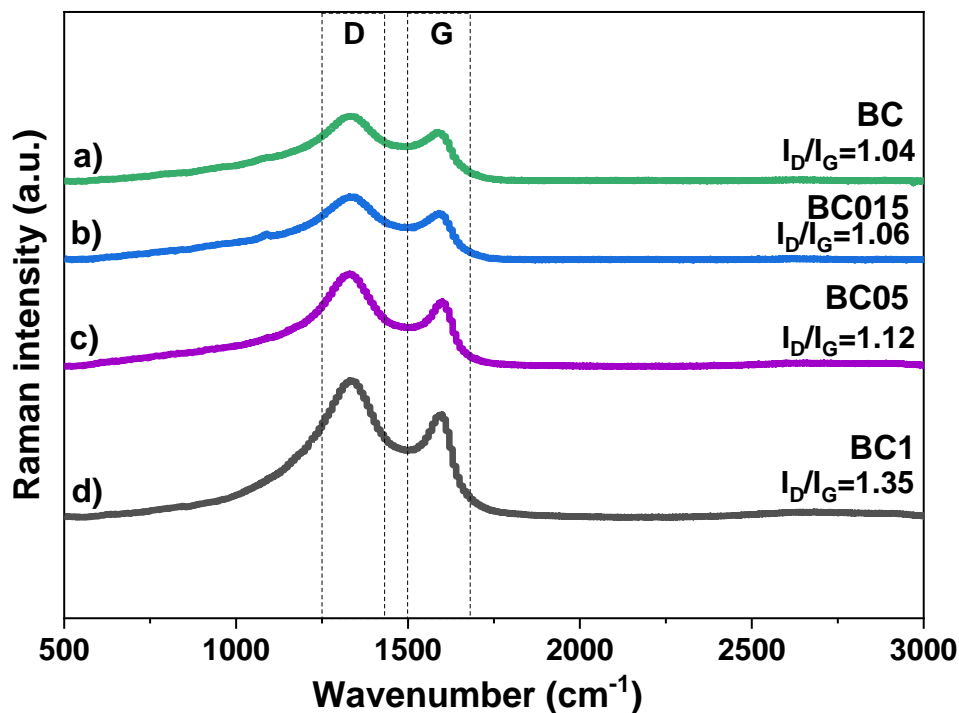
Figure 4.2 Raman spectra of a) BC, b) BC015, c) BC05, and d) BC1.

4.1.3 Chemical composition by EDS.

Table 4.1 depicts the chemical composition and standard deviation of BS, and non-functionalized and functionalized BC. BS is composed of C, O, and several other elements. After pyrolysis, the concentration of C clearly diminishes while that of O remains about the same at BC, BC015, BC05, and BC1, which show the presence of 15 elements including several heteroatoms. Regarding only the BC, the concentration of C increases after the functionalization. Being biocarbons of such heterogeneous chemical composition, it is not an easy task to control the evolution of the elements after pyrolysis and functionalization [57]. For instance, the concentration of N and Si is slightly higher at BC05, compared to BC, BC015 and BC1. Meanwhile, that of K is higher at BC related to the other biocarbons. Nevertheless, it is well known that the presence of heteroatoms improves the catalytic behavior of carbon-based catalysts [127]

Table 4.1 Chemical composition of BS, non-functionalized and functionalized BC catalysts by EDS.

Catalyst	Chemical Composition (wt. %)														
	C	O	N	Si	Ca	K	Al	Fe	P	Mg	Na	Zn	S	Ti	Cl
BS	72.68 ±2.09¥	19.04 ±0.89	4.70 ±0.44	1.17 ±0.52	0.72 ±0.54	0.03 ±0.07	0.25 ±0.15	0.16 ±1.10	0.13 ±0.05	0.13 ±0.04	0.42 ±0.04	0.05 ±0.03	0.44 ±0.25	0.01 ±0.02	0.07 ±0.07
BC	36.78 ±6.10	19.43 ±3.25	1.21 ±0.33	10.87 ±0.72	8.02 ±2.17	15.37 ±4.67	1.84 ±0.20	2.79 ±1.72	0.75 ±0.06	0.46 ±0.06	0.32 ±0.08	1.02 ±0.87	0.59 ±0.11	0.53 ±0.28	0.05 ±0.09
BC015	47.63 ±2.48	21.06 ±1.24	1.21 ±0.25	10.27 ±0.84	7.50 ±1.18	4.80 ±0.75	2.13 ±0.15	2.14 ±0.39	0.78 ±0.06	0.57 ±0.06	0.23 ±0.14	1.17 ±0.60	0.12 ±0.02	0.37 ±0.11	ND
BC05	43.80 ±0.82	21.14 ±0.85	1.44 ±0.28	11.34 ±0.33	8.80 ±0.53	5.76 ±0.29	2.32 ±0.11	2.36 ±0.15	0.91 ±0.16	0.64 ±0.04	0.18 ±0.05	0.74 ±0.13	0.13 ±0.12	0.41 ±0.11	0.02 ±0.05
BC1	46.70 ±4.57	18.56 ±1.50	1.38 ±0.65	9.59 ±0.50	8.67 ±1.76	5.95 ±1.05	2.01 ±0.37	3.15 ±1.22	0.77 ±0.13	0.56 ±0.07	0.22 ±0.06	1.46 ±0.65	0.29 ±0.20	0.63 ±0.26	0.05 ±0.07

¥Standard deviation, ND: not detected.

4.1.4 Identification of functional groups utilizing Fourier Transform Infrared (FT-IR) Spectroscopy

Figure 4.3 shows the FTIR spectra of the BC catalysts. The broad bands between 3600 – 3800 cm^{-1}, with peaks at 3779.22 and 3677.04 cm^{-1}, correspond to v(O-H) stretch vibrations [128]. The peaks in the 1676-1720 cm-1 interval are ascribed to C=O species [129]. The nitrated aromatic compounds NH_2 emerge at ca. 1574-1591 cm^{-1}, attributed to the N-species contained at the BC samples. Meanwhile, the bands at 1234-1247 cm^{-1} are ascribed to C-O stretching vibrations from esters and phenols [128, 130, 131, 132]. The bands in the 918 - 826 cm^{-1} interval is assigned to the aromatic C-H vibrations [120]. The appearance of two C-H peak bands at the BC catalysts is commonly observed at biocarbons obtained from high temperature pyrolysis treatment [133].
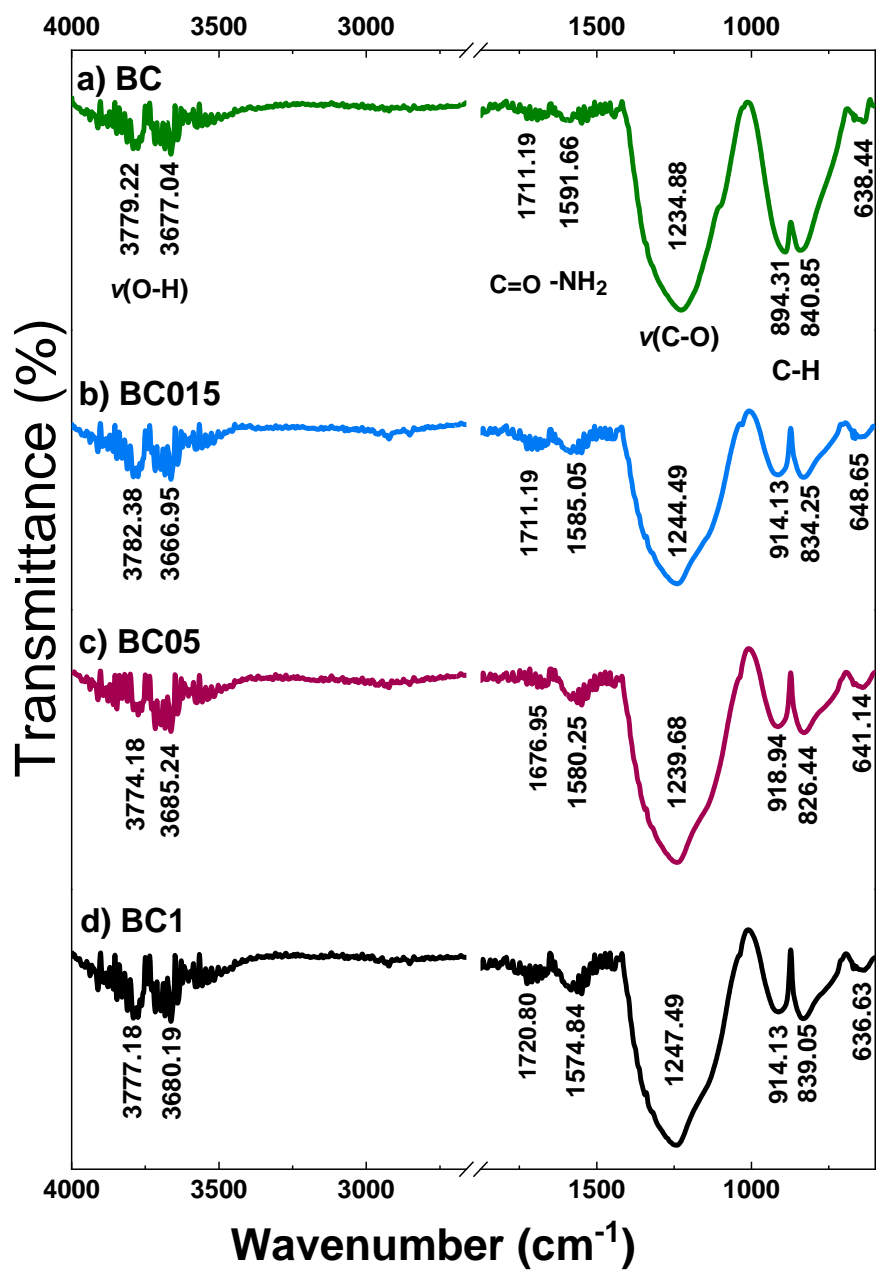
Figure 4.3 FTIR spectra of a) BC, b) BC015, c) BC05, and d) BC1.

4.1.5 Scanning Electron Microscopy of BC

Figure 4.4 shows SEM micrographs of BC and functionalized BC, which show a heterogeneous morphology with irregular and agglomerated particles [111]. The morphology of all BC-based catalysts was similar, with porous features.
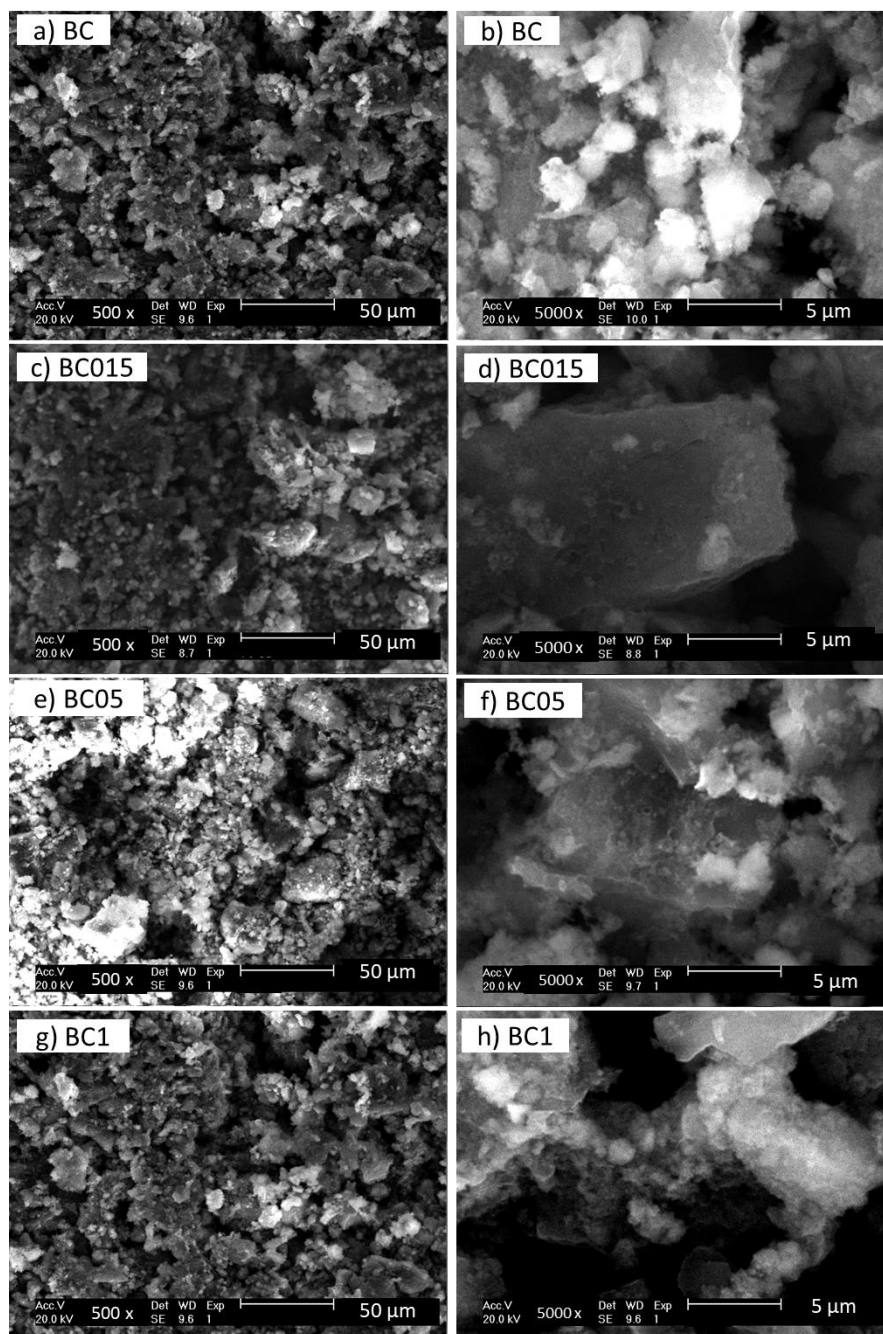
Figure 4.4 SEM micrographs of a-b) BC, c-d) BC015, e-f) BC05, and g-h) BC1.

4.1.6 Chemical mapping of biocarbon

Meanwhile, Figure 4.5 displays the FESEM elemental mapping of BC, BC015, BC05, and BC1, confirming the presence of C, O, heteroatoms like S, P, K, and N, as well as several other elements. This analysis confirms the chemical composition determined by EDS. Moreover, the porous nature of the catalysts can be confirmed from the micrographs.
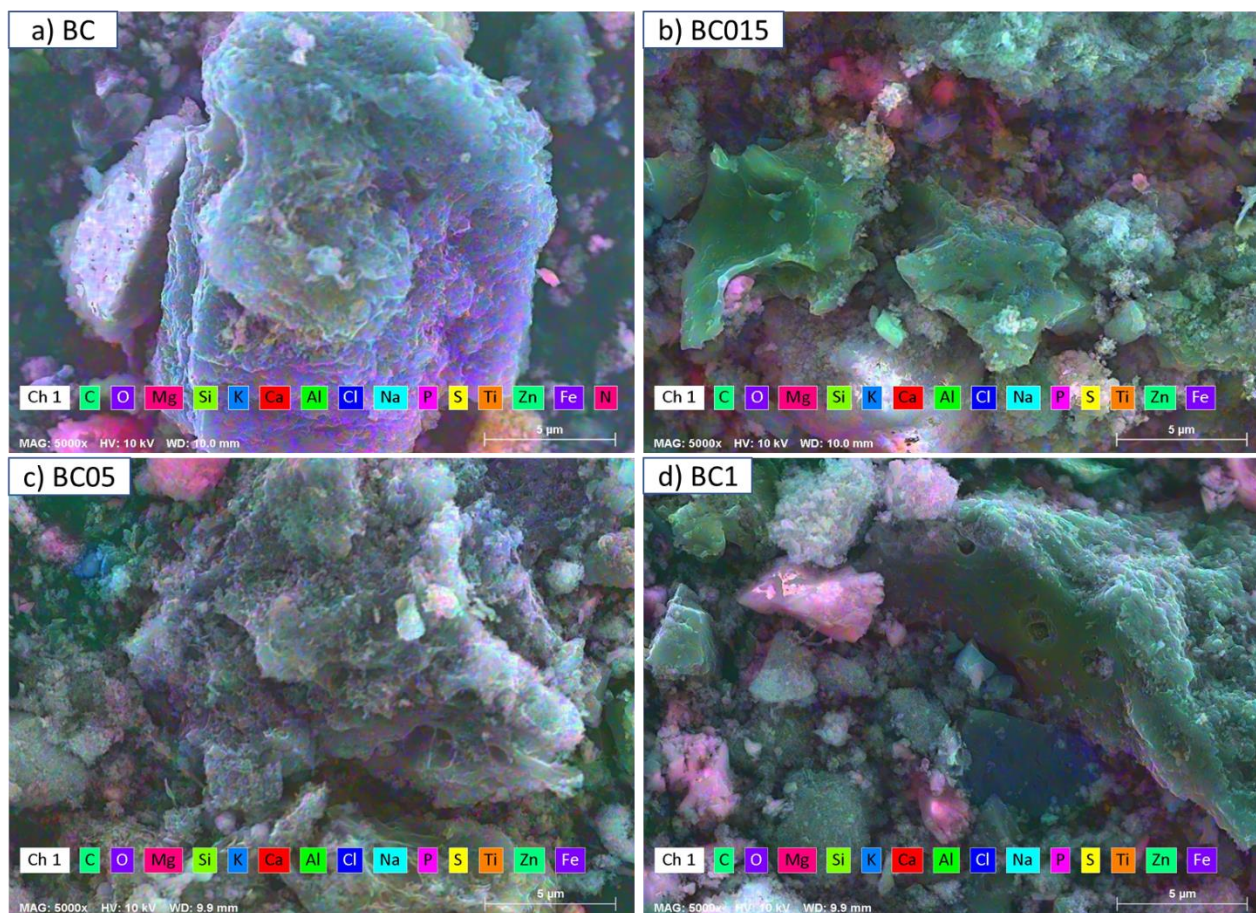
Figure 4.5 Elemental mapping by FESEM. a) BC; b) BC015; c) BC05 and d) BC1.

4.1.7 Organic elemental analysis

In table 4.2 it is showed the organic elemental analysis of the BC-catalysts in Table YY indicates a C content of roughly 29 wt.%. After functionalization with methanol, the O content decreases, while that of N and total organic carbon (TOC) increases. Among the functionalized catalysts, BC015 shows the highest O, N, and TOC concentration.

Table 4.2 Organic elemental composition of BC, BC015, BC05 and BC1.

CATALYST	CHEMICAL COMPOSITION (wt%)				
	C	H	O	N	TOC
BC	29.76	1.20	14.49	1.03	22.30
BC015	29.79	1.24	10.90	1.27	28.10
BC05	28.60	1.30	10.35	1.21	27.40
BC1	29.26	1.02	10.33	1.26	27.60

4.1.8 HRTEM Analysis of biocarbon

Figure 4.6 shows a HRTEM micrograph of BC, in which its crystalline structure is confirmed since ordered lattice fringes can be observed, as in the area highlighted by the red rectangle. Some of those fringes may be ascribed to graphitic carbon phases of the porous BC, in agreement with its elemental composition [134].
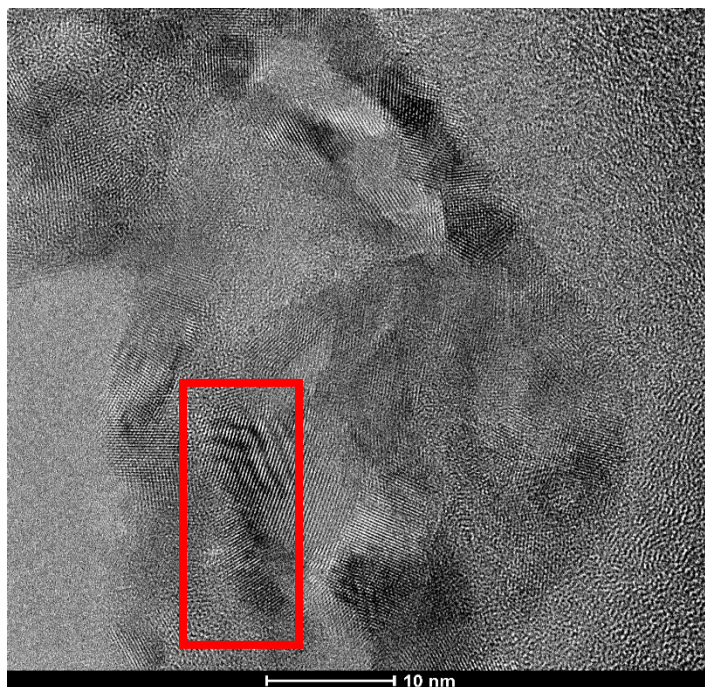
Figure 4.6 HRTEM micrograph of BC.

4.1.9 Desorption of N₂- BET Analysis

 The N_2 adsorption/desorption isotherms of BC, BC015, BC05, and BC1 are shown in Figure 4.7. The isotherms are of the IVa type with an H3 hysteresis loop [98]. That of BC has an open hysteresis at low P/Po, characteristic of slit or bottle-shaped pores [93, 97]. Moreover, the isotherms of BC015, BC05, and BC1 have a steep increase in adsorption at high P/P0, a characteristic commonly found in micro-mesoporous structures [135, 93].
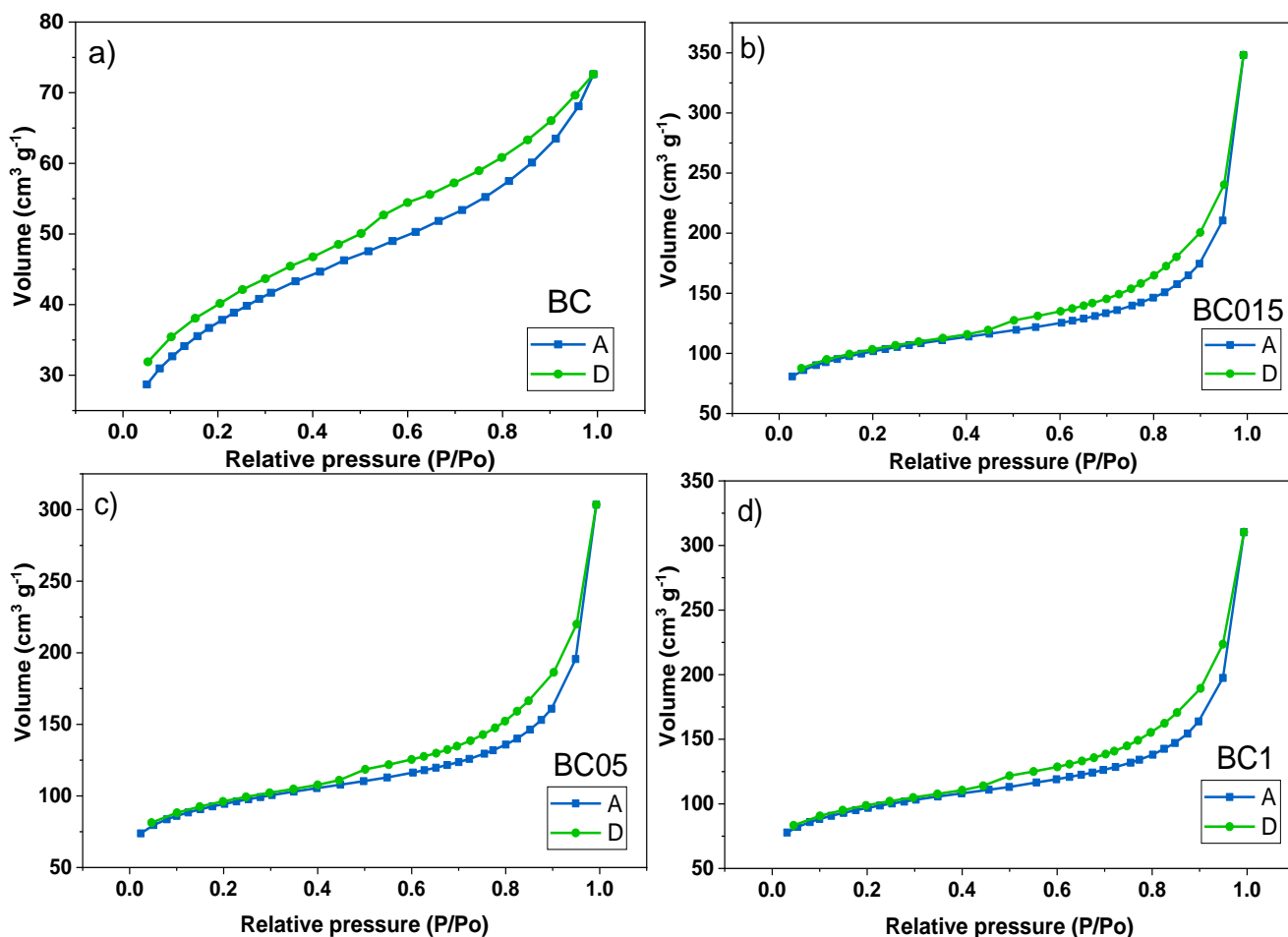
Figure 4.7 N_2 adsorption (A)/desorption (D) isotherms of a) BC, b) BC015, c) BC05, and d) BC1

Table 4.3 shows that the specific surface area increased from 129.3 m^2 g^{-1} to 364.5 m^2 g^{-1} of BC015, i.e., when the biocarbon is functionalized with 0.15 M MeOH . Then, there is a slight decrease at BC05 and BC1. The average pore size also increases from 3.47 of BC to more than 5.5 nm at the functionalized biocarbons (5.90 nm at BC015).   The

average pore size is also larger at the functionalized biocarbons (0.538 cm^3 g^{-1} at BC015). These features indicate the mesoporous nature of the BC catalysts, with enhanced textural values by BC015.

Table 4.3 Textural properties of BC, BC015, BC05, and BC1.

Sample	Surface Area (m^{2}g^{-1})	Average pore size (nm)	Total pore volume (cm^{3}g^{-1})
BC	129.3	3.47	0.112
BC015	364.5	5.91	0.538
BC05	338.6	5.54	0.469
BC1	347.2	5.53	0.480

4.1.10 Surface chemical composition by X-Ray Photoelectron Spectrometry of Non-functionalized and functionalized BC catalysts.

Table 4.4 shows the surface chemical composition of BS, BC, BC015, BC05, and BC1, determined from the XPS survey characterization. The number of elements increases from 6 to 9 from the biomass to pyrolyzed BC, with a significant decrease in the C concentration, while that of O increases. The concentration of the Si and N heteroatoms also increases while elements such as the K and Fe (among others) emerge at BC, compared to BS. BC015, BC15, and BC1 show similar C and O content, with variations in those of other elements and the appearance/disappearance of some more compared to BC. These elements were C, O, Si, N, Ca, K, Al, Fe, Mg, B, P, and S, and were listed by their atomic percentage at Table 3.9. Meanwhile, only six elements will be discussed due the higher concentration detected in most of the BS and BC samples [136]. In the appendix B are shown the deconvolutions of the eight elements, also is included a table with information of binding energy shift, the FWHM and the atomic percentage of each chemical species detected in the spectra.

Table 4.4 XPS survey parameters of BS, BC, BC015, BC05, and BC1.

Catalyst	C 1s	O 1s	Si 2p	N 1s	Ca 2p	K 2p	Al 2p	Fe 2p	Mg 1s	B 1s	P 2s	S 2p
						at%						
BS	80.01	14.3	1.95	1.57	1.73	ND	ND	ND	ND	ND	ND	0.45
BC	36.6	40.74	10.19	2.02	1.93	5.33	1.37	1.03	0.78	ND	ND	ND
BC015	39.67	39.16	9.95	1.43	1.76	1.99	0.81	0.91	0.87	3.45	ND	ND
BC05	39.77	39.49	9.88	0.98	1.89	2.15	1.63	0.86	1.16	ND	2.19	ND
BC1	38.25	42.01	10.61	0.79	1.91	ND	2.34	0.37	0.86	2.85	ND	ND

ND: not detected

Figure 4.8 shows the high-resolution spectra of BS and the biocarbons in the C 1s region. The species with the highest concentration at BS is the C=C sp^2 bond, followed by C-C sp^3 C-OH, and C=O (Table 4.4) [137, 138]. Additional to these species, BC and the functionalized catalysts show the presence of the -COOH carboxylic species. The C=C sp^2 bond has also the highest concentration at BC, BC015, BC05, and BC1 (Table YY).

The higher content of sp^2 bonds compared to the sp^3 species at the BC corroborates the observations from Raman spectra, in which the D band is more intense than the G one, indicating their disorder structure.
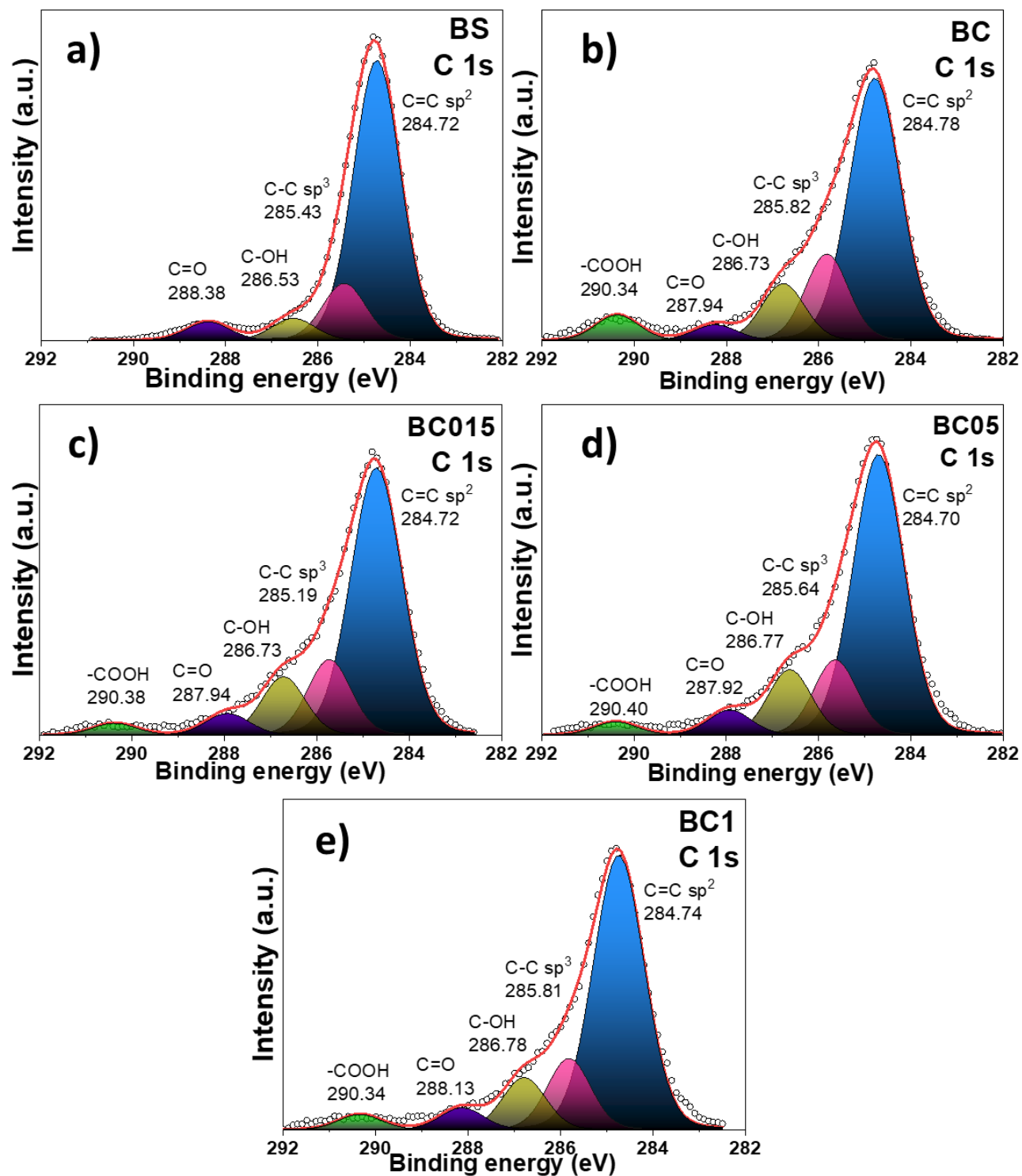
Figure 4.8 High-resolution spectra of a) BS, b) BC, c) BC015, d) BC05, and e) BC1 in the C 1s region.

The high-resolution spectra in the O 1s region (Figure 4.9) show bonds at BS ascribed to C=O, C-OH (with the highest concentration, Table 4.5, and C-O species [139]. Meanwhile, BC, BC015, BC05, and BC1 show the C-OH, C-O, and O-C=O bonds. At these catalysts, the C-O species has the highest concentration (Table 4.5). Therefore, there is an important effect of the functionalization on the formation of new O-species and on their relative concentration, compared to BC.
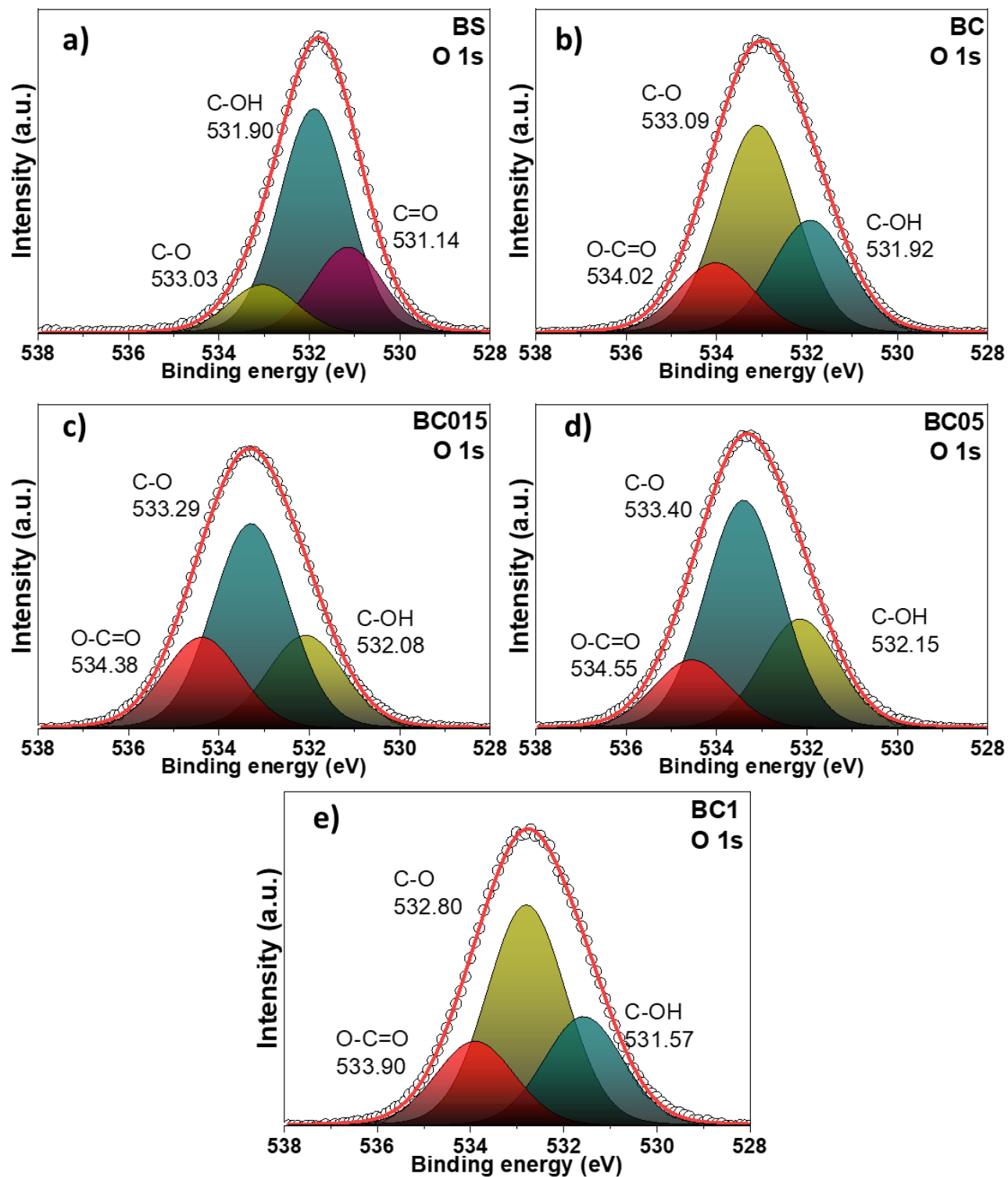
Figure 4.9 High resolution spectra of a) BS, b) BC, c) BC015, d) BC05, and e) BC1 in the O 1s region

Figure 4.10 shows the high-resolution spectra in the N 1s region. At BS, three peaks can be observed, attributed to the N-pyridinic, amine, and N-pyrrolic species at BEs of 398.98, 399.90, and 400.79 eV, respectively (Table 4.5) [137, 126]. It is important to mention that the presence of heteroatoms such as N can improve the catalytic activity of carbon-based catalysts in electrochemical reactions [140]. Moreover, it has been reported that N-atoms doping the carbon structure attract electrons, creating a positive charge density on adjacent C-atoms, resulting in highly favorable surface for the adsorption of O-species [141].

Meanwhile, some changes were observed in the N 1s region after the biomass is subjected to pyrolysis. For instance, the signal at ca. 401 eV at BC, BC015, BC05, and BC1 can be ascribed to the N-graphitic species. Additionally, functionalized BC015, BC05, and BC1 show a peak attributed to Si_3N_4 bonds at about 397-398 eV (Table 4.5), demonstrating: i) the relevant effect of pyrolyzing the biomass, and ii) the influence of functionalizing BC with methanol on the development of N-species. Such behavior has been also observed at the FTIR spectra, with the increase on intensity of the N-H bonds due to organic compounds in the ca. 1574-1591 cm^{-1} interval [141].

Moreover, there is an effect of the functionalization on the relative concentration of the N-species. The highest content at BC is that of N-graphitic, while that at BC015 and BC05 is N-pyrrolic. Meanwhile, BC1 shows a higher relative concentration of the amine species.
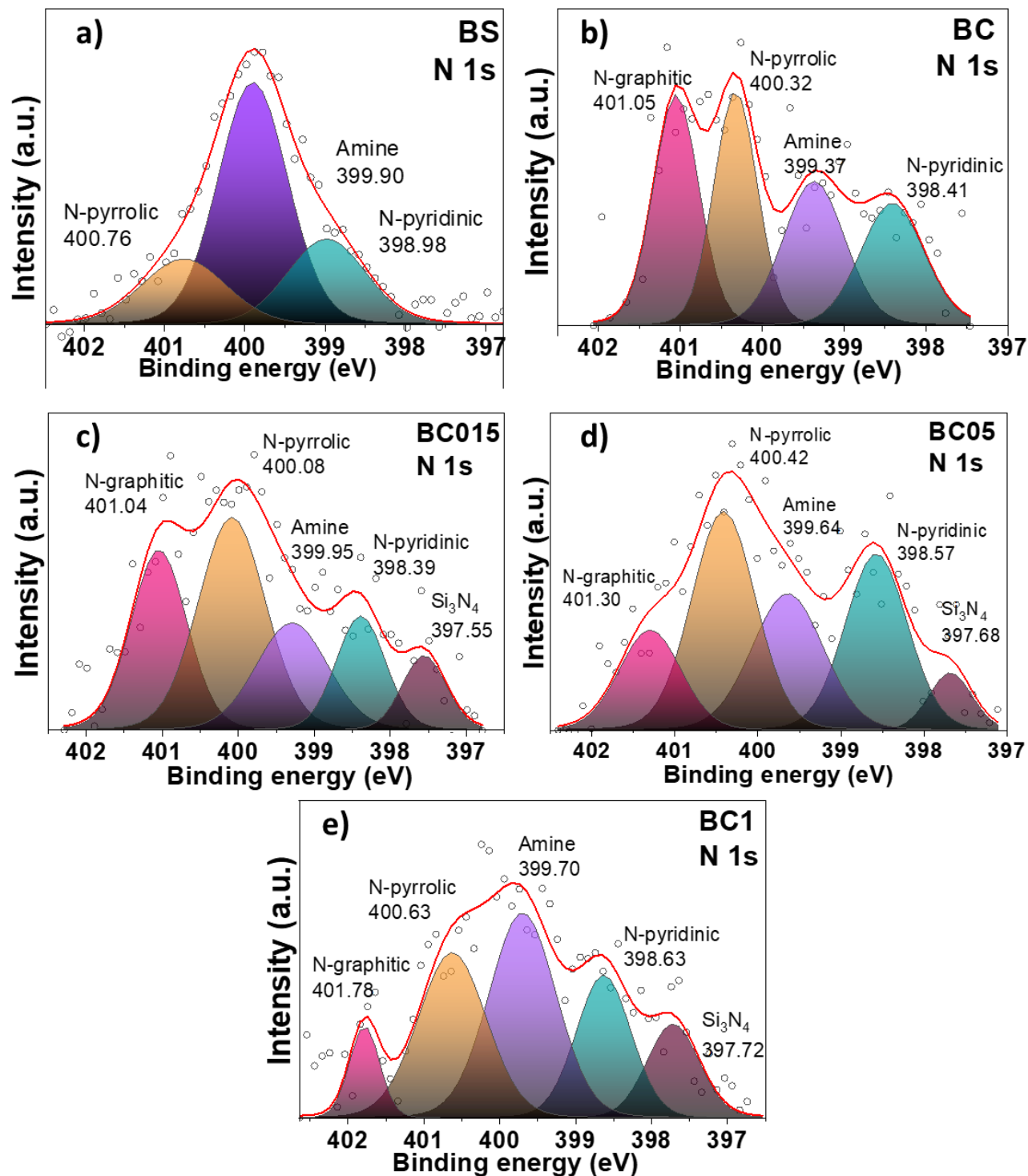
Figure 4.10 High-resolution spectra of a) BS, b) BC, c) BC015, d) BC05, and e) BC1 in the N 1s region.

Figure 4.11 shows the high-resolution spectra in the Si 2p region of BS and the biocarbons. At the former, the Si_3N_4, SiC, and SiO_2 species at BEs of 101.88, 102.68 and 103.88 eV, respectively, have been identified (Table 4.5) [142]. After heat treatment, the Si_3N_4 bonds are no longer observed. Instead, a peak ascribed to silicates (SiO_x) is detected at about 104-105 eV at BC, BC015, BC05, and BC1, being the species with the highest relative concentration.

The differences between BS and the biocarbons, and among the BC series of catalysts, are thus attributed to the important effect of pyrolysis and functionalization on their surface chemical composition. These results confirm that the catalysts obtained from sewage sludge have several heteroatoms on their surface chemistry, the presence of which has been reported to enhance the electrochemical performance of these type of structures in several applications.
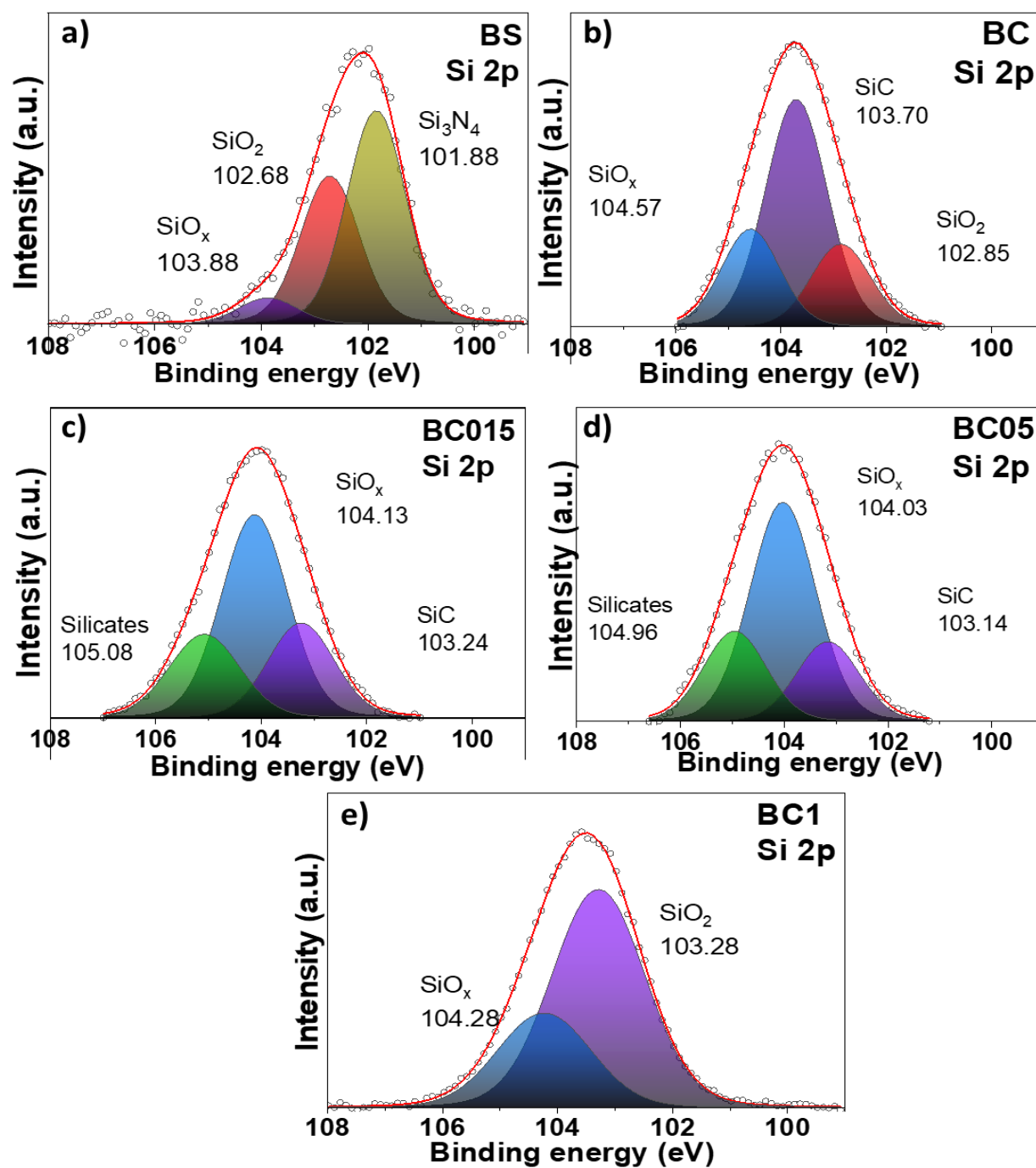
Figure 4.11 High-resolution spectra of a) BS, b) BC, c) BC015, d) BC05, and e) BC1 in the Si 2p region.

Table 4.5 XPS data of BS, BC, BC015, BC05, and BC1.

CATALYST	STATE	SPECIES	BE (eV)	COMPOSITION (at%)
BS	C 1s	C=C sp^2	284.72	75.80
		C-C sp^3	285.43	14.10
		C-OH	286.53	5.40
		C=O	288.38	4.60
	O 1s	C=O	531.14	24.00
		C-OH	531.90	62.40
		C-O	533.03	13.60
	N 1s	N-pyridinc	398.88	23.10
		Amine	399.90	57.90
		N-pyrrolic	400.76	19.00
	Si 2p	Si$_3$N$_4$	101.88	55.20
		SiO$_2$	102.68	38.10
		SiC	103.88	6.70
BC	C 1s	C=C sp^2	284.78	62.80
		C-C sp^3	285.82	17.50
		C-OH	286.77	11.50
		C=O	284.24	3.10
		COOH	290.37	5.10
	O 1s	C-OH	531.92	28.90
		C-O	533.09	53.10
		O-C=O	534.02	18.00
	N 1s	N-pyridinc	398.41	20.80
		Amine	399.37	13.90
		N-pyrrolic	400.32	27.20
		N-graphitic	401.05	28.20
	Si 2p	SiO$_2$	102.85	19.90
		SiC	103.70	57.00
		SiO$_x$	104.57	23.10
BC015	C 1s	C=C sp^2	284.72	65.40
		C-C sp^3	285.74	15.60

		C-OH	286.73	12.10
		C=O	287.94	4.50
		COOH	290.38	2.40
	O 1s	C-OH	532.08	24.00
		C-O	533.29	52.60
		O-C=O	534.38	23.40
	N 1s	Si_3N_4	397.55	8.00
		N-pyridinc	398.39	13.70
		Amine	399.95	18.80
		N-pyrrolic	400.08	34.90
		N-graphitic	401.04	24.60
	Si 2p	SiC	103.24	24.40
		SiO_x	104.13	52.60
		Silicates	105.08	22.90
BC05	C 1s	$C=C\ sp^2$	284.70	65.00
		$C-C\ sp^3$	285.64	14.80
		C-OH	286.63	12.80
		C=O	287.92	4.90
		COOH	290.40	2.60
	O 1s	C-OH	532.15	26.90
		C-O	533.40	56.10
		O-C=O	534.55	16.90
	N 1s	Si_3N_4	397.68	5.70
		N-pyridinc	398.57	25.30
		Amine	399.64	22.60
		N-pyrrolic	400.42	32.20
		N-graphitic	401.30	14.30
	Si 2p	SiC	103.14	19.90
		SiO_x	104.03	57.50
		Silicates	104.96	22.60
BC1	C 1s	$C=C\ sp^2$	284.74	66.90
		$C-C\ sp^3$	285.81	14.70
		C-OH	286.78	10.80
		C=O	288.13	4.50

	COOH	290.34	3.10
O 1s	C-OH	531.14	24.00
	C-O	531.90	62.40
	O-C=O	533.03	13.60
N 1s	Si_3N_4	397.72	12.10
	N-pyridinc	398.63	19.30
	Amine	399.70	34.00
	N-pyrrolic	400.63	27.80
	N-graphitic	401.78	6.80
Si 2p	SiC	103.28	69.60
	SiO_x	104.28	30.40

4.1.11 Morphology of bioanodes

Figure 4.12 shows SEM micrographs of the bioanodes: a-b) BC + *B. subtilis*, c-d) BC015 + *B. subtilis*, e-f) BC05 + *B. subtilis*, and g-h) BC1 + *B. subtilis*. The bacillar morphology of the bacteria and the biofilm grown on the carbonaceous materials, forming a web-like matrix having fibrillar networks is clearly observed [55]. Such features are commonly found in biofilms developed by *B. subtilis* on biocarbons [108, 143] suggest a good biocompatibility between the elements forming the bioanode.
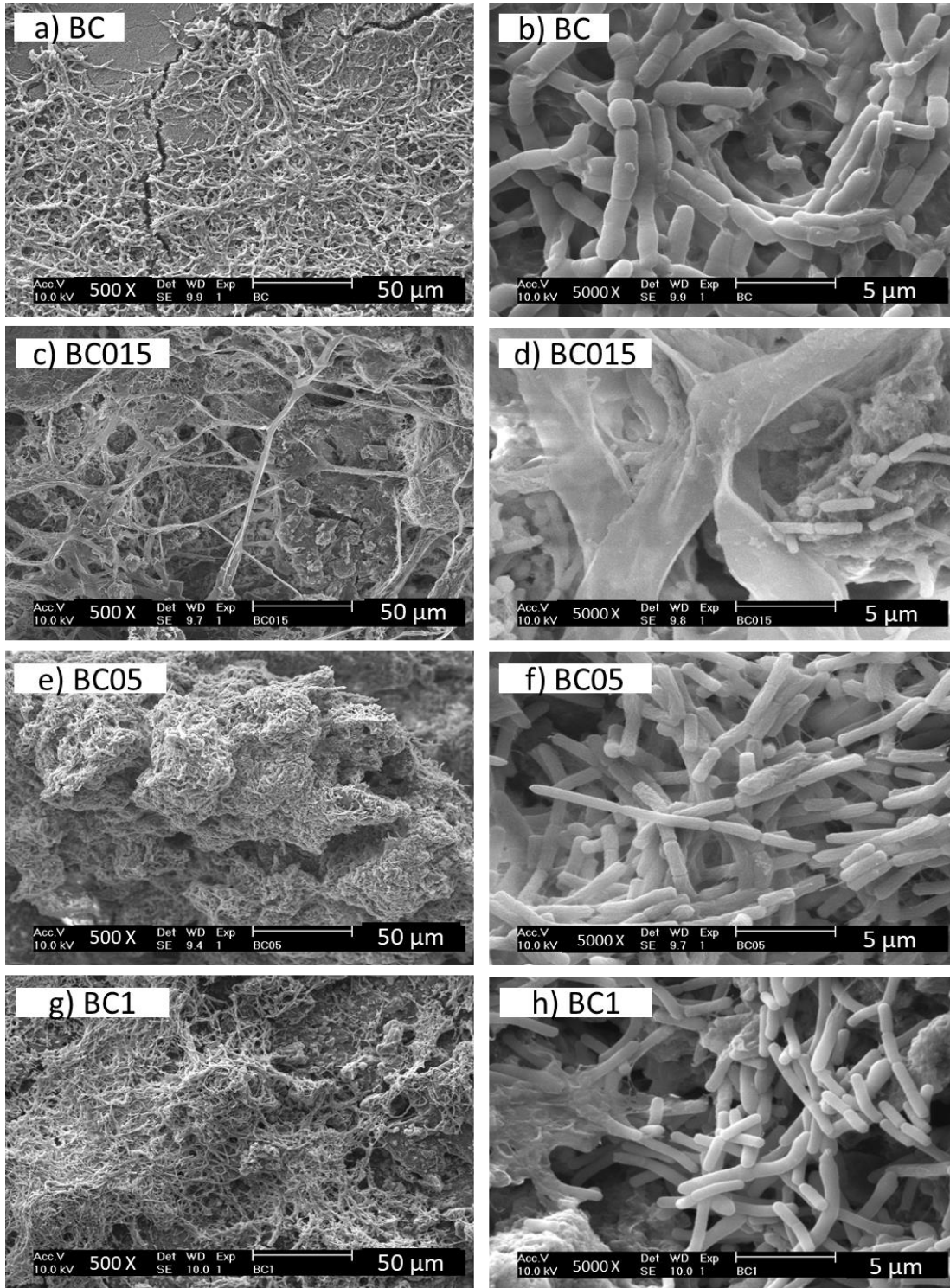
Figure 4.12 Low and high magnification SEM micrographs of a-b) BC, c-d) BC015, e-f) BC05, and g-h) BC1, having a biofilm of *B. subtilis*.

4.2 Electrochemical characterization in half cell

The CVs of the anodes containing a catalyst layer of the BC, BC015, BC05, and BC1 catalysts in PWW (pH 7.1) are shown in Figure 4.13. BC shows a quasi-rectangular CV typical of carbonaceous materials. Meanwhile, the shape of the functionalized BC catalysts changes, indicating a variation in the adsorption/desorption mechanism of species, nevertheless maintaining a quasi-capacitive behavior.

The j values generated by the functionalized BC is higher than that of non-functionalized BC, indicating that the functionalization with methanol enhances the catalytic activity of BC in PWW. Among the catalysts, BC05 delivers the highest j values over the potential scanned.
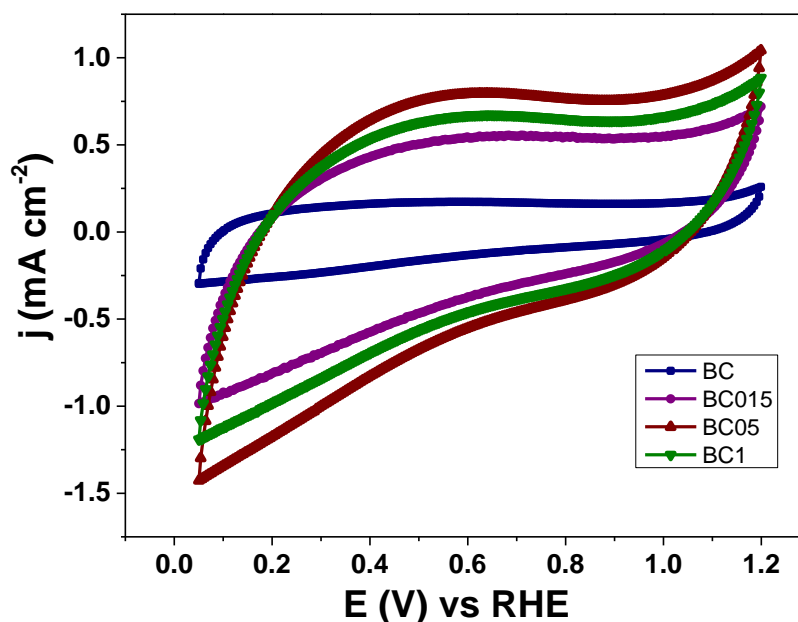
Figure 4.13 CVs of BC, BC015, BC05, and BC1, Substrate: PWW (pH= 7.1). Scan rate: 20 mV s^{-1}.

4.2.1 Electrochemical characterization of BC bioanodes

The CVs of the a) BC + *B. subtilis*, b) BC015 + *B. subtilis*, c) BC05 + *B. subtilis*, and BC1 + *B. subtilis* bioanodes in PWW with pH= 7.1 are shown in Figure 4.14. For comparison purposes, the CVs of the anodes (i.e., without EAM biofilm) are also depicted in the Figure. As can be seen, the shape and slope of the CVs of BC + *B. subtilis* and BC015 + *B. subtilis*

changes due to the presence of the EAM biofilm, delivering higher j values at the most positive and negative potentials than their anode counterparts, and demonstrating enhanced bioelectrochemical behavior.

It has been reported that higher j values in the anodic direction are due to the faster oxidation reactions and/or electron transfer, while an increase in the cathodic scan can be ascribed to a lower accumulation of metabolic intermediates [108]. These results show that the functionalization with methanol 0.15 M has a positive effect in the bioelectrochemical behavior of both, BC and OMC catalysts (see the previous Chapter).

Meanwhile, the BC05 + *B. subtilis* and BC1 + *B. subtilis* bioanodes generate lower *j* values compared to their corresponding anodes, suggesting a poor biocompatibility between catalyst and EAM. Therefore, the BC + *B. subtilis* and BC015 + *B. subtilis* bioanodes have been selected for the next part of the electrochemical evaluation.
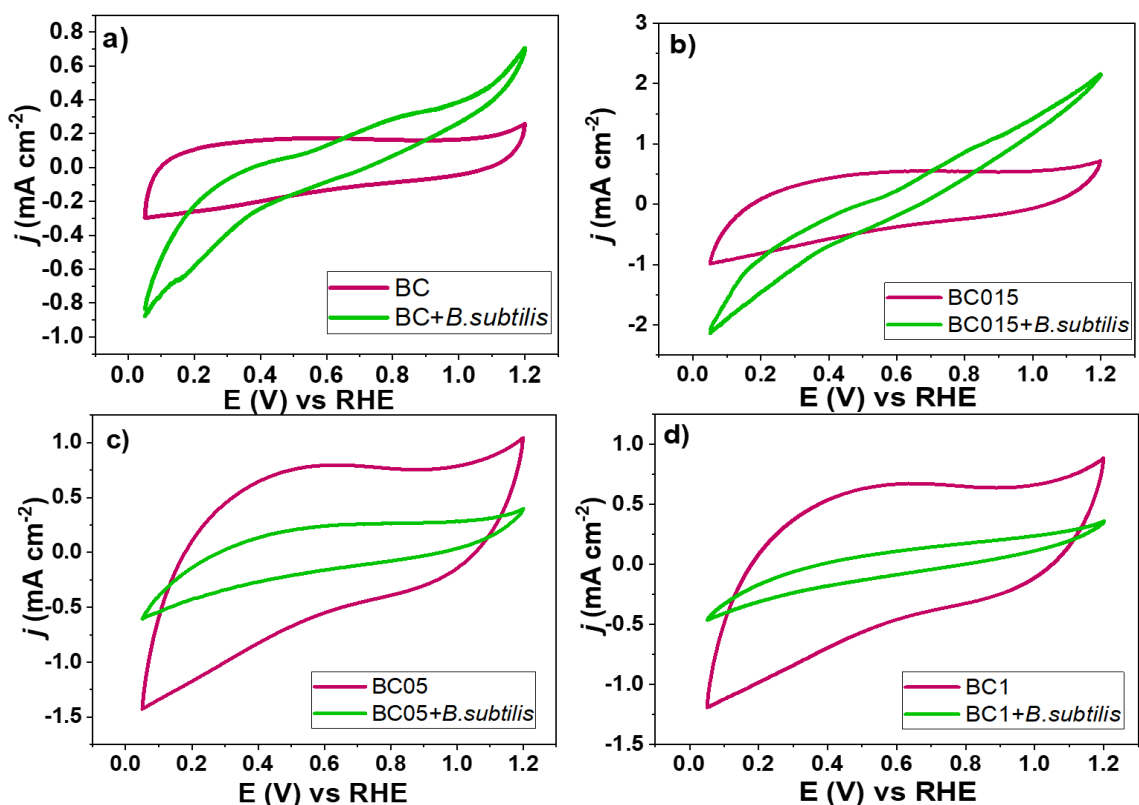
Figure 4.14 CVs showing a comparison of the catalytic activity of the a) BC + *B. subtilis*, b) BC015 + *B. subtilis*, c) BC05 + *B. subtilis*, and BC1 + *B. subtilis* bioanodes with their corresponding anodes. Substrate: PWW (pH= 7.1). Scan rate: 20 mV s^{-1}.

4.2.2 Performance of bioanodes in the MFC

Figure 4.15 shows the a) polarization and b) power density curves of the MFC equipped with the BC + *B. subtilis* bioanode, with PWW as the substrate, tested at Days 0, 3 and 7. At Day 0, the OCV is 0.383 V, delivering a maximum j of 82.64 mA m^{-2}, with P_{cell}= 5.48 mW m^{-2} (Table 4.6). After 3 days of operation, the performance decreases in terms of OCV, but the MFC generates a higher j compared to Day 1, delivering P_{cell}= 10.61 mW m^{-2}. At Day 7 of the test, the OCV and j values decrease compared to Day 3, producing a P_{cell} of 6.40 mW m^{-2}. Such decrease in bioelectrochemical activity can be attributed to the immature biofilm presented by this date, when the bioanode is enough mature could develop an adequate redox enzyme and could generate higher current densities [110].
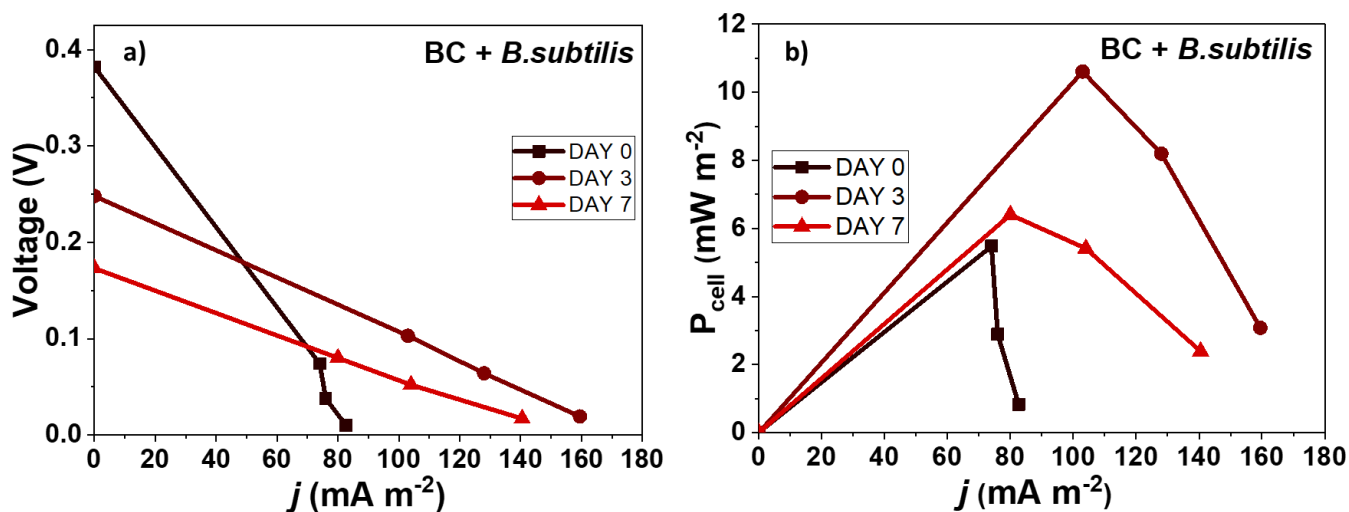
Figure 4.15 a) V-j and b) P_{cell}-j curves of the MFC equipped with the BC + *B. subtilis* bioanode at Days 0, 3 and 7. Membrane: Nafion 117. Cathode: Pt/C. Anode substrate: PWW. Cathode electrolyte: O2-saturated phosphate buffer solution. T_{cell}: ambient.

Figure 4.16 shows the a) polarization and b) power density curves of the MFC equipped with the BC015 + *B. subtilis* bioanode, also with PWW as the substrate, at 0, 3 and 7 days of testing. At Day 0, the OCV is 0.417 V, delivering a maximum j of 74.4 mA m^{-2}, with P_{cell}= 5.04 mW m^{-2} (Table 4.6). After 3 days of operation, the overall performance decays,

delivering P_{cell}= 1.85 mW m^{-2}. One possible explanation for the reduced bioelectrochemical activity is the microbial log phase, a stage where the microorganisms use their metabolic energy to grow in the media instead of producing electricity. This phase occurs during a certain time interval and affects the performance of the system decreasing the power density [110, 111].

At Day 7, the OCV increases compared to Day 3, but remains lower than Day 0. Interestingly, j increases to 148.8 mA m^{-2}, delivering the maximum P_{cell}= 11.66 mW m^{-2}, a possible explanation for the oscillating behavior of the microbial fuel cell (MFC) is that the microorganism is adapting to the environmental conditions and reaching a stationary phase of its growth. This could affect the electron transfer from the PWW to the anode, and, thus, the bioenergy production. Another possibility is that the bioanode, composed of BC015 + *B. subtilis*, is undergoing dynamic changes in its biofilm structure and composition, which could result in the formation or elimination of other bacteria that influence the electrochemical performance of the MFC, decreasing the power density [108, 143].
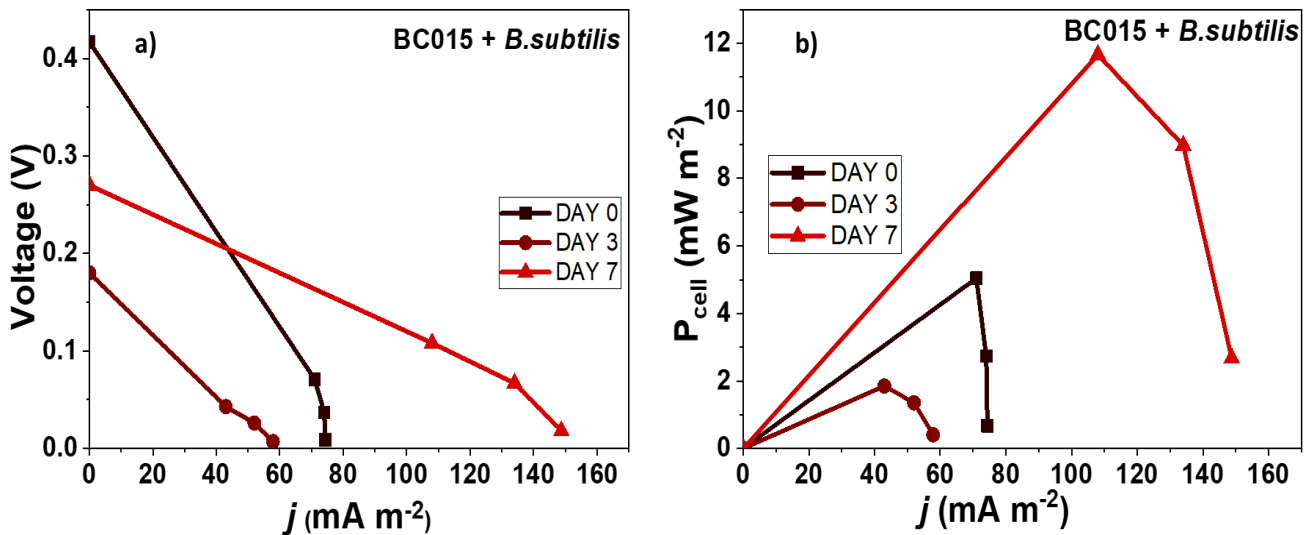
Figure 4.16 a) V-j and b) P_{cell}-j curves of the MFC equipped with the BC015 + B. subtilis bioanode at Days 0, 3 and 7. Membrane: Nafion 117. Cathode: Pt/C. Anode substrate: PWW. Cathode electrolyte: O$_2$-saturated phosphate buffer solution. T_{cell}: ambient.

A comparison of the performance of the BC + *B. subtilis* and BC015 + *B. subtilis* bioanodes show that the highest OCV is generated in both cases at Day 0, with a similar P_{cell} (Table 4.6). Afterwards, BC + *B. subtilis* shows a higher performance at Day 3 compared to Day 7, while the opposite is observed for BC015 + *B. subtilis*. Therefore, the adaptation, growth, and stability of the EAM is different for both catalysts. Thus, the highest P_{cell} is obtained at Day 3 in the case of BC + *B. subtilis*, while Day 7 is the most performing time at BC015 + *B. subtilis*. The P_{cell} delivered at Day 7 with BC015 + *B. subtilis* is the highest from the MFC equipped with a biocarbon catalyst (Table 4.6).

Table 4.6. Parameters of the MFC operating with the BC + *B. subtilis* and BC015 + *B. subtilis* bioanodes, with PWW as the substrate.

Bioanode	V_{cell} (V)			j (mA m^{-2})			P_{cell} (mW m^{-2})		
	Day 0	Day 3	Day 7	Day 0	Day 3	Day 7	Day 0	Day 3	Day 7
BC + *B. subtilis*	0.38	0.24	0.17	82.64	174.6	140.5	5.48	10.61	6.4
BC015 + *B. subtilis*	0.42	0.18	0.27	74.4	57.9	148.8	5.04	1.85	11.6

5. Properties of Pharmaceutical Wastewater (PWW)

5.1 Determination of settleable solids

Table 5.1 depicts the settleable solids determined from 3 samples of PWW, at 10 and 60 min. The Mexican norm NOM-073-ECOL-1994 [144], stipulates that the maximum quantity of settleable solids that could be discharged to effluents of water is 150 mgL^{-1} which is 0.15 mLL^{-1}. The results of the PWW collected here are above such limit, confirming the importance of treatment of PWW.

Table 5.1 Settleable solids of PWW

PWW sample	Settleable solids Time (min)	
	10	60
S1	54.0 mL L^{-1}	42.0 mL L^{-1}
S2	28.0 mL L^{-1}	23.5 mL L^{-1}
S3	13.0 mL L^{-1}	12.5 mL L^{-1}

5.2 Physicochemical characterization

Table 5.2 shows the physicochemical parameters of PWW. It is interesting to note that some values differ from our previous research [96, 145]. For instance, the pH is 7.10 in this study, compared to 9.6 before. Even more, the Chemical Oxygen Demand (COD) is ca. 14,200, lower than the 27,603 reported previously by the lab group [143]. The differences have been ascribed to the type of chemicals produced by the company that provided the samples, i.e., more production of penicillin before versus mainly ampicillin now (personal communication).

Table 5.2 Properties of Pharmaceutical Wastewater

Parameters	Value
pH	7.10
Specific conductance (mS cm^{-1})	29.22
Oxidation and Reduction Potential (mV)	53.40
Resistance (ohm cm^{-1})	52.79
Temperature (°C)	23.37
Chemical Oxygen Demand (mg L^{-1})	14191.51

Tables 5.3 and 5.4 show some of the properties of determined at Days 0 and 7 using the OMC + *B. subtilis* and OMC015 + *B. subtilis* bioanodes. Overall, the pH value increases from Day 0 to Day 7 with the four bioanodes, becoming more alkaline, an indication of the bioelectrochemical performance of B. subtilis in basic media [108]. In the case of the specific conductance, it suffers slight variations. Meanwhile, the redox potential which is used to describe the overall reducing or oxidizing capacity of a system. In well-oxidized water, if oxygen concentrations remain above ~1 mg O_2 L^{-1}, the redox potential will be highly positive, reaching values above 300-500 mV. Microbial mediated redox processes can decrease the redox potential to values as low as -300 mV.

Redox potential is a measure of how easily a system can transfer electrons. It indicates whether a system is more likely to reduce or oxidize other substances. In water with high oxygen levels, such as well-oxidized water, the redox potential is high and positive, meaning that the system can easily oxidize other substances. However, in water with low oxygen levels, such as water influenced by microbial activity, the redox potential is low and negative, meaning that the system can easily reduce other substances. [146]. Even though the values of redox potential show no trend at the four bioanodes, at the Days 7 it has values as low as -46.23 mV, indicating the mediated processes at the MFC. Temperature and resistance of the MFC also show slight variations.

Table 5.3 Properties of PWW at Days 0 and 7 using the OMC + *B. subtilis* and OMC015 + *B. subtilis* bioanodes in the MFC.

Parameter	BIOANODE			
	OMC + *B. subtilis*		OMC015 + *B. subtilis*	
	DAY 0	DAY 7	DAY 0	DAY 7
pH	7.18 ± 0.01¥	8.01 ± 0.01	7.04 ± 0.01	8.07 ± 0.01
Specific conductance (mS cm^{-1})	18.73 ± 0.19	19.37 ± 0.06	16.90 ± 0.09	17.73 ± 0.12
Redox potential (mV)	1.13 ± 0.60	-42.43 ± 0.31	9.73 ± 0.65	-46.23 ± 0.43
Temperature (°C)	23.43 ± 0.23	24.87 ± 0.21	22.03 ± 0.35	28.23 ± 0.06
Resistance (ohm cm^{-1})	53.39 ± 0.54	51.65 ± 0.18	59.19 ± 0.33	56.23 ± 0.08

¥Std deviation

Table 5.4 Properties of PWW at Days 0 and 7 using the BC + *B. subtilis* and BC015 + *B. subtilis* bioanodes in the MFC.

Parameter	BIOANODE			
	BC + *B. subtilis*		BC015 + *B. subtilis*	
	DAY 0	DAY 7	DAY 0	DAY 7
pH	7.10 ± 0.01¥	7.84 ± 0.01	7.19 ± 0.01	7.91 ± 0.01
Specific conductance (mS cm^{-1})	18.86 ± 0.14	20.04 ± 0.06	19.19 ± 0.07	19.00 ± 0.09
Redox potential (mV)	5.43 ± 0.38	-37.40 ± 0.17	-0.10 ± 0.60	-38.67 ± 0.31
Temperature (°C)	21.40 ± 0.00	25 ± 0.00	20.33 ± 0.15	27.43 ± 0.12
Resistance (ohm cm^{-1})	52.79 ± 0.00	49.98 ± 0.04	52.09 ± 0.19	52.64 0.25

¥Std deviation

5.3 Chemical Oxygen Demand (COD) of PWW in the MFC

COD is defined as the amount of oxygen equivalents consumed in the chemical oxidation of organic matter by a strong oxidant (e.g., potassium dichromate).

The principle of COD detection is that nearly all organic compounds can be fully oxidized to carbon dioxide using a strong oxidizing agent under acidic conditions. The COD detection is used to quantify the number of organics in water. A relatively high COD value indicates a high-water pollution by organic matter [147].

Table 5.5 depict the COD values from the PWW in the MFC, using the different bioanodes. The results show that OMC015 + *B. subtilis*, BC + *B. subtilis*, and BC015 + *B. subtilis* promote a decrease in COD at Day 7, indicating the oxidation of organic compounds in the PWW by the bacteria. The effect is more evident at OMC015 + *B. subtilis* and BC + *B. subtilis*. Meanwhile, the OMC + *B. subtilis* bioanode shows an opposite effect, without degradation of organic compounds in the PWW. The BC + *B. subtilis* bioanode has the highest performance in terms of COD removal, with a 12% decrease when comparing Day 7 to Day 1.

Table 5.5 Determination of Chemical Oxygen Demand measurements

Bioanode	COD mg L^{-1}		
	DAY 0	DAY 3	DAY 7
OMC + *B. subtilis*	13861.59 ± 253.74$^{¥}$	14644.65 ± 645.06	21900.93 ± 8972.55
OMC015 + *B. subtilis*	14845.13 ± 4645.43	11953.47 ± 1684.16	12479.78 ± 4558.51
BC + *B. subtilis*	14448.69 ± 1471.05	14241.19 ± 524.20	11413.49 ± 153.96
BC015 + *B. subtilis*	12558.12 ± 432.17	14049.15 ± 1011.07	12308.83 ± 573.71

$^{¥}$Std. Deviation

6. Conclusions

Conclusions

- The BC series of catalysts presented several heteroatoms as nitrogen species which are demonstrated enhance the electrochemical behavior of the carbonaceous materials.

- The pyrolysis treatment modified the surface chemical composition of BC, compared to BS, forming nitrogen species which enhance electrochemical behavior of the BC materials. These modifications were proved with Raman, FTIR, and XRD techniques.

- The surface functionalization with methanol influenced the surface chemical composition of the BC and OMC series of catalysts, corroborated with XPS detecting the presence of -OH functional groups on the surface of the materials.

- Functionalization with methanol increased the relative concentration of the nitrogen pyrrolic species at BC015, BC05 and BC1, compared to BC, which could enhance the electrochemical behavior.

- All the carbonaceous materials presented a biofilm formed over the bioanode, showing the biocompatibility between the material and the bacteria *B. subtilis*.

- The current densities obtained from the bioanodes were observed between the day 3 and the day 7 of the MFC experiments, proving the relationship between the bacteria growing in the PWW and the electron transfer process from the bioanode.

- The four materials selected (OMC, OMC015, BC, and BC015) to forming the bioanodes were capable to generate higher current densities compared to the other functionalized carbon materials.

- The OMC015, in the day 3 of the experiment, was the material which delivered the higher current density, compared to the other four tested materials, due its chemical composition and biocompatibility with the bacteria.

- The BC bioanode present a comparable current density and was capable to degrade organic compounds from the PWW.

7. References

References

[1] K.O. Callaghan, Technologies for the utilization of biogenic waste in the bio-economy, Food Chem. (2016) 2-11.

[2] S. García-Mayagoitia, F. Fernández-Luqueño, D. Morales-Acosta, N.M. Sánchez-Padilla, J.C. Carrillo-Rodríguez, I.L. Alonso-Lemus, F.J. Rodríguez-Varela. Evaluation of Order Mesoporus Carbon as Anode for Microbial Fuel Cells Applications. ECS Trans. 77 (2017) 1351-1357.

[3] H. Hassan, B. Jin, E. Donner, S. Vasileiadis, C. Saint, S. Dai. Microbial community and bioelectrochemical activities in MFC for degrading phenol and producing electricity: Microbial consortia could make differences. Chem Eng J. 332 (2018) 647-657.

[4] J. Xiong, M. Hu, X. Li, H. Li, X. Liu, G. Cao, W. Li. Porous graphite: A facile synthesis from ferrous gluconate and excellent performance as anode electrocatalyst of microbial fuel cell. 2018, Biosens Bioelectron. 109 (2018) 116-122.

[5] F. Nourbakhsh, M. Pazouki, M. Mohsennia. Impact of modified electrodes on boosting power density of microbial fuel cell for effective domestic wastewater treatment: A case study of Tehran. J Fuel Chem Technol. 45 (2017) 871-879.

[6] V.K. Tyagi, S.L. Lo. Sludge: A waste or renewable source for energy and resources recovery? Renew Sust Energy Rev. 25 (2013) 708-728.

[7] Z. Ahmad, L. Yao, J. Wang, D. Gang, F. Islam, Q. Lian, M. Zappi. Neodymium Embedded Ordered Mesoporous Carbon (OMC) for Enhanced Adsorption of Sunset Yellow: Characterizations, Adsorption Study and Adsorption Mechanism. Chem Eng Sci. 359 (2019) 814-826.

[8] T. Minh, J. Song, A. Deb, L. Cha, V. Srivastava and M. Sillanpää. Biochar based catalysts for the abatement of emerging pollutants: A review. Chem Eng J, 394, 124856 (2020) 1-25.

[9] Z. Ismail, A. Habeeb. Experimental and modeling study of simultaneous power generation and pharmaceutical wastewater treatment in microbial fuel cell based on mobilized biofilm bearers. Renew Energ. 101 (2017) 1256-1265.

[10] S. Lakhani, D. Acharya, R. Sakariya, D. Sharma, P. Patel, M. Shah and M. Prajapati. A comprehensive study of bioremediation for pharmaceutical wastewater treatment. Cleaner Chem Eng, 4, 100073 (2022) 1-10.

[11] T. Tommasi, G. Lombardelli. Energy sustainability of Microbial Fuel Cell (MFC): A case study., J Power Sources. 356 (2017) 448-447.

[12] V. Sharma, P.P. Kundu. Biocatalysts in microbial fuel cells. Enzyme Microb Tech. 47 (2010) 179-188.

[13] V. Nimje, C. Chen, C. Chen, J. Jean, A. Reddy, C. Fan, H. Liu and J. Chen. Stable and high energy generation by a strain of *Bacillus subtilis* in a microbial fuel cell. J Power Sources. 190, 2 (2009) 258-263.

[14] K. Elsaid, E. Sayed, M. Abdelkareem, A. Baroutaji y A. Olabi. Environmental impact of desalination processes: Mitigation and control strategies., Sci. Total Environ. 740, 140125 (2020) 1-16.

[15] T. Wilberforce, E. Sayed, M. Abdelkareem, K. Elsaid y A. Olabi. Value added products from wastewater using biolectrochemical systems: Current trends and perspectives. J. Water Process. Eng. 39, 101737 (2021) 1-17.

[16] M. Potter. Electrical effects accompanying the decomposition of organic compounds. Proc. Royal Soc. B. 84, 571, (1911) 260-276.

[17] E. Chingate-Barbosa. Simulación de una cámara anódica y el efecto de su composición sobre la eficiencia de una Celda de Combustible Microbiana., Bogotá, Colombia: Universidad Nacional de Colombia, (2019).

[18] T. Ida and B. Mandal. Microbial fuel cell design, application and performance: A review. Mater Today Proc. 76 (2023) 88-94.

[19] S. Roller, H. Bennetto, G. Delaney, J. Mason, J. Stirling y C. Thurston. Electron-transfer Coupling in Micorbial Fuel Cells: 1. Comparison of Redox-mediator Reduction Rates and Respiratory Rates of Bacteria. J Chem Tech Biotechnol. 34B(1984) 3-12.

[20] B. Kim, D. Park, P. Shin, I. Chang y H. Kim. Mediator-Less Biofuel Cell. United States Patente 5976719, 2 November 1999.

[21] D. Holzman. Microbe Power! Environ Health Perspect. 113, 11(2005) A754-757.

[22] B. Logan, D. Call, S. Cheng, H. Hamelers, T. Sleutels, A. Jeremiasse, R. Rozendal. Microbial Electrolysis Cells for High Yield Hidrogen Gas Production from Organic Matter. J Am Chem Soc. 42,23 (2008) 8630-8640.

[23] C. Moore, S. Minteer, R. Martin. Microchip-Based Ethanol/Oxygen Biofuel Cell. Lab Chip. 5 (2005) 218-225.

[24] A. Pandit, R. Mahadevan. In *silico* Characterization of Microbial Electrosynthesis for Metabolic Engineering of Biochemicals. Microb Cell Fact. 10, 76 (2011) 1-14.

[25] T. Sleutels, A. Ter Heijne, C. Buisman, H. Hamelers. Bioelectrochemical Systems: An Outlook for PracticalApplications. Chem Sus Chem. 5 (2012) 1012-1019.

[26] T. Krieg, A. Sydow, U. Schröder, J. Schrader, D. Holtman. Reactor Concepts for Bioelectrochemical Syntheses and Energy Conversion. Trends Biotechnol. 32, 12 (2014) 645-655.

[27] I. Gajda, J. Greenman, I. Ieropoulos. Recent Advancements in Real-World Microbial Fuel Cell Applications. Curr Opin Electrochem. 11 (2018)78-83.

[28] N. Tabassum, N. Islam and S. Ahmed. Progress in microbial fuel cells for sustainable management of industrial effluents. Process Biochem. 106 (2021) 20-41.

[29] L. Hong, S. Cheng, L. Huang, B. Logan. Scale-up of Membrane-free Single-chamber Microbial Fuel Cell. J Power Sources. 179, 1 (2008) 274-279.

[30] P. Aelterman, K. Rabaey, H. The Pham, N. Boon, W. Verstraete. Continuous Electricity Generation at High Voltages and Currents Using Stacked Microbial Fuel Cells. Environ Sci Technol 51 (2006) 3388-3394.

[31] L. Zhuang, Y. Yuan, Y. Wang, S. Zhou. Long-term Evaluation of a 10-liter Serpentine-type Microbial Fuel Cell Stack Treating Brewery Wastewater. Bioresour Technol. 123 (2012) 406-412.

[32] N. Gao, Y. Fan, Y. Qiu, W. Geier, H. Liu. Novel Trickling MIcrobial Fuel Cells for Electricity Generation from Wastewater. Chemosphere. 248, 126058 (2020) 1-7.

[33] M. Blatter, L. Delabays, C. Furrer, G. Huguenin, C. Cachelin, F. Fisher. Stretched 1000-L MIcrobial Fuel Cell. J Power Sources. 483, nº 229130 (2021) 1-14.

[34] P. Nakhate, H. Patil, V. Shah, T. Salvi, K. Marathe. Process Validation of Integrated Bioelectrochemical and Membrane Reactor for Synchronous Bioenergy Extraction and Sustainable Wastewater Treatment at a Semi-pilot Scale. Biochem Eng J. 151, 107309 (2019) 1-13.

[35] A. Mohamed, H. Zmuda, P. Ha, E. Coats, H. Beyenal. Large-scale Switchable Potentiostatically Controlled/Microbial Fuel Cell Bioelectrochemical Wastewater Treatment System. Bioelectrochemistry. 138, 107724 (2021) 1-12.

[36] W. Zhi, Z. Ge, Z. He, H. Zhang. Methods for understanding microbial community structures and functions in microbial fuel cells: A review., Bioresource Technol. 171 (2014) 461-468.

[37] N. Zhu, X. Chen, T. Zhang, P. Wu, P. Li, J. Wu. Improved performance of membrane free single-chamber air-cathode microbial fuel cells with nitric acid and ethylenediamine surface modified activated carbon fiber felt anodes, Bioresource Technol. 102 (2011) 422-426.

[38] R. Ryoo, S. Hoon Jooy, S. Jun, Synthesis of highly ordered carbon molecular Sieves via Template mediated structural transformation. J Phys Chem B. 103 (1999) 7743-7746.

[39] D. Morales-Acosta, F.J. Rodríguez-Varela, R. Benavides. Template-free synthesis of ordered mesoporous carbon: Application as support of highly active Pt nanoparticles for the oxidation of organic fuels. Int J Hydrogen Energ. 41 (2016) 3387-3398.

[40] S. Mohan, S. Varjani and A. Pandey. Microbial Fuel Cell Configurations: An Overview. Microbial Electrochemical Technology. Elsevier. (2018) 407-435.

[41] F. Harnisch, U. Schröder, Selectivity versus mobility: separation of anode and cathode in microbial bioelectrochemical systems, Chem Sus Chem, 2 (2009) 921-926.

[42] X. Zhang, S. Cheng, X. Wang, X. Huang, B.E. Logan. Separator characteristics for increasing performance of microbial fuel cells. Environ Sci Technol. 43 (2009) 8456-8461

[43] S. Flimban, S. Hassan, M. Rahman and S.E. Oh. The effect of Nafion membrane fouling on the power generation of a microbial fuel cell. Int J Hydrogen Energ. 30 (2018) 1-9.

[44] S. Angioni, L. Millia, G. Bruni, C. Tealdi and P. Mustarelli. Improving performances of Nafion based membranes for microbial fuel cells with silica based, organically functionalized mesostructured fillers. J Power Sources. 334 (2016) 120-127.

[45] M. Lu, Y. Qian, L. Huang, X. Xie, and W. Huang. Improving the performance of MIcrobial Fuel Cells through Anode Manipulation. Chem Plus Chem. 80, 8 (2015) 1216-1225.

[46] E. Heidrich, T. Curtis and J. Dolfing. Determination of the Internal Chemical Energy of Wastewater. Environ Sci Technol. 45 (2011) 827-832.

[47] Y. Hindatu, M. Annuar and A. Gumel. Mini-review: Anode modification for improved performance of microbial fuel cell. Renew Sust Energ Rev. 73 (2017) 236-248.

[48] M. Rahimnejad, A. Adhami, S. Darvari, A. Zirepour and S. Oh. Microbial fuel cell as new technology for bioelectricity generation: A review. Alex Eng J. 54 (2015) 745-756.

[49] S. Cheng and B. Logan. Ammonia treatment of carbon clothe anodes to enhance power generation of microbial fuel cells., Electrochem Comm. 9 (2007) 492-496.

[50] E. Koroglu, H. Yoruklu, A. Demir and B. Ozkaya. Chapter 3.9: Scale-Up and Commercialization Issues of the MFCs: Challenges and Implications. Microbial Electrochemical Technology. Elsevier. (2019) 565-583.

[51] Z. Du, H. Li and T. Gu. A state of art review on microbial fuel cells: a promising technology for wastewater treatment and bioenergy. Biotech Adv. 25 (2007) 464-482.

[52] B. Gutarowska and A. Michaelski. Microbial degradation of woven fabrics and protection against biodegradation. INTECH (2012).

[53] A. Mehdinia, E. Zael, A. Jabbari. Multi-walled carbon nanotube/SnO2 nanocomposite: a novel anode material for microbial fuel cells. Electrochim Acta, 130 (2014) 512-518.

[54] K. Dolch, J. Danzer, T. Kabbeck, B. Bierer, J. Erben, A. H. Förster, J. Maisch, P. Nick, S. Kerzenmacher, J. Gescher. Characterization of microbial current production as a function of microbe-electrode-interactions. Bioresource Technol. 157 (2014) 284-292

[55] S. García-Mayagoitia, F. Fernández-Luqueño, D. Morales-Acosta, J. Carrillo-Rodríguez, M. García-Lobato, L. De la Torre-Saenz, I. Alonso-Lemus and F. Rodríguez-Varela. Energy Generation from Pharmaceutical Residual Water in Microbial Fuel Cells Using Ordered Mesoporous Carbon and *Bacillus subtilis* Bioanode. 7 (2019) 12179-12187.

[56] S.H. Joo, S.J. Choi, I. Oh, J. Kwak, Z. Liu, O. Terasaki R. Ruoo. Ordered nanoporous arrays of carbon supporting high dispersions of platinum nanoparticles. Nature, 412 (2001) 169-172.

[57] R. Chávez-Alcázar and F. Rodríguez-Varela, Aplicación de un biocarbón obtenido de losods de aguas residuales comosoporte de nanoestructuras núcleo-coraza Ni@Pt para promover las reacciones de Evolución y de Reducción de Oxígeno. Cinvestav Unidad Saltillo. (2021) 1-84.

[58] A. Torres-Nuñez, F. Rodríguez-Varela and M. Sánchez-Castro, Biocarbones a partir de desechos de ajo (*Allium sativum L.*) y su funcionalización con compuestos organometálicos de Cu como soportes de nanocatalizadores de Pt para las reacciones de Evolución de Hidrógeno y Oxígeno. Cinvestav Unidad Saltillo. (2021) 1-96.

[59] J. Lee, K.H. Kim, E.E. Kwon. Biochar as a catalyst. Renew Sust Energ Rev. 77 (2017) 70-79.

[60] A.U. Rajapaksha, S.S. Chen, D.C.W. Tsang, M. Zhang, M. Vithanage, S, Mandal Engineered/designer biochar for contaminant removal/immobilization from soil and water: potential and implication of biochar modification, Chemosphere, 148 (2016) 276-291.

[61] R. Rojas-Remis and L. Mendoza-Espinosa. Utilización de biosólidos para la recurperación energética en México. Rev. P+L. 7, 2 (2012) 74-94.

[62] M. Li, Y. Li, X. Yu, J. Guo, L. Xiang, B. Liu, H. Zhao, M. Xu, N. Feng, P. Yu, Q. Cai, C. Mo. Improved Bio-electricity Production in Bio-electrochemical Reactor for Wastewater Treatment Using Biomass Carbon Derived from Sludge Supported Carbon Felt Anode. Sci Total Environ. 726, 138573 (2020) 1-10.

[63] G. Kumar, V. Sarathi and K. Nahm. Recent Advances and Challenges in the Anode Architecture and Their Modifications for the Applications of Microbial Fuel Cells. Biosens Bioelectron. 43 (2013) 461-475.

[64] K. Rabaey and W. Verstraete. Microbial fuel cells: novel biotechnology for energy generation. Trends biotechnol. 23 (2005) 291-298.

[65] N. Xiao, R. Wu, J. Huang and P. Selvaganapathy. Anode surface modification regulates biofilm community population and the performance of micro-MFC based biochemical oxygen demand sensor. Chem Eng Sci. 221, 115691 (2020) 1-9.

[66] A. Paitier, A. Godain, D. Lyon, N. Haddour, T.M. Vogel. Microbial fuel cell anodic microbial population dynamics during MFC start-up. Biosens Bioelectron, 92 (2017) 357-363.

[67] B.E. Logan, B. Hamelers, R. Rozendal, U. Shröder, J. Keller, S. Freguia, P. Alterman, W. Verstraete, K. Rabaey. Microbial fuel cells: methodology and technology. Environ Sci Technol. 40 (2006) 5181-5192.

[68] J.W. Costerton. Chapter 1. Direct Observations. The Biofilm primer. Springer, Berlin-New York (2007) 70

[69] F. Krackle, I. Vassilev, J.O. Krömer. Microbial electron transport and energy conservation - the foundation for optimizing bioelectrochemical systems. Microbiology. 6, 575 (2015) 1-18.

[70] H. Hassan, B. Jin, S. Dai, T. Ma, C. Saint. Chemical impact of catholytes on *Bacillus subtilis*-catalised microbial fuel cell performance for degrading 2,4-dichlorophenol. Chem Eng J. 301 (2016) 103-114.

[71] A.A.S. Al-Gheethi, N. Ismail. Biodegradation of Pharmaceutical Wastes in Treated Sewage Effluents by Bacillus subtilis 1556WTNC. Environ Process. 1 (2014) 459-481.

[72] A. Franks, K. Nevin. Microbial Fuel Cells, A Current Review. Energies. 3 (2010) 899-919.

[73] M. Zhou, J. Yang, H. Wang, T. Jin, D. Hassett, T. Gu. Chapter 9: Bioelectrochemistry of Microbial Fuel Cells and their Potential Applications in Bioenergy. Bioenergy Research: Advances and Applications. Elsevier. (2014) 131-152.

[74] C. Pfeffer, S. Larsen, J. Song, M. Dong, F. Besenbacher, R. Meyer, K. Kjeldsen, Y. Gorby, M. El-Naggar, K. Leung, A. Schramm, N. Risgaard-Petersen, L. Nielsen. Filamentous Bacteria Transport Electrons Over Centimetre Distances. Nature. 491 (2012) 218-221.

[75] K. Rabaey, J. Rodríguez, L. Blackall, J. Keller, P. Gross, D. Batstone, W. Verstraete, K. Nealson. Micorbial Ecology Meets Electrochemistry: Electricity-Driven and Driving Communities. ISME J. 1 (2007) 9-18.

[76] M. Sun, L. Zhai, W. Li, H. Yu. Harvest and Utilization of Chemical Energy in Wastes by Microbial Fuel Cells. Chem Soc Rev. 45 (2016) 2847-2870.

[77] C. Santoro, C. Arbizzani, B. Erable, I. Ieropoulos. Microbial Fuel Cells: From Fundamentals to Applications. A review. J Power Sources. 356 (2017) 225-244.

[78] D. Harris. Quantitative Chemical Analysis, 8th ed., New York, NY: W. H. Freeman and Company. (2010) 279-392.

[79] S. Jung, J. Lee, Y.K. Park, E. Kwon. Bioelectrochemical Systems for a Circular Bioeconomy. Bioresource Technol. 300, 122748 (2020) 1-9.

[80] D. Pant, G. Van Bogaert, L. Diels, K. Vanbroekhoven. A review of substrates used in microbial fuel cells (MFCs) for sustainable energy production. Bioresource Technol. 101 (2010) 1533-1543.

[81] W. Li, H. Yu and B. Rittmann. Reuse Water Pollutants. Nature. 528 (2015) 29-31.

[82] P. Nakhate, H. Patil, V. Shah, T. Salvi, K. Marathe. Process Validation of Integrated Bioelectrochemical and Membrane Reactor for Synchronous Bioenergy Extraction and Sustainable Wastewater Treatment at a Semi-pilot Scale. Biochem Eng J. 151, 107309 (2019) 1-13.

[83] J. Fornero, M. Rosenbaum, L. Angenent. Electric Power Generation from Municipal, Food, and Animal Wastewaters Using Microbial Fuel Cells. Electroanalysis. 22, (2010) 832-843.

[84] R. Singh Rana, P. Singh, V. Kandari, R. Singh, R. Dobhal, S. Gupta. A review on characterization and bioremediation of pharmaceutical industries´ wastewater: an Indian perspective. Appl Water Sci. 7 (2017) 1-12.

[85] F. López-Valdez, F. Fernández-Luqueño, M. Luna-Guido, R. Marsch, V. Olalde-Portugal , L. Dendooven. Microorganisms in sewage sludge added to an extreme alkaline saline soil affect carbon and nitrogen dynamics. Appl Soil Ecol. 45 (2010) 225-231.

[86] T. Schulze, G. Streck, A. Paschke, Sampling and Conservation. Treatise on Water Science Germany Volume 3. Elsevier. (2011) 131-152.

[87] L. Wang, Y. Wu, Z. You, H. Bao, L. Zhang, J. Wang. Electrochemical impedance spectroscopy (EIS) reveals the role of microbial fuel cell-ceramic membrane bioreactor (MFC-CMBR): Electricity utilization and membrane fouling. Water Res. 222, 118854 (2022) 1-13.

[88] Dirección Nacional de Medio Ambiente. Manual de Procedimientos Analíticos para Aguas y Efluentes. Ministerio de Vivienda, Ordenamiento Territorial y Medio Ambiente (1996).

[89] L. Pawlowski. Standard methods for the examination of water and wastewater, Science of The Total Environment. A. Greenberd, L. Clesceri and A. Eaton, Eds., Water Environment Federation,142 (1994) 227-228.

[90] Secretaría de Economía. Análisis de Agua-Determinación de la demanda química de oxígeno en aguas naturales, residuales y residuales tratadas- método de prueba (NMX-AA-030-SCFI-2001). (2001).

[91] X. Ma, H. Yuan and M. Hu. A Simple Method for Synthesis of Ordered Mesoporous Carbon. Diamond Rel Mat. 98, 107480 (2019) 1-11.

[92] A. Bharti and G. Cheruvally. Influence of various carbon nano-forms as supports for Pt catalyst on proton exchange membrane fuel cell performance. J Power Sources 196 (2017) 196-205.

[93] X. Ma, H. Yuan and M. Hu. A simple method for synthesis of ordered mesoporous carbon. Diam Relat Mater. 98, 107480 (2019) 1-11.

[94] Q. Lian, M. Konggidinata, Z. Ahmad, D. Gang, L. Yao, R. Subramaniam, E. Revellame, W. Holmes and M. Zappi. Combined effects of textural and surface properties of modified ordered mesoporous carbon (OMC) on BTEX adsorption. J Hazardous Materials. 377 (2019) 381-390.

[95] J. Lilloja, M. Mooste, E. Kibena-Põldsepp, A. Sarapuu, A. Kikas, V. Kisand, M. Käärik, J. Kozlova, A. Treshchalov, P. Paiste, J. Aruväli, J. Leis, A. Tamm, S. Holdcroft and K. Tammeveski. Cobalt-, iron- and nitrogen-containing ordered mesoporous carbon-based catalysts for anion-exchange membrane fuel cell cathode. Electrochim Acta. 439, 41676 (2023).

[96] S. García-Mayagoitia, F. Fernández-Luqueño, D. Morales-Acosta, J. Carrillo-Rodríguez, M. García-Lobato, L. De la Torre-Saenz, I. Alonso-Lemus and F. Rodríguez-Varela. Energy Generation from Pharmaceutical Residual Water in Microbial Fuel Cells Using Ordered Mesoporous Carbon and Bacillus Subtilis as Bioanode. ACS Sustain Chem Eng. 7 (2019) 12179-12187.

[97] P. Maziarka, C. Wurzer, P. Arauzo, A. Dieguez-Alonso, O. Masek and F. Ronsse, Do you BET on routine? The reliability of N2 physisorption for the quantitative assessment of biochar's surface area. Chem Eng J. 418, 129234 (2021)1-41.

[98] M. Thommes, K. Kaneko, A. Neimark, J. Olivier, F. Rodríguez-Reinoso, J. Rouquerol and K. Sing. Physisorption of gases, with special reference to the evaluation of surface area and pore size distribution (IUPAC Technical Report). Pure App Chem. 87 (2015) 1051-1069.

[99] X. Kan, F. Song, G. Zhang, G. Zheng, Q. Zhu, F. Liu and L. Jiang. Sustainable design of co-doped ordered mesoporous carbons as efficient and long-lived catalysts for H2S reutilization. Chem Eng Sci, 269, 118483, (2023).

[100] J. Menéndez, A. Arenillas, B. Fidalgo, Y. Fernández, L. Zubizarreta, E. Calvo and J. Bermúdez. Microwave heating processes involving carbon materials. Fuel Process Technol. 91, 1 (2010) 1-8.

[101] C. Weidenthaler, A. Lu, W. Schmidt and F. Schüth. X-ray photoelectron spectroscopic studies of PAN-based ordered mesoporous carbons (OMC). Microporous Mesoporous Mater. 88 (2006) 238-243.

[102] N. Wang, Z. Yu, Y. Zhang, C. Zhu, J. Hu, X. Yang, F. Shi. One-step Direct Synthesis of Ordered Mesoporous Carbon Supported Tungsten Trioxide for Photocatalytic Degradation of Rhodamine B. Mater. 301, 130324 (2021) 1-4.

[103] J. Carrillo-Rodríguez, A. Garay-Tapia, B. Escobar-Morales, J. Escorcia-García, M. Ochoa-Lara, F. Rodríguez-Varela and I. Alonso-Lemus. Insight into the performance and stability of N-doped Ordered Mesoporous Carbon Hollow Spheres for the ORR: Influence of the nitrogen species on their catalytic activity after ADT. Int J Hydrogen Energy. 46, 51 (2021) 26087-26100.

[104] S. Pérez-Rodríguez, D. Sebastián and M. Lázaro. Electrochemical oxidation of ordered mesoporous carbons and the influence of graphitization. Electrochim Acta. 303 (2019) 167-175.

[105] X. Wan, Y. Li, H. Xiao, Y. Pan and J. Liu. Hydrothermal synthesis of nitrogen-doped ordered mesoporous carbon via lysine-assisted self-assembly for efficient CO2 capture. R Soc Chem. 10 (2020) 2932-2941.

[106] N. Patel, D. Rai, D. Chauhan, U. Mishra and B. Bhunia. Carbon Nanotube Based Anodes and Cathodes for Microbial Fuel Cells. Microbial Fuel Cells: Materials and Applications. Materials Research Forum LLC, 46 (2019) 125-150.

[107] J. Modestra and S. Mohan. Bio-electrocatalyzed electron efflux in Gram positive and Gram negative bacteria: an insight into disparity in electron transfer kinetics. RSC adv. 4 (2014) 34045-34055.

[108] O. Duarte-Urbina, F. Rodríguez-Varela, F. Fernández-Luqueño, G. Vargas-Gutiérrez, M. Sánchez-Castro, B. Escobar-Morales and I. Alonso-Lemus. Bioanodes containing catalysts from onion waste and Bacillus subtilis for energy generation from pharmaceutical wastewater in a microbial fuel cell. New Journal of Chemistry, (2021) 12634-12646.

[109] T. Liu, Y. Yu, T. Chen and W. Chen. A Synthetic Microbial Consortium of Shewanella and Bacillus for Enhanced Generation of Bioelectricity. Biotechnol Bioeng. 114, 3 (2017) 526-532.

[110] P. Serra, A. Espíritu-Santo and M. Magrinho. A steady-state electrical model of a microbial fuel cell through multiple-cycle polarization curves. Renew Sustain Energy Rev. 117, 109439 (2020) 1-19.

[111] K. Masoodi, S. Lone and R. Rasool, "Growth of bacterial cultures and preparation of growth curve," in Advanced Methods in Molecular Biology and Biotechnology, Academic Press, 2021, pp. 163-166.

[112] D. Pinto, T. Coradin and C. Laberty-Robert. Effect of anode polarization on biofilm formation and electron transfer in Shewanella oneidensis/graphite fel microbial fuel cells. Bioelectrochemistry, 120 (2018) 1-9.

[113] R. Ramasamy, Z. Ren, M. Mench and J. Regan. Impact of initial biofilm growth on the anode impedance of microbial fuel cells. Biotechnol Bioeng. 101 (2008) 101-108.

[114] L. Lan, J. Li, Q. Feng, L. Zhang, Q. Fu, X. Zhu and Q. Liao. Enhanced current production of the anode modified by microalgae derived nitrogen-rich biocarbon for microbial fuel cells. Int J Hydrogen Energ. 45, 6 (2020) 3833-3839.

[115] A. Manohar, O. Bretschger, K. Nealson and F. Mansfeld. The use of electrochemical impedance spectroscopy (EIS) in the evaluation of the electrochemical properties of a microbial fuel cell. Bioelectrochemistry. 72, 2 (2008) 149-154.

[116] Z. Ren, R. Ramasamy, S. Cloud-Owen, H. Yan, M. Mench and J. Regan. Time-course correlation of biofilm properties and electrochemical performance in single-chamber microbial fuel cells. Bioresource Technol. 102, 1 (2011) 416-421.

[117] Y. Katharria, S. Kumar, F. Singh, J. Pivin, D. Kanjilal. Synthesis of buried SiC using an energetic ion beam. J Phys D Appl Phys. 39 (2006) 3969-3973.

[118] E. Antunes, J. Schumann, G. Brodie, M. Jacob, P. Schneider. Biochar produced from biosolids using a single-mode microwave: characterization and its potential for phosphorus removal. J Environ Manage. 196 (2017) 119-126.

[119] A. Ukwatta, A. Mohajerani, N. Eshtiaghi, S. Setunge. Variation in physical and mechanical properties of fired-clay bricks incorporating ETP biosolids. J Clean Prod. 119 (2016) 76-85.

[120] I. Ismail, G. Singh, P. Smith, S. Kim, J. Yang, S. Talapaneni, A. Vinu. Oxygen Functionalized Porous Activated Biocarbons with High Surface Area Derived from Grape Marc for Enhanced Capture of CO_2 at Elevated-pressure. Carbon. 160 (2020) 113-124.

[121] S. Vaughn, F. Dinelli, J. Kenar, M. Jackson, A. Thomas, S. Peterson. Physical and chemical properties of pyrolyzed biosolids for utilization in sand-based turfgrass rootzones. Waste Manage. 76 (2018) 98-105.

[122] D. Render, T. Samuel, H. King, M. Vig, S. Jeelani, R. Babu, V. Rangari. Biomaterial-Derived Calcium Carbonate Nanoparticles for Enteric Drug Delivery. J Nanomater. 2016, 3170248 (2016) 1-8.

[123] Y. Shen, A. Xie, Z. Chen, W. Xu, H. Yao, S. Li, L. Huang, Z. Wu, X. Kong. Controlled synthesis of calcium carbonate nanocrystals with multimorphologies in different bicontinuos microemulsions. Mat Sci Eng A - Struct. 443 (2007) 95-100.

[124] M. Nash, B. Opayke, Z. Wu, M. Mondeshki, S. Wolf. Simple X-Ray diffraction techniques to identify MG calcite, dolomite and magnesite in tropical coralline algae and assess peak asymmetry. J Sediment Res. 83 (2013) 1084-1098.

[125] J. Harris, I. Mey, M. Hajr, M. Mondeshki, S. Wolf. Pseudomorphic transformation of amorphous calcium carbonate films follow spherulitic growth mechanisms and can give rise to crystal lattice tilting. Cryst Eng Comm. 17 (2015) 6831-6837.

[126] I. Alonso-Lemus, M. Figueroa-Torres, D. Lardizabal-Gutierrez, P. Bartolo-Perez, J. Carrillo-Rodriguez, F. Rodríguez-Varela. Converting chicken manure into highly active N-P co-doped metal-free biocarbon catalysts: effect of chemical treatment on their catalytic activity for the ORR.Sust Energy Fuels. 3 (2019) 1307-1316.

[127] N. Devi, M. Hariram and S. Vivekanadhan. Modification techniques to improve the capacitive performance of biocarbon materials. J Energy Storage. 33, 101870 (2021).

[128] K. Onchoke, C. Franclemont and P. Weatherford. Structural characterization and evaluation of municipal wastewater sludge (biosolids) from two rural wastewater treatment plants in East Texas, USA. Spectrochim Acta Part A: Molecular and Biomolecular Spectroscopy. 204 (2018) 514-524.

[129] L. Deng, H. Yuan, L. Qiang, L. Wang, H. Hu and Y. Chen. Municipal sludge-derived carbon dots-decorated, N-doped hierarchical biocarbon for the electrochemical reduction of carbon dioxide. Resour Conserv Recy. 177, 105980 (2022) 1-10.

[130] P. Larkin, Infrared and Raman Spectroscopy. Principles and Spectral Interpretation. Elsevier (2011).

[131] P. Soler-Rovira, E. Madejón, P. Madejón, C. Plaza. In situ remediation of metal-contaminated soils with organic amendments: Role of humic acids in copper bioavailability. Chemosphere. 79 (2010) 844-849.

[132] S. Jamari, J. Howse. The Effect of the Hydrothermal Carbonization Process on Palm Oil Empty Fruit Bunch. Biomass Bioenerg. 47 (2012) 82-90.

[133] Y. Shao, C. Guizani, P. Grosseau, D. Chaussy, D. Beneventi. Biocarbons from Microfibrillated Cellulose/Lignosulfonate Precursors: A Study of Electrical Conductivity Development During Slow Pyrolysis. Carbon. 129 (2018) 357-366.

[134] G. Singh, J. Lee, R. Bahadur, A. Karakoti, J. Yi and A. Vinu, "Highly graphitized porous biocarbon nanosheets with tuneable Micro-Meso interfaces and enhanced layer spacing for CO2 capture and LIBs," Chem Eng J, vol. 433, no. 134464, pp. 1-11, 2022.

[135] G. Singh, R. Bahadur, J. Lee, I. Kim, A. Ruban, J. Davidraj, D. Semit, A. Karakoti, A. Al Muhtaseb, A. Vinu. Nanoporous activated biocarbons with high surface areas from alligator weed and their excellent performance for CO2 capture at both low and high pressures. Chem Eng J. 406, 126787 (2021) 1-11.

[136] Thermo Fisher Scientific. XPS Elements Table. (2020). [Online]. Available: https://xpssimplified.com/elements/.

[137] R. Wang, C. Wang, Z. Zhao, J. Jia, Q. Jin. Energy recovery from high-ash municipal sewage sludge by hydrothermal carbonization: Fuel characteristics of biosolid products. Energy. 186 (2019) 115848, 1-11.

[138] J. Carrillo-Rodríguez, S. García-Mayagoitia, R. Pérez-Hernández, M. Ochoa-Lara, F. Espinosa-Magaña, F. Fernández-Luqueño, P. Bartolo-Pérez, I. Alonso-Lemus, F. Rodríguez-Varela. Evaluation of the novel Pd-CeO$_{2\text{-NR}}$ electrocatalyst supported on N-doped graphene for the Oxygen Reduction Reaction and its use in a Microbial Fuel Cell. J Power Sources 414 (2019) 103-114.

[139] M. Del Bubba, B. Anachini, Z. Bakari, M. Bruzzoniti, R. Camisa, C. Caprini, L. Checchini, D. Fibbi, A. El Ghadraoui, F. Liguori, S. Orlandini. Physicochemical properties and sorption capacities of sawdust-based biochars and commercial activated carbons towards ethoxylated alkylphenols and their phenolic metabolites in effluent wastewater from textile district. Sci Total Environ.708 (2020) 135217, 1-14.

[140] I. Alonso-Lemus, B. Escobar-Morales, D. Lardizabal-Gutierrez, L. De la Torre-Saenz, P. Quintana-Owen, F.J. Rodríguez-Varela. Short communication: Onion skin waste-

derived biocarbon as alternative non-nobel metal electrocatalyst towards ORR in alkaline media. Int J Hydrogen Energ 44 (2019) 12409-12414.

[141] L. Zhou, P. Fu, D. Wen, Y. Yuan, S. Zhou. Self-Constructed Carbon Nanoparticles-Coated Porous Biocarbon From Plant Moss as Advanced Oxygen Reduction Catalysts. Appl Catal B: Environ. 181 (2016) 635-643.

[142] E. Vereda-Alonso, A. García de Torres, M. Siles-Cordero, J. Cano-Pavón. Quantitative determinations of SiC and SiO2 in new ceramic materials by Fourier transform infrared spectroscopy. Talanta 75 (2008) 424-431.

[143] I. Alonso-Lemus, C. Cobos-Reyes, M. Figueroa-Torres, B. Escobar-Morales, K. Aruna, P. Akash, F. Fernández-Luqueño and F. Rodríguez-Varela. Green Power Generation by Microbial Fuel Cells Using Pharmaceutical Wastewater as Substrate and Electroactive Biofilms (Bacteria/Biocarbon). J Chem.(2022) 1-11.

[144] Instituto Nacional de Ecología, NOM-073-ECOL-1994 Norma Oficial Mexicana que establece los límites máximos permisibles de contaminantes en las descargas de Aguas residuales a Cuerpos receptores provenientes de las Industrias farmacéuticas y farmoquímica, México D.F., 1994.

[145] S. García-Mayagoitia, F. Rodríguez-Varela and F. Fernández-Luqeño. Tesis. Aplicación de Matrices Carbonosas como Ánodos para Producción de Energía Eléctrica y Reducción de Compuestos Orgánicos por Bacillus subtilis. CINVESTAV, Unidad Saltillo (2016).

[146] M. Sondergaard. Redox Potential. Encyclopedia of Inland Waters. Academic Press (2009) 852-859.

[147] D. Li, S. Liu. Chapter 8 - Water Quality Detection for Lakes. Water Quality Monitoring and Management. Academic Press (2019) 221-231.

Appendix A.

1. **Deconvoluted XPS spectra of non-functionalized and functionalized OMC.**

1.1 Deconvoluted XPS spectra of OMC015
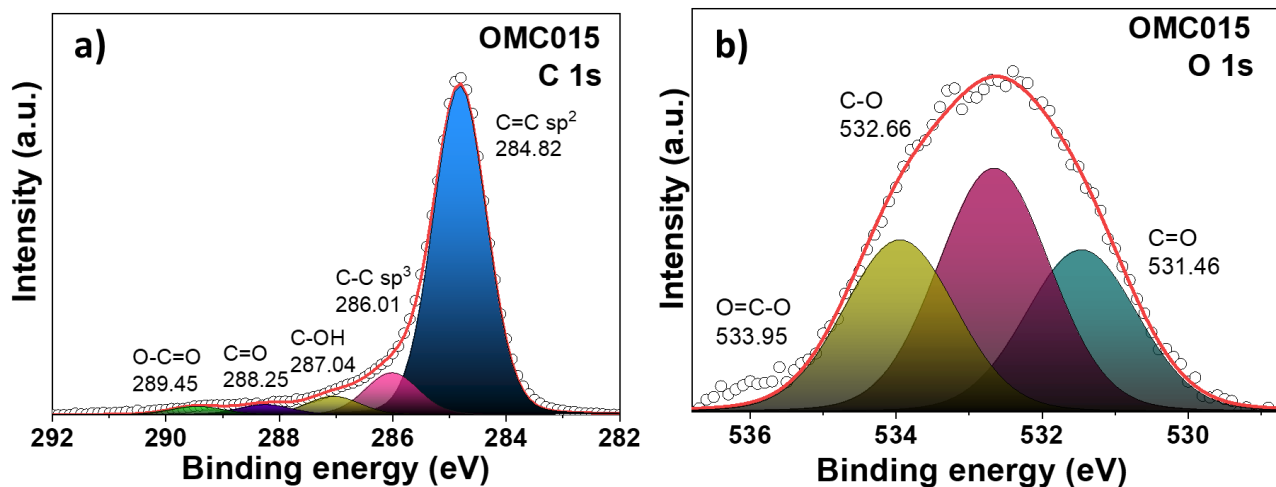
1.2 Deconvoluted XPS spectra of OMC05
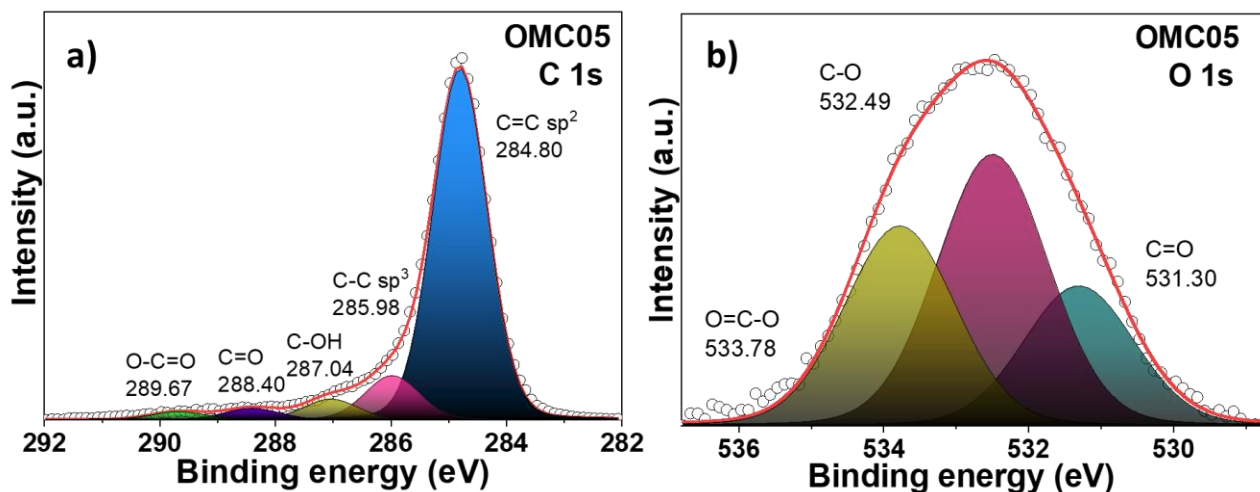
1.3 Deconvoluted XPS spectra of OMC1
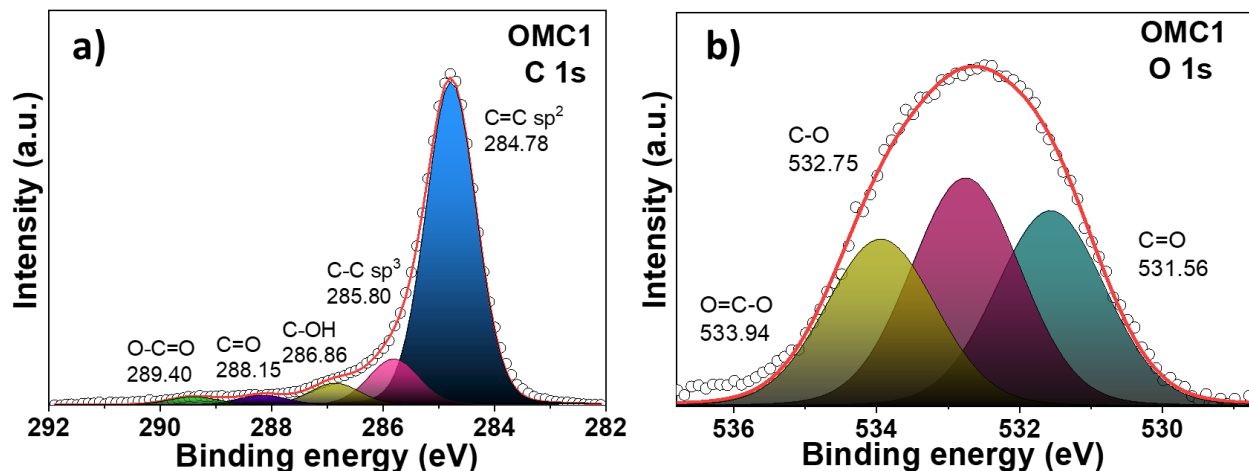
Table A.1 X-ray photoelectron parameters of OMC materials.

CATALYST	STATE	SPECIES	BE (eV)	COMPOSITION (at%)	FWHM
OMC	C1s	C=C sp^2	284.82	79.1	1.10
		C-C sp^3	285.91	12	1.10
		C-O	286.99	4.8	1.10
		C-OH	288.27	2.5	1.10
		C=O	289.62	1.6	1.10
	O 1s	C=O	531.26	37.6	1.80
		C-O	532.77	43.1	1.80
		O-C=O	534.09	19.3	1.80
OMC015	C1s	C=C sp^2	284.82	80.7	1.05
		C-C sp^3	286.01	10.3	1.10
		C-OH	287.04	4.5	1.10
		C=O	288.25	2.5	1.10
		O-C=O	289.45	2	1.10
	O 1s	C=O	531.46	28.1	1.80
		C-O	532.66	42.1	1.80
		O-C=O	533.95	29.8	1.80
OMC05	C1s	C=C sp^2	284.8	80.7	1.10
		C-C sp^3	285.98	10.2	1.10
		C-OH	287.04	4.7	1.10
		C=O	288.4	2.6	1.10
		O-C=O	289.67	1.8	1.10
	O 1s	C=O	531.3	22.9	1.80
		C-O	532.49	44.4	1.80
		O-C=O	533.78	32.7	1.80
OMC1	C1s	C=C sp^2	284.78	79.1	1.06
		C-C sp^3	285.8	11.3	1.06
		C-OH	286.86	5.3	1.06
		C=O	288.15	2.3	1.06
		O-C=O	289.4	2	1.06
	O 1s	C=O	531.56	33.1	1.80
		C-O	532.75	38.6	1.80
		O-C=O	533.94	28.3	1.80

Appendix B.

2. Deconvoluted XPS spectra of BS, non-functionalized and functionalized BC.

2.1 Deconvoluted XPS spectra of BS

2.2 Deconvoluted XPS spectra of BC

a) BC C 1s — C=C sp² 284.78; C-C sp³ 285.82; C-OH 286.73; C=O 287.94; -COOH 290.34

b) BC O 1s — O-C 533.09; O-C=O 534.02; C-OH 531.92

c) BC N 1s — N-graphitic 401.05; N-pyrrolic 400.32; Amine 399.37; N-pyridinic 398.41

d) BC Si 2p — SiC 103.70; SiOₓ 104.57; SiO₂ 102.85

e) BC Ca 2p — Ca 2p₃/₂ 348.16; Ca 2p₁/₂ 351.76

f) BC K 2p — K2p₃/₂ 294.42; K2p₁/₂ 297.17

g) BC Al 2p — AlOOH 74.58; Al₂O₃ 75.48; Al(OH)₃ 73.58

h) BC Fe 2p — FeOOH 712.41; Fe³⁺ 2p₁/₂ 726.14; Fe³⁺ 2p₃/₂ 723.56; FeCO₃ 715.60; FeCO₃ 719.43; Fe₂O₃ 709.67; Fe 2p₁/₂ 729.14

2.3 Deconvoluted XPS spectra of BC015

2.4 Deconvoluted XPS spectra of BC05

a) BC05 C 1s
- -COOH 290.40
- C=O 287.92
- C-OH 286.77
- C-C sp^3 285.64
- C=C sp^2 284.70

b) BC05 O 1s
- O-C 533.40
- O-C=O 534.55
- C-OH 532.15

c) BC05 N 1s
- N-pyrrolic 400.42
- Amine 399.64
- N-pyridinic 398.57
- N-graphitic 401.30
- Si$_3$N$_4$ 397.68

d) BC05 Si 2p
- SiO$_x$ 104.03
- Silicates 104.96
- SiC 103.14

e) BC05 Ca 2p
- Ca 2p$_{3/2}$ 347.98
- Ca 2p$_{1/2}$ 351.57

f) BC05 K 2p
- K 2p$_{3/2}$ 294.42
- K 2p$_{1/2}$ 297.17

g) BC05 Al 2p
- Al$_2$O$_3$ 75.28
- AlOOH 74.48

h) BC05 Fe 2p
- Fe$_2$O$_3$ 713.22
- Fe 2p$_{1/2}$(FeO) 724.42
- Fe 2p$_{3/2}$ sat 717.40
- Fe 2p$_{1/2}$(Fe$_2$O$_3$) 727.22
- Fe2p$_{3/2}$ sat 720.87
- Fe$_2$O$_3$ 710.35
- Fe 2p$_{1/2}$ sat 731.48

2.5 Deconvoluted XPS spectra of BC1

a) BC1 C 1s
- -COOH 290.34
- C=O 288.13
- C-OH 286.78
- C-C sp^3 285.81
- C=C sp^2 284.74

b) BC1 O 1s
- O-C 532.80
- O-C=O 533.90
- C-OH 531.57

c) BC1 N 1s
- N-graphitic 401.78
- N-pyrrolic 400.63
- Amine 399.70
- N-pyridinic 398.63
- Si$_3$N$_4$ 397.72

d) BC1 Si 2p
- SiC 103.28
- SiO$_x$ 104.28

e) BC1 Ca 2p
- Ca 2p$_{3/2}$ 347.29
- Ca 2p$_{1/2}$ 350.84

f) BC1 K 2p
- K 2p$_{3/2}$ 294.48
- K 2p$_{1/2}$ 297.17

g) BC1 Al 2p
- Al$_2$O$_3$ 75.18
- AlOOH 74.28

h) BC1 Fe 2p
- Fe 2p$_{1/2}$ 728.53
- Fe 2p$_{1/2}$ 725.97
- Fe 2p$_{1/2}$ (FeO) 723.92
- Fe2p$_{3/2}$ sat 716.29
- Fe$_2$O$_3$ 713.23
- Fe$_2$O$_3$ 710.29

Table A.2 X-ray photoelectron parameters of OMC materials.

CATALYST	STATE	SPECIES	BE (eV)	COMPOSITION (at%)	FWHM
BS	C 1s	C=C sp2	284.72	75.80	1.20
		C-C sp3	285.43	14.10	1.10
		C-OH	286.53	5.40	1.10
		C=O	288.38	4.60	1.10
	O 1s	C=O	531.14	24.00	1.80
		C-OH	531.90	62.40	1.80
		O-C	533.03	13.60	1.80
	N 1s	N-pyridinc	398.88	23.10	1.15
		Amine	399.90	57.90	1.02
		N-pyrrolic	400.76	19.00	1.24
	Si 2p	Si_3N_4	101.88	55.20	1.30
		SiO_2	102.68	38.10	1.29
		SiC	103.88	6.70	1.30
	Ca 2p	Ca 2p3/2	347.29	67.70	1.60
		Ca 2p1/2	350.84	32.30	1.60
	K 2p	ND			
	Al 2p	ND			
	Fe 2p	ND			
	S 2p	C-S-C	163.39	32.00	1.00
		C-SH	164.29	15.00	1.00
		C=O	164.97	10.00	1.00
		sulfite	167.99	15.00	1.00
		sulfate	169.03	14.00	1.00
		sulfate	169.86	14.00	1.00
BC	C 1s	C=C sp2	284.78	62.80	1.30
		C-C sp3	285.82	17.50	1.10
		C-OH	286.77	11.50	1.10
		C=O	284.24	3.10	1.10
		COOH	290.37	5.10	1.10
	O 1s	C-OH	531.92	28.90	2.00
		O-C	533.09	53.10	2.00
		O-C=O	534.02	18.00	2.00
	N 1s	N-pyridinc	398.41	20.80	0.65
		Amine	399.37	13.90	0.89
		N-pyrrolic	400.32	27.20	0.62
		N-graphitic	401.05	28.20	0.62
	Si 2p	SiO_2	102.85	19.90	1.33
		SiC	103.70	57.00	1.38
		SiO_x	104.57	23.10	1.30

	Ca 2p	Ca 2p3/2	348.16	69.30	1.83
		Ca 2p1/2	351.76	30.70	1.73
	K 2p	K 2p3/2	294.42	68.40	2.16
		K 2p1/2	297.17	31.60	2.03
	Al 2p	Al(OH)3	73.58	13.30	1.24
		AlOOH	74.58	61.60	1.25
		Al2O3	75.48	25.10	1.26
	Fe 2p	Fe2O3	709.67	11.60	2.44
		FeOOH	712.41	30.50	3.45
		FeCO3	715.60	12.10	3.59
		Fe(III) Fe 2p3/2 sat	719.43	10.90	4.05
		Fe(III) Fe 2p3/2	723.56	11.30	2.85
		Fe(III) Fe 2p1/2	726.14	11.60	2.95
		Fe(II) Fe 2p1/2 sat	729.42	12.00	4.34
BC015	C 1s	C=C sp2	284.72	65.40	1.30
		C-C sp3	285.74	15.60	1.10
		C-OH	286.73	12.10	1.10
		C=O	287.94	4.50	1.10
		COOH	290.38	2.40	1.10
	O 1s	C-OH	532.08	24.00	2.00
		O-C	533.29	52.60	2.00
		O-C=O	534.38	23.40	2.00
	N 1s	Si3N4	397.55	8.00	0.68
		N-pyridinc	398.39	13.70	0.76
		Amine	399.95	18.80	1.11
		N-pyrrolic	400.08	34.90	1.04
		N-graphitic	401.04	24.60	0.87
	Si 2p	SiC	103.24	24.40	1.48
		SiO_x	104.13	52.60	1.49
		Silicates	105.08	22.90	1.57
	Ca 2p	Ca 2p3/2	348.06	67.20	2.30
		Ca 2p1/2	351.67	32.70	2.32
	K 2p	K 2p3/2	294.48	66.40	2.05
		K 2p1/2	297.17	33.60	2.06
	Al 2p	AlOOH	74.57	57.00	1.42
		Al2O3	75.58	43.00	1.42
	Fe 2p	Fe2O3	711.92	17.10	2.12
		Fe2O3	714.06	40.00	2.75
		Fe 2p3/2 sat	716.96	13.70	2.43
		Fe(III) Fe 2p3/2 sat	719.95	5.00	2.50

		Fe 2p1/2 (FeO)	722.53	1.60	1.03
		Fe 2p1/2 (FeO)	724.98	9.40	2.25
		Fe 2p1/2 (Fe2O3)	727.40	9.90	1.68
		Fe(II) Fe 2p1/2 sat	729.34	3.20	1.09
BC05	C 1s	C=C sp2	284.70	65.00	1.30
		C-C sp3	285.64	14.80	1.10
		C-OH	286.63	12.80	1.10
		C=O	287.92	4.90	1.10
		COOH	290.40	2.60	1.10
	O 1s	C-OH	532.15	26.90	2.00
		O-C	533.40	56.10	2.00
		O-C=O	534.55	16.90	2.00
	N 1s	Si3N4	397.68	5.70	0.61
		N-pyridinc	398.57	25.30	0.88
		Amine	399.64	22.60	1.02
		N-pyrrolic	400.42	32.20	0.91
		N-graphitic	401.30	14.30	0.88
	Si 2p	SiC	103.14	19.90	1.42
		SiO$_x$	104.03	57.50	1.49
		Silicates	104.96	22.60	1.42
	Ca 2p	Ca 2p3/2	347.98	66.80	2.27
		Ca 2p1/2	351.57	33.20	2.28
	K 2p	K 2p3/2	294.48	67.00	2.02
		K 2p1/2	297.07	33.00	2.03
	Al 2p	AlOOH	74.48	47.60	1.35
		Al2O3	75.28	52.40	1.34
	Fe 2p	Fe2O3	710.35	7.10	2.58
		Fe2O3	713.22	32.70	4.17
		Fe 2p3/2 sat	717.40	15.90	4.57
		Fe 2p3/2 sat	720.87	6.60	3.85
		Fe 2p1/2 (FeO)	724.42	11.80	3.42
		Fe 2p1/2 (Fe2O3)	727.22	12.20	3.38
		Fe(III) Fe 2p1/2 sat	731.48	13.70	4.01
BC1	C 1s	C=C sp2	284.74	66.90	1.30
		C-C sp3	285.81	14.70	1.10
		C-OH	286.78	10.80	1.10
		C=O	288.13	4.50	1.10
		COOH	290.34	3.10	1.10
	O 1s	C-OH	531.14	24.00	2.00
		O-C	531.90	62.40	2.00
		O-C=O	533.03	13.60	2.00
	N 1s	Si3N4	397.72	12.10	0.81

	N-pyridinc	398.63	19.30	0.85
	Amine	399.70	34.00	1.05
	N-pyrrolic	400.63	27.80	1.06
	N-graphitic	401.78	6.80	0.47
Si 2p	SiC	103.28	69.60	1.91
	SiO_x	104.28	30.40	1.92
Ca 2p	Ca 2p3/2	348.07	66.80	2.30
	Ca 2p1/2	351.67	33.20	2.32
K 2p	K 2p3/2	294.48	66.60	2.06
	K 2p1/2	297.17	33.40	2.07
Al 2p	AlOOH	74.28	80.00	1.23
	Al2O3	75.18	20.00	1.61
Fe 2p	Fe2O3	710.29	7.10	2.58
	Fe2O3	713.23	32.70	4.17
	Fe 2p3/2 sat	716.29	15.90	4.57
	Fe 2p3/2 sat	723.92	6.60	3.85
	Fe 2p1/2 (FeO)	725.97	11.80	3.42
	Fe 2p1/2 (Fe2O3)	728.53	12.20	3.38
	Fe(III) Fe 2p1/2 sat	731.48	13.70	4.01